Final Technical Report
1/9/02

# Project Title: Numerical Analysis Of Three Component Induction Logging In Geothermal Reservoirs

DOE Agreement Number DE-FG07-00ID13955

Submitted to

Procurement Services Division
U. S. DOE, Idaho Operations Office
Attention: Carol L. Van Lente
850 Energy Drive
Idaho Falls, ID 83401-1563

By

Dr. David L. Alumbaugh
University of Wisconsin-Madison
Department of Civil and Environmental Engineering
Geological Engineering Program
2258 Engineering Hall
1415 Engineering Drive
Madison, WI 53706

## Table of Contents

# Chapter 1 - Introduction

## 1. Project Purpose:

This project is supporting the development of the 'Geo-BILT', geothermal, electromagnetic-induction logging tool that is being built by ElectroMagnetic Instruments, Inc. The tool consists of three mutually orthogonal magnetic field antennas, and three-component magnetic field receivers located at different distances from the source. In its current configuration, the source that has a moment aligned along the borehole axis consists of a 1m long solenoid, while the two trans-axial sources consist of 1m by 8cm loops of wire. The receivers are located 2m and 5m away from the center of the sources, and five frequencies from 2 kHz to 40 kHz are being employed. This study is numerically investigating 1) the effect of the borehole on the measurements, and 2) the sensitivity of the tool to fracture zone-geometries that might be encountered in a geothermal field. The benefits of the results are that they will lead to a better understanding of the data that the tool produces during its testing phase and an idea of what the limitations of the tool are.

## 2. Project Objectives

1) To understand the effect of the borehole on the measurements and test methods for removing the effect. Measurements where both the source and receivers are oriented perpendicular to the borehole (here referred to as the coplanar configuration) are known to be more sensitive to conductivity contrasts between the borehole and the formation than the traditional coaxial data. Here we will numerically determine how significant these effects are and analyze methods for reducing the effects.

2) To test the sensitivity of the Geo-BILT tool to different fracture zone geometries. Here the objective is being met by running a series of numerical models to analyze the depth away from the borehole to which the Geo-BILT tool configuration is sensitive, how dip of the fracture zone effects the measurements, the vertical resolution of the tool, the differences between the response of dipole and finite-sized sources the tool employs, and how anisotropy within the fracture zone effects the results.

Chapter 2 addresses the issues outlined under objective 1), while Chapter 3 focuses on issues raised under Objective 2).

# Chapter 2 - Numerical Modeling of borehole effects using a 3-component EM induction logging tool

## 1. Introduction

Electromagnetic (EM) induction logging has been used for years to determine near borehole properties. Traditional EM logging methods use a coaxial source-receiver configuration and can thus only produce a 2-D estimate of bulk formation resistivity. Interpretation of data acquired using this configuration is limited to cylindrical geometries about the borehole. Such assumptions are not valid in zones of complex structure or in anisotropic media if the well is not perpendicular to bedding.

The present study involves forward modeling of the response of an experimental 3-component EM induction-logging tool (GeoBILT), which Electro Magnetic Instruments (EMI) Inc. is building. This tool uses both a 3-component source and receiver to give 4 unique source-receiver combinations: Coaxial, coaxial null-coupled, coplanar, and coplanar null-coupled (Alumbaugh and Wilt, 2001). Both coaxial configurations have the source aligned parallel with the borehole axis; with the full coupled having the receiver also parallel to the borehole axis and the null coupled having the receiver perpendicular to the borehole axis. Both coplanar configurations have the source and receiver perpendicular to the borehole axis; with the full coupled having the receiver parallel to the source, and the null coupled having the receiver perpendicular to the source. These source-receiver combinations, along with relatively large offsets, when inverted are expected to yield true a 3-dimensional image of formation resistivity. The current version of the tool consists of at least one tri-axial source and two 3-component receivers located at 2 and 5m offset. The tool will operate at frequencies in the range of 2 to 20 kHz.

This study will focus on the coaxial and coplanar configurations (Figure 1), while the null-coupled configurations are investigated for specific cases only. The sensitivity for the coaxial configuration is minimized along the borehole axis (Figure 2) and therefore, the borehole effect is not expected to be significant (Alumbaugh and Wilt, 2001). The coplanar configuration, however, exhibits sensitivity that is maximized along the borehole axis (Figure 3), and thus the borehole may contribute to a considerable portion of the tool response. The effect of a borehole of variable diameter and variable conductivity will be investigated, for both source-receiver configurations. We will also explore the effect of an off-center source-receiver in a large borehole, and the effect of borehole-fracture interaction. Model results will be compared to analytic solutions, where available.

The effectiveness of both frequency differencing and a multi-coil differencing will be evaluated for removing the borehole effect. The frequency differencing technique uses measurements at multiple frequencies at the same source-receiver offset. The multi-coil differencing technique uses measurements made at a single frequency and multiple source/receiver offsets.

## 2. Induction logging

The first induction-logging tool was developed in 1948 (Doll, 1949), and was designed for use in wells drilled with highly resistive drilling mud. More recently their application has expanded to both dry holes and holes with more conductive drilling

fluids. A typical induction-logging tool (Figure 4) is composed of multiple transmitters and receivers oriented in the coaxial configuration. Here, both the source and receiver have their dipole moment axes aligned parallel to the borehole axis and are positioned at various offsets (~1-3m) along the borehole. The coaxial configuration is favorable for several reasons, including good depth of penetration, good signal to noise ratio, and sensitivity that is minimized along the borehole axis (Alumbaugh and Wilt, 2001). The major limitation, however, is that this configuration can only produce a 2-D estimate of bulk formation resistivity. Interpretation of data acquired using this configuration is, therefore, limited to cylindrical geometries about the borehole.

The present study also includes the coplanar configuration, in which both the source and receiver have their axes aligned perpendicular to the borehole axis and parallel to each other. This configuration is commonly used for surface prospecting, but is rarely used in for borehole logging. The coplanar configuration has lower signal to noise ratio and a smaller depth of penetration than the coaxial configuration, and has sensitivity, which is maximized along the borehole axis (Alumbaugh and Wilt, 2001). This configuration does, however, provide some directional sensitivity, which is lacking with the coaxial configuration.

The transmitter coil consists of an induction coil that uses a sinusoidal, time varying current to produce a magnetic field. The frequencies used, ~1-50 kHz, combined with typical conductivities encountered, require the use of Maxwell's equations to describe the behavior of currents, electrical, and magnetic fields associated with the EM induction method (Keller and Frischknecht, 1966). The current produces a primary magnetic field, or "free-space" field, in accordance with the Biot-Savart law, which relates a time varying current ($I_0\ e^{-i\omega t}$) to a corresponding magnetic field (H). The magnetic field induces eddy currents in any conductive bodies (formation) in the vicinity (Figures 1a and b). The electrical field produced by these eddy currents can be described by Faraday's law, which relates a time varying magnetic field ($\delta b/\delta t$), to a corresponding electrical field (E), which has both a real and imaginary component. These eddy currents produce a secondary (scattered) magnetic field in the formation. The secondary and primary magnetic fields produce a voltage in the receiver coil.

## 3. Previous Studies

Approximate theory of induction logging was first developed by Henry Doll in the late 40's (Doll, 1949). Doll's theory is based on the assumption that one can neglect the interaction of induced currents at sufficiently low frequencies for a resistive medium. The phase of the induced currents is $90^0$ out of phase from the primary field, regardless of the distance from the transmitter. The measured signal, therefore, is the sum of the signals created by currents in the medium and depends on the conductivity of the region surrounding the logging device only. This treatment is termed the "geometrical factor", in which the apparent conductivity of a formation can be calculated by assigning relative importance to the various regions in the vicinity of the sonde, or logging device, based on the the coil arrangement.

Doll's geometric factor approach, however, is insufficient to describe the measured response in the vicinity of highly conductive bodies, at high frequencies, and at significant distances from the transmitter. Approximate theory to include the interaction between induced currents or "skin effect" was introduced by Moran and Kunz (1962), for

induction logging with a two coil sonde in various borehole environments. Methods of solutions were developed for: a homogeneous conducting medium, invaded, infinitely thick beds, two adjacent noninvaded beds, and a thin bed inbedded in a homogeneous medium. This approximate theory, however, assumes cylindrical symmetry with respect to the borehole axis and is developed for a two coil sonde in the coaxial configuration only. Approximate theory to include more complex scenarios was subsequently developed.

Gianzero (1978) compared theoretical solutions with experimental results for an off-center induction logging tool. It was discovered that it was not necessary to include the "skin effect", in the theoretical analysis order to match experimental data. This analysis, however, was conducted for the coaxial configuration only and did not take into account a finite length source.

Howard (1981) develops theory to deal with vertical fractures that intersect a borehole filled with conductive fluid. The formulation is developed for source and receiver coil axes that are perpendicular to the borehole axes. This, however, is not a configuration that is commonly used. Other authors have developed methods to model the response from concentric layers about a borehole, simulating an invasion zone, and borehole casing. Wait (1984) presents a generalized formulation for any number of concentric homogenous layers about a borehole. This method is developed for a finite length source and receiver arranged in the coaxial configuration. Gianzero and Anderson (1984) provide an alternate formulation with specific application to the low frequency electromagnetic thickness tool (ETT), high frequency deep propagation tool (DPT), as well as moderate frequency induction logging arrays. Chew (1984) offers exact formulation in terms of an integral, and then presents an iterative scheme to compute the approximate solutions. A comparison between numerical integration and approximate solutions are offered for three and eight medium cases.

Anderson (1986) used a forward modeling technique to simulate the tool response in laminated zones and dipping beds. 2-d axial symmetry was assumed for the laminated zone analysis, while a 3-d code was used for the dipping bed scenarios. Anderson found that the behavior of apparent conductivity in laminated zones was linear in relation to the percentage of sand and shale presenting, and thus predictable. The dipping bed analysis showed that dip makes beds appear thicker, and that thin and resistive beds are more affected by dip than thick and conductive beds.

Only recently has attention been focused on the response from a 3-component induction logging instrument. Alumbaugh and Wilt (2001) present a numerical study on the sensitivity of a 3-component, long offset imaging tool. They present a sensitivity analysis for the four unique source-receiver configurations in a homogeneous half-space to determine realistic frequency and source-receiver combinations. Their analysis also included an inversion for the response from a horizontal well that penetrates an oil bearing sandstone, shale, and brine filled sandstone sequence. The beds are both faulted and dipping. A comparison between and image created using a single polarization source and one using three orthogonal sources indicates that the three component source can offer better estimate of 3-d geometry. The main drawback of three-component data is that its inversion requires significant computing power.

## 4. Methods

The tool response using coaxial and coplanar configurations will be determined using a frequency domain, finite difference (FD) method (Newman and Alumbaugh, 1995). The scattered fields are calculated on a staggered grid (Yee, 1966), in which the electric fields are assigned to the cell edges and the magnetic fields to the faces (Newman and Alumbaugh, 1995). In this scheme, the conductivity is computed halfway along a given cell edge. The average conductivity can then be evaluated by tracing the line integral of the magnetic field centered on the midpoint of the cell edge (Wang and Hohmann, 1993). The scattered fields are evaluated at each grid point, and the electric fields at each receiver are determined by bilinear interpolation. After the electric fields are calculated, the magnetic fields are determined by applying a numerical approximation to Faraday's law for the scattered electrical fields surrounding the receiver. The finite difference method is fully three dimensional, allowing for several different borehole diameter and conductivity scenarios, as well invasion zones and fractures to be investigated.

All numerical modeling is conducted on a desktop pc, with a 1 GHz chip and 1 GB of RAM. Model run time for a single source with ten receivers, at two frequencies ranged from 0.5 to ~6 hours depending on model complexity and source type.

Models consist of a 3 dimensional grid with a cylindrical borehole aligned parallel to the z-axis and located at x = y = 0 (Figures 5a-c). The borehole extends the entire model space in the z direction. The 3-dimensional staggered grid has been shown to be adequate in representing a cylindrical borehole, provided the node spacing is small enough in relation to the borehole diameter (Newman and Alumbaugh, 2001). The cylindrical nature of the borehole allows us to simplify our models by making them symmetric about the y-axis, thus reducing the number of y grid nodes by half. Some of the models included in this study are symmetric about the y-axis (Figures 6a and b). Y-symmetry was used in order to reduce the number of grid nodes for models that required either a large model space, or finer grid node spacing. A larger model space was used for the profile models, and finer grid node spacing was necessary for the variable conductivity models, due to the larger induction numbers relating to higher conductivity boreholes. A typical model that is not symmetric about the y-axis has 70 nodes in the x and y direction, and 125 in the z direction while a model with y-symmetry has only 35 in the y direction.

The models are constructed of a grid composed of non-uniform sized cells. Grid node spacing within the borehole is 0.02m in the x and y direction, and 0.05m in the z direction (in the vicinity of the source and receivers). Node spacing increases incrementally in the x and y direction, outside of the borehole, to a maximum of approximately 2.6m at the grid edge. Node spacing increases incrementally in the z direction as well, to a maximum of approximately 1.5m at the grid edge. The resulting overall grid dimensions are approximately 30m in the x direction, 15m in the y direction and 15m in the z direction.

In all cases, except the off-center and the fracture models, the source is located at x = y = 0, and z = 5m. Nine receivers are located directly below the source, the first one at 1.0m away and the rest at 0.5m increments from the source in the + z direction, resulting in a 5m long source receiver array. Five meters corresponds to the largest offset currently in use with the EMI tool. Source/receiver location for the off-center case is the same as

above, except the array is off set in the x direction to x = 0.16m. There are three sets of fracture models: one set with a 5m source-receiver array in three different locations, one with a 2m source-receiver pair, and one with a 4.5m source-receiver pair. These are described further in the results section.

The response using 4 different source types has been calculated. For the coaxial configuration, both a point dipole source and a 1m long solenoid source were used. The 1m solenoid source was simulated by integrating a series of magnetic dipoles along the axis of the borehole. This source has with no width in the x or y direction. The coplanar configuration also has two source types, a point dipole source and a loop. The loop source consists of a rectangular loop which is 1m long along the borehole axis and is 0.08m wide. The loop source is oriented with its moment in the +y direction. Results presented in the sections 7-9 are for the finite length source, unless otherwise noted. These finite length sources are dictated by the EMI GeoBILT tool specifications.

The borehole effect will be determined for each model, by comparison of the total quadrature component of the magnetic field with the quadrature component of the primary field, expressed as a percent. The primary field is the 'free space' field, and is equivalent to the response in the absence of any scatterers. The following equation is used:

$$[\ (QH_p - QH_t) / QH_p\ ] * 100. \qquad (1)$$

Here, $QH_p$ is the quadrature component of the primary field and $QH_t$ is the quadrature component of the total field. In some cases, $QH_t$ for a model with a borehole will be compared to the $QH_t$ for a similar model without a borehole. Since the models consist of a borehole in a homogenous background, with the exception of the fracture models, any difference between the primary and total quadrature field is due to the borehole only. The percent difference between the primary and total quadrature field will be calculated at each frequency as a function of source-receiver offset.

## 5. Numerical Checks

The accuracy of the model algorithm for simulating these types of borehole models is evaluated by comparison to analytic solutions. Ki Ha Lee at Lawrence Berkley National Labs provides an analytic solution for the coaxial configuration for different diameter and conductivity boreholes. Figures 7a-c show a comparison between the FD model results and the analytic solution for 0.01 and 100 S/m, 0.1m diameter boreholes in a 1.0 S/m background, and for a 10 S/m, 0.4m borehole in a 1.0 S/m background. Model results agree well with the analytic solution. The 0.01 S/m borehole results differ by less than 1% at all source-receiver offsets used, the 100 S/m borehole results are differ by less than 2% at 1.0m offset and less than 1% at greater offsets. The 0.4m borehole results differ by less than 5% at 1m offset and by less than 1% at offsets greater than 3m. The increase error at short offsets is due to the fact that there are a fewer number of cells between the source and receiver as you decrease the separation and thus the linear approximation employed in the FD solutions breaks down.

Berthold Kriegshauser of Baker Atlas provided analytic results for the coplanar configuration for a 10 S/m, 0.1m diameter borehole in a 1 S/m background. Comparison of these analytic solutions with the model results can be seen in Figure 7d. Agreement is

quite good, with results differing by less than 2% at all source-receiver offsets except for 3.5m at 20 kHz where it is 4.5%. This relatively large error is due to the fact that the total quadrature values cross zero between 3 and 4m offset, thus a small difference between the FD model and the analytic results is amplified.

**6. Point source versus Finite length source comparisons**

Numerical solutions are calculated for both point and finite length sources. The finite length source models take longer to compute, however they simulate the actual source configuration, and therefore are more realistic. If no significant difference between the point and finite length source results exists, future models could employ a point source to save computing resources.

The point source and extended source model results for 0.01 and 100 S/m boreholes, using the coaxial configuration can be seen in Figures 8a and b. The absolute value of the total quadrature components of the magnetic field (normalized by the transmitter moment) is shown as a function of source receiver offset. The absolute value of each solution is used, so that the results could be plotted on log scale to accommodate the wide range of values. The results show that there is a slight shift between the data sets, which is the largest at short offsets. The percentage difference between the point source and finite length source results is ~3% at 2.0m offset and ~1% at 5.0m offset for both the 0.01 and 100 S/m boreholes.

A comparison between the results from the point and finite length source has been made for the coplanar configuration as well. The finite length source consists of a loop that is 1.0m in length and 0.08m in width. The coplanar configuration results for the 0.01 and 100 S/m borehole models using point source and loop source can be seen in Figure 8b. Similar to the coaxial configuration, the finite length coplanar source results are shifted from the point source results. At 2m offset, the shift for the 0.01 S/m borehole is 6% at 2 kHz and 10 % at 20 kHz, and 1 % at 2 kHz and 8% at 20 kHz for the 100 S/m borehole. At 5m offset, the shift is for the 0.01 S/m borehole is 3% at 2 kHz and 4% at 20 kHz, and 17% at 2 kHz and 5% at 20 kHz for the 100 S/m borehole. This large difference may be a result of instability in the solution, and not differences in the source type as the 2 kHz results using the extended source oscillate above and below the point source results.

These results indicate that the finite length source results are significantly different than the point source results, and are thus more appropriate. All of the results presented in the following sections were computed using a finite length source, unless otherwise noted.

**7. Centered Borehole Simulations**

7.1 Variable borehole conductivity

The effect of the borehole on the tool response will first be evaluated for boreholes of different conductivities. Models consist of 0.1m diameter boreholes in a homogeneous 1.0 S/m background. Mud resistivity values include 0.01, 0.1, 10, and 100 S/m.

The results for the coaxial configuration at 2 and 20 kHz are shown in Figure 9a, and the values for the percent difference between the primary and total quadrature components are shown in Figure 9b. The magnitude of the borehole effect is similar for both frequencies, with the percent difference values for 20 KHz being only slightly

larger. Values of percent difference at 2 and 5m offset are less than zero for 0.01, 0.1 and 10 S/m boreholes at both 2 and 20 kHz. The 100 S/m borehole model produces percent difference values that are ~-9 % at 2m offset and ~-1% at 5m offset.

The results for the coplanar configuration at 2 and 20 kHz are shown in Figure 9c and the percent difference between the primary and total quadrature components is shown in Figure 9d. Similar to the coaxial results, the amplitude of the quadrature component of the primary field decreases with increasing offset, however there is a zero crossing between 3.0 and 3.5m offset for the 20 kHz results. The zero crossing produces a magnification of the separation between the primary quadrature and the total quadrature between 3.0 and 4.0m offsets. When the absolute value of the 20 kHz results is taken, the zero crossing produces a minimum value. The less conductive boreholes, 0.01 and 0.1 S/m, have percent difference values that range from –2 to –7% at 2m offset and from –3 to 1% at 5m offset. The 10 S/m borehole model has percent difference values that are ~5% at 2m offset and ~1% at 5m offset. The 100 S/m borehole has the largest percent difference values which reduce from 10% at 2m offset to 2 % at 5m offset for 2 kHz, and from 25% at 2m offset to –9% at 5m offset for 20 kHz. The 1m offset value for the 100 S/m borehole at 20 kHz appears to have an anomalously low value. This is possibly due to Numerical error, as the number of grid nodes in-between the source and receiver is too small for an induction number that high.

These results show that the borehole effect decreases with increasing source-receiver offset, and increases with increasing borehole conductivity. The effect of the borehole is larger for the coplanar configuration than the coaxial configuration. Also, the zero crossing produced at 20 kHz for the coplanar configuration moves to shorter offset with increasing borehole conductivity and diameter.

7.2. Variable borehole diameter

The magnitude of the borehole effect for three borehole diameters including 0.1, 0.2, and 0.4m, has also been examined (figure 10a and b). Each model consists of a 10.0 S/m borehole, in a 1.0 S/m background. The 0.1m case is identical to the 10 S/m case from the variable borehole conductivity analysis.

The results for the coaxial configuration are shown in Figure 11a and the percent difference between the primary and total quadrature fields for these models can be seen in Figure 11b. As was seen for the variable conductivity models, percent difference decreases with increasing offset for all cases. Values of percent difference are also found to increase with increasing borehole diameter. At 2m offset, percent difference values increase from less than 1% for a 0.1m borehole, to ~-14% for a 0.4m borehole. Values are smaller at 5m offset, ranging from ~0% for a 0.1m borehole to -2% for a 0.4m borehole.

The results for the coplanar configuration are shown in Figure 11c and the percent difference values are shown in Figure 11d. Similar to the coaxial results, percent difference values decrease with increasing offset, and increase with increasing borehole diameter. These values are also significantly lower for 2 than 20 kHz. At 2 kHz, values of percent difference at 2m offset increase from 3 to 27% for 0.1 to 0.4m diameter boreholes, while at 5m offset the increase is 1 to 9%. At 20 kHz values increase from 6 to 66% for 0.1 to 0.4 diameter boreholes, and from –2 to –24 % at 5m offset. The 20 kHz data has the same zero crossing that was evident in the previous sections. This zero

crossing, represented by a minimum value, moves to shorter source-receiver offsets with increasing borehole diameter. The 1m offset value for the 0.4 m borehole at 20 kHz has an anomalously low value, similar to the 0.1 m diameter, 100 S/m borehole case. Once again, the source-receiver separation may be too small for an induction number this high, resulting in numerical error in the solution.

These results indicate that the borehole effect decreases with increasing source receiver offset, increases with increasing frequency, and increases with increasing borehole diameter. The effect of the borehole is larger for the coplanar configuration than the coaxial, and is significant for the 0.4m diameter borehole out to 5m offset.

7.3. Borehole and invasion zone models

The magnitude of the effect of a more realistic combination of a borehole and invasion zone is investigated for two different scenarios. One model has a 0.1m diameter borehole with a 0.8m diameter invasion zone and the other has a 0.1m borehole with a 1.2m invasion zone (Figures 12a and b). The conductivity of the invasion zone for both models is 3.0 S/m, the borehole is 10.0 S/m, and the background is 1.0 S/m.

The coaxial configuration results for the two invasion zone models, is shown in Figure 13a, and the percent difference between the primary and total quadrature is shown in Figure 13b. Values of percent difference for the 0.8m invasion zone model are similar to those for the 0.4m diameter borehole, with values of ~-13% at 2m offset and ~-2% at 5m offset. As expected, percent difference values are even larger for the 1.2m invasion zone, with values of ~-27% at 2m offset and ~-5% at 5m offset.

Figure 13c shows the coplanar configuration results for invasion zone, while Figure 13d shows the percentage difference between the primary and total. As was seen with the coaxial configuration, the coplanar results for a 0.8m invasion zone are similar to those for a 0.4m diameter borehole. Values of percent difference are smaller at 5m offset than 2m offset. Also, the percent difference is larger for the 1.2m invasion zone than for the 0.8m invasion zone. The minimum values cause by the zero crossing in the 20 kHz data moves to shorter offsets with increasing invasion zone diameter, as was seen earlier with the increasing borehole diameter. The extremely high percent difference values at offsets between 2.5 and 4.0 are a result of the zero crossing.

## 8. Off-center borehole simulations

8.1 Maximum-coupled

The response of a source-receiver array that is off-center is investigated in a 0.4m borehole. The model is identical to the 0.4m borehole case in the previous section, however the source and receivers are located at x = 0.16m, y = 0 (Figure 14). This serves to simulate a tool that is along the edge of the borehole.

The coaxial configuration (Hzz) results for both the centered and off-center array can be seen in Figure 15a. The effect of the borehole is slightly smaller for the off-center array compared to the centered array, with total quadrature values shifted away from the centered total quadrature values and towards the primary quadrature. The coplanar configuration (Hxx) shows a similar relationship (Figure 15b), with the off-center total quadrature values shifted towards the primary quadrature.

8.2 Null-coupled

The geometry of the model is not symmetric about the array in the off-center case as was the case for the centered array. This asymmetry leads to non-zero results for the null-coupled configurations. Figure 15c shows the coplanar null-coupled (Hxy) and the coaxial null-coupled (Hzx and Hzy) results for the off-center array in the 0.4m diameter borehole.

The coaxial null-coupled configuration has sensitivity (Figure 16) that minimized along the borehole axis, and is maximized in the plane of the receiver (Alumbaugh and Wilt, 2001). Since the array is located in the + x direction, but along the y = 0 plane, a receiver polarized in the x direction will have unequal amounts of if its positive and negative regions of sensitivity in the borehole, thus producing a non-zero response. Due to symmetry, the Hzy component should be zero, and thus the ~1E-11 values shown indicate the level of error associated with this numerical method.

The coplanar null-coupled configuration has sensitivity that is minimized along the borehole axis as well as the x and y axes and it has its maximum sensitivity along the x the y diagonal (Alumbaugh and Wilt, 2001). The off-center array using this configuration will primarily have the background and only some portions of the borehole in the region of maximum sensitivity. These values should also be zero, due to symmetry, and thus the ~1E-8 values are due to error associated with the numerical method.

## 9. Borehole interaction with fracture

The final models in this study examine the interaction of a conductive horizontal fracture with a borehole and invasion zone. This analysis includes results from a 5m source-receiver array located above, across, and below the fracture (Figure 17); as well as from 2 and 4.5m source-receiver offset arrays, which cross the fracture in discrete increments (Figure 18). The latter analyses simulate an actual borehole logging run. Two sets of models have been used, ones that contain a fracture, borehole and invasion zone, and ones that contain a fracture only. Results for models with the borehole, invasion zone, and fracture are compared with those from models that include a fracture only. The fracture used is 1.0m in thickness and extends horizontally in the x-y plane across the entire model space. The models that include a borehole and invasion zone have a 0.1m diameter borehole and a 0.8m diameter invasion zone, which expands to 1.6m in diameter within the fracture (Figure 19). The background has a conductivity of 1 S/m, the borehole is 10 S/m, the invasion zone is 3 S/m outside the fracture and 6 S/m in the fracture and the fracture itself is 2 S/m.

### 9.1 5m Source-Receiver Array

The results for the array located above, across, and below the fracture are shown in Figures 20a-c. Comparison of the total quadrature values from the model with the fracture to those from the model with the fracture, borehole, and invasion zone show that the addition of the borehole and invasion zone cause a 'static shift' where by the response appears to maintain the same shape across the fracture, but is shifted to either larger or smaller values. The results for the coaxial configuration show that the shift decreases with increasing source-receiver offset. Values of percent difference between the model with the borehole and invasion zone, and the model with fracture only reduce from ~10% at 2m offset to ~2% at 5m offset.

Values of percent difference for the coplanar configuration are larger than those for the coaxial configuration, but decrease with increasing offset as well. The 2 kHz results have percent difference a value of ~26% at 2m offset and and ~6% at 5m offset for the arrays above and below the fracture. The array across the fracture, however, has percent difference values that don't decrease as much and are 24% at 5m offset.

For the coaxial configuration, the static shift caused by the borehole is ~10% at 2.0m offset, while at 5.0m offset the shift is reduced to ~2%. This suggests that at 5.0m offset it is not necessary to correct the total quadrature response in order to correctly detect the signal from the fracture. However, the results for the coplanar configuration show significantly larger shifts corresponding to the addition of the borehole and invasion zone at both offsets. At 2.0m offset, the shift is up to 75%, and at 5m offset the shift can be as high as 36%. These results indicate that the borehole effect is more significant for the coplanar configuration even out to 5.0m offset. Therefore, if the coplanar configuration is to be useful in detecting horizontal features, a technique to remove the effect of the borehole and invasion zone must be employed

9.2 2.0m Source-Receiver offset profile

The results from a simulation of a 2.0m long tool that encounters a conductive horizontal feature (Figure 18), is shown in Figure 21. Here, the model space is similar to that of the previous section; however, the total quadrature is calculated at 0.5m intervals across the fracture, using a fixed source-receiver separation. The total quadrature for both the coaxial and coplanar configurations at 2 and 20 kHz is plotted versus source-receiver midpoint. Values of total quadrature are plotted on a linear scale.

The coaxial and coplanar configuration results at 2 kHz are not extremely sensitive to the fracture, and show only a small perturbation in the vicinity of the fracture. The results from the model that includes a borehole has a slightly larger response from the fracture, than from the model without the borehole. The results at 20 kHz are significantly more sensitive to the fracture. Here the separation between the results from the model with the borehole and the model without the borehole is large away from the fracture, and even larger near the fracture. The percentage difference between the results from the model with the borehole and the model without the borehole can be seen in Figure 22. Values for the coaxial configuration increase from ~11% away from the fracture to ~21% near the fracture. Those for the coplanar configuration at 2 kHz increase from ~27% away from the fracture to >100% near the fracture, and from ~70% to >2700% near the fracture at 20 kHz. This increase in the borehole effect is in the vicinity of the horizontal fracture is at least partially due to the expanded invasion zone in the fracture.

9.3 4.5m Source-Receiver offset profile

Next we examine the results from the horizontal fracture models with a 4.5m long tool, instead of a 2.0m long one (Figure 18). The large model space required for a 4.5m offset array in multiple locations made it necessary to use a parallel computing platform, precluding usage of the PC that the previous models were run on. Unfortunately the extended source code is not currently available for the parallel platform and thus a point

source had to be used for the coaxial configuration models. The coplanar data are for the same 0.08 by 1.0m loop as in the previous examples. The coaxial and coplanar configuration results for the 4.5m source-receiver offset profile at 2 and 20 kHz can be seen in Figure 23a-d. The results at 2 kHz are similar to the 2.0m source-receiver offset results, with both configurations showing only a small response from the fracture. At 20 kHz, the response from the fracture is greater for both configurations; however the overall response is significantly smaller than for the 2.0m offset results. Values of percent difference between the models with and without the borehole can be seen in Figure 24a and b. This figure shows that similar to the results from the previous section, the borehole effect increases when the source and receiver is near the horizontal fracture. Values of percent difference for the coaxial configuration increase from ~2% away from the fracture to ~5% near the fracture. Values for the coplanar configuration at 2 kHz increase from ~14% away from the fracture to ~50% near the fracture, while the percentage difference remains ~35% at all locations at 20 kHz.

## 10. Post Acquisition Processing

To this point, discussion has involved analyzing the magnitude of the borehole effect for various diameters and conductivities. We have shown that the borehole effect can be significant, especially at for the coplanar configuration, at short offsets, and at higher frequencies. In this section we examine methods by which the borehole effect can be reduced. Two methods will be evaluated: frequency differencing and multi-coil differencing.

### 10.1 Frequency differencing

The first method that will be examined is a frequency differencing technique. This technique involves measurements made using two frequencies at the same source receiver offset. Analysis of Doll's theory of induction logging using a coaxial configuration has shown that any conducting medium can be divided into two regions, the internal and external area (Kaufman and Keller, 1989). The internal area, which is adjacent to the induction probe, has induced currents that are shifted $90^0$ in phase from the primary field and have density that is defined by the primary magnetic flux. The extent of the internal area is determined by the frequency and medium conductivity. Currents induced in the internal area have little influence on current density in the external area.

If frequency and medium conductivities produce an induction number such that the boundary between the internal and external area is located within the formation, i.e. the borehole is entirely within the internal area, then the frequency differencing technique can significantly reduce the effect of a borehole (Kaufman and Keller, 1989). For a two-coil probe, operating at different frequencies, the quadrature component of the magnetic field can be written:

$$\begin{aligned} Q\,H_z(\omega_1) &= \sigma_i[\omega_1 \mu L^2 / 2] + f(\omega_1, L, \sigma_3) \\ Q\,H_z(\omega_2) &= \sigma_i[\omega_2 \mu L^2 / 2] + f(\omega_2, L, \sigma_3) \end{aligned} \qquad (2)$$

Where $\omega_1$ and $\omega_2$ are the frequencies of coil one and two, $\sigma_i$ is the frequency independent apparent conductivity of the of the internal area when the conductivity of the external

area is equal to infinity, L is the probe length, and $f(\omega,L,\sigma_3)$ depends on frequency, probe length and medium conductivity only. If the current in each coil equal, then the following function does not depend on the distribution of conductivities in the internal zone:

$$QH_z(FD) = QH_z(\omega_2) - [\omega_2 / \omega_1]\, QH_z(\omega_1). \quad (3)$$

Here, $QH_z(FD)$ is the quadrature component of the magnetic field after frequency differencing. Frequency differencing is achieved by applying equation (3) to both the primary quadrature and total quadrature responses at the 2 and 20 kHz, and then comparing the results as in the previous sections. Kaufman and Keller (1989) formulated this technique for use with the coaxial configuration; however in this study we apply it to both the coaxial and coplanar results. The effectiveness of the frequency differencing technique is then evaluated for both configurations.

The total and primary quadrature results after frequency differencing for the coaxial and coplanar configurations are shown in Figures 25a-c. The results for the boreholes of variable conductivity (Figure 25a) show that after frequency differencing, there is almost no separation between the total and primary quadrature values for either configuration. Values of percent difference between the total and primary quadrature after frequency differencing are <3% at both 2 and 5m offset. This indicates that the effect of the borehole has been almost completely removed.

The results for the variable diameter borehole after frequency differencing are shown in Figure 25b. The coaxial results are similar to those for the variable conductivity borehole, with the total quadrature values being nearly identical to the primary quadrature. Values of percent difference between the total and primary quadrature are less than 3% at both 2 and 5m offsets. The coplanar results also have total quadrature values that are near the primary quadrature values, except for the 0.4m borehole that deviates at offsets shorter than 3.0m. This deviation, however, may be due to numerical instability of the solutions, or the zero crossing that occurs between 2 and 3m offset. Values of percent difference between the total and primary quadrature remain below 3% at 2 and 5m.

Figure 25c shows the total and primary quadrature results after frequency differencing for the models that include a borehole and invasion zone. The borehole effect is significantly reduced for both the coaxial and coplanar configurations compared to the 2 and 20 kHz results. At short offsets, values of percent difference are slightly larger for the coplanar configuration than the coaxial configuration; however, both models produce percent difference values that are less than 2% at 5m offset. This is a significant reduction compared to the non-differenced data.

The frequency differencing technique has been demonstrated to remove the borehole effect for various conductivities and diameters, however, for it to be truly effective, it must also preserve the signal from features extending away from the borehole. We next apply the frequency differencing technique to the models that contain a conductive horizontal fracture. Figures 26a-c show the total quadrature results for the models that have an array above, across, and below a 1m thick horizontal fracture. Frequency differencing has significantly reduced the borehole effect for the coaxial configuration. The percent difference between the total quadrature results from the model with the borehole and invasion zone, and the model with the fracture only, are 3%

at 2m offset and 2% at 5m offset for all three array locations. The values of percent difference are only slightly larger for the coplanar results, at 2m and 5m offset, the percent difference is ~4%.

The frequency difference technique is next applied to the results from the 2.0 and 4.5m source-receiver offset profiles across the fracture. The total quadrature results for both the coaxial and coplanar configurations for the 2.0m source-receiver offset profile, after frequency differencing are shown in Figures 27a and b. The figures show that the differencing technique has reduced the separation between the results from model with the borehole and the model without the borehole away from and near the fracture. This reduction in the borehole effect is especially significant for the coplanar configuration. The coaxial configuration has percentage difference values at 2.0m offset that increase from ~3% away from the fracture to ~8% near the fracture and from ~2 to ~4% for 4.5m offset. The 2.0m results are significantly reduced from the non-differenced values, however, the 4.5m results are show a minimal reduction. The coplanar configuration results at 2.0m offset cross over each other near the edges of the fracture, producing percentage difference values which are ~5% away from the fracture and between 13 and -9% near the fracture. The 4.5m offset coplanar results also cross over, and have percent difference values that are ~1% away from the fracture and from 8 to ~-13% near the fracture. Both the 2.0 and 4.5m coplanar results are reduced significantly compared to the non-differenced values. In addition to removing the borehole effect, however, frequency differencing has reduced the amplitude of the response from the fracture, significantly decreasing the signal to noise ratio.

These results indicate that frequency differencing is effective at removing the borehole effect for the coaxial and coplanar configurations in many different situations. The effect of 0.1m diameter boreholes that have conductive mud of less than 100 S/m can be effectively eliminated. Also, the borehole effect from a borehole of diameter up to 0.4m with mud of 10 S/m, and for invasion zones of 3 S/m and 1.2m diameter can also be significantly reduced. These results also indicate that frequency differencing will not remove the response from a horizontal feature, such as a fluid filled fracture. An additional virtue of the frequency differencing technique is that it removes the zero crossing for the higher frequency coplanar results, and therefore aids in data interpretation. A major drawback of the frequency differencing technique, however, is that it reduces the sensitivity of the measurements, and thus increases the signal to noise ratio. This is evidenced by the reduction of the magnitude of the response from the horizontal conductive fracture after differencing.

10.2 Multi-coil differencing

Another technique that may be used to reduce the borehole effect is multi-coil differencing. This technique involves the measurement made with multiple source-receiver offsets at a single frequency. In our case, we use a single source and two receivers, one at 2.0m and one at 5.0m offset. Similar to the frequency differencing mentioned above, this technique attempts to remove the signal from the internal area, while preserving that from the external area (Kaufman and Keller, 1989). Multi-coil differencing is achieved by applying the following equation:

$$QH\,(MCD) = QH\,(5m) - QH\,(2m) * [H_{air}\,(5m) / H_{air}\,(2m)]. \qquad (4)$$

Here, QH (MCD) is the quadrature component of the magnetic field after multi-coil differencing, QH (5m) and (2m) are the quadrature components of the magnetic field at 5 and 2 meters offset, and $H_{air}$ is the magnitude of the total magnetic field in air or 'free space field, at 5 and 2m offset. The air values were obtained by calculating the response at 2 and 5m offsets in a 0 S/m homogeneous background. The ratio $H_{air}$ (5m) / $H_{air}$ (2m) is equal to 6.4e-2 at both 2 and 20 kHz, for both the coaxial and coplanar configurations. In practice, values for a specific array can be obtained by operating the tool in the air, at the surface.

The percent difference values between the primary and total quadrature component of the magnetic field, after differencing, can be seen in Table 1. The magnitude of the borehole effect at 5 m offset for the coaxial configuration is relatively small, therefore, a comparison of the percent difference for the raw data (at 5m offset) and the multi-coil data show that multi-coil technique offers almost no significant reduction in the borehole effect. In some cases, such as for the invasion zone models at 20 kHz, the values of percent difference between the total and quadrature are actually larger after differencing.

Since the borehole effect at 5 m offset for the coplanar configuration is significant, the multi-coil differencing is more effective for the coplanar configuration than for the coaxial. Values of percent difference between the total and primary quadrature after differencing can be seen in Table 1. Comparison of the percent difference for the raw data (at 5m offset) and the multi-coil data show that the multi-coil technique reduces the borehole effect significantly. Values of percent difference for a 100 S/m borehole are less than 1% after differencing, compared to 19% at 20 kHz. Values of percent difference for a 0.4m borehole reduce from –24 to –3.5% at 20 kHz after multi-coil differencing. The response from a 1.2m invasion zone is also significantly reduced, with percent difference of -24%, compared to –63% at 20 kHz. The effectiveness of the multi-coil differencing technique at removing the effect of the borehole while preserving the signal from a horizontal feature is evaluated by applying the technique to the models that contain a conductive horizontal fracture. The values of percent difference between the total quadrature from the fracture models that contain a borehole and invasion zone, and those that contain a fracture only are shown in Table 1. The coaxial configuration has values of percent difference that are ~0% at 2 kHz and ~5% at 20 kHz for arrays located above, across, and below the fracture. These are not significantly lower than those for the raw data at 5m offset. Values of percent difference for the array above, across, and below the fracture using the coplanar configuration are not significantly reduced at 2 kHz; however, the 20 kHz data show a large reduction. Here, values of percent difference at 20 kHz, at 5m offset, reduce from ~32% to ~8% after differencing.

## 11. Discussion

The borehole effect has been shown to increase with increasing borehole conductivity and diameter, however, this relationship is yet to be quantified. The magnitude of the borehole effect can be expressed in terms of percentage difference between the total and primary quadrature fields. All of the models included in this study, with the exception of the fracture models, consist of borehole in a homogeneous half-space; therefore any deviation of the total quadrature from the primary quadrature can be attributed to the borehole only.

One way to characterize a source-receiver array in a borehole environment is by using the induction number. The induction number is defined as:

$$I = \Delta\sigma\, \omega\, \mu\, L^2. \tag{5}$$

Here, $\Delta\sigma$ is the difference between the background and borehole conductivity, $\omega$ is angular frequency (given by $2\pi f$, where $f$ is the frequency in Hertz), $\mu$ is the magnetic permeability of free space, and L is a characteristic length (in our case the borehole diameter). Figure 28 shows a plot of the induction number ($I$) versus the absolute value of the percentage difference between the total and primary quadrature. Percentage difference values include those from the variable conductivity, variable diameter, and invasion zone models. The data are presented for both the coaxial and coplanar data at 2 and 20 kHz using a 5m source-receiver offset. The figure shows that percent difference increases approximately linearly with the induction number. The different configurations and frequencies, however, all have different relationships. The results for the coplanar configuration can be fit with trendlines that have significantly higher slopes than the results for the coaxial configuration. Similarly, the 2 kHz data produces higher slopes than the 20 kHz data, indicating that the borehole effect is frequency dependant. This indicates that although the borehole effect can be said to increase linearly with the induction number, a single equation cannot be applied to data from different configurations and/or frequencies.

## 12. Conclusions

We have used a finite difference approach to evaluate the dependence of the borehole effect on borehole diameter and conductivity, for both the coaxial and coplanar configurations at 2 and 20 kHz. The degree to which a borehole and invasion zone affects the response from a conductive horizontal fracture has also been investigated. This research has been done in relation to a three-component, long-offset EM induction tool that is currently being developed by EMI. The magnitude of the borehole effect is quantified by taking the percent difference of the total and primary quadrature fields for a given source-receiver offset.

The influence of the borehole has been shown to increase with increasing borehole conductivity for a given background conductivity using both the coaxial and coplanar configurations. Decreasing the conductivity to below that of the background does not produce a significant borehole effect. Increasing the borehole diameter and adding a conductive invasion zone are both found to increase the response from the borehole. The borehole effect increases with increasing frequency, with values of percent difference being larger at 20 kHz than at 2 kHz. In general, the coplanar configuration is more sensitive to the borehole than the coaxial configuration. For example, values of percent difference between the total and primary quadrature at 2m offset and at 20 kHz are 66% at 2m offset for a 0.4m borehole using the coplanar configuration, compared to 15% for the coaxial configuration. The borehole effect decreases with increasing source-receiver offset. At 5.0m offset, the borehole response for the coaxial configuration is generally insignificant, while the coplanar configuration can have significant borehole effects. This is primarily true for the large diameter boreholes models, and the models with a borehole and invasion zone. The magnitude of the borehole effect has been shown to increase

linearly with the induction number. Each configuration and frequency, however, has a unique slope for this relationship.

Due to the cylindrical symmetry about the x-y axis, the null-coupled components (Hzx, Hzy, and Hxy) for a centered array are zero. A source-receiver array that is off-center in the +x direction, produces a reduction in the full-coupled (i.e. Hxx and Hzz) response from the borehole, as well as a non-zero Hzy component. An array that is off-center in an arbitrary direction will also produce a non-zero Hzx component.

The presence of a borehole and invasion zone has been shown to produce a "static shift" in the total quadrature response to a conductive horizontal feature. This shift affects the magnitude of the response, while preserving the shape of the profile across the fracture. A horizontal fracture that causes an expansion of the invasion zone has been shown to produce an increased borehole effect in the vicinity of the fracture.

Two techniques have been implemented to reduce the borehole effect; multi-coil differencing and frequency differencing. The multi-coil differencing technique has been shown to be more effective at removing the borehole effect for the coplanar configuration, and had negligible effect on the coaxial results. This technique was unable to completely remove the borehole effect for the 0.4m diameter borehole and the invasion zone models. The frequency differencing technique was found to be effective at removing the borehole effect for both the coaxial and coplanar configurations. This technique was also shown to be able to reduce the borehole effect, while preserving the response from a horizontal feature. The frequency differencing technique, however, reduces the sensitivity of the measurements significantly, thus decreasing the signal to noise ratio.

## 13. References cited

Alumabugh, D.L., and Wilt, M.J., A numerical sensitivity study of three dimensional imaging from a single borehole. *Petrophysics*, 42, 1, 19-31, 2001.

Anderson, B., The analysis of some unsolved induction interpretation problems using computer modeling. *The Log Analyst*, 27, 5, 60-73, 1986.

Chew, W.C., Response of a current loop antenna in an invaded borehole. *Geophysics*, 49, 1, 81-91, 1984.

Doll, H.G., Introduction to induction logging and application to logging of wells drilled with oil base mud. *Journal of Petroleum Technology*, 1, 148-162, 1949.

Gianzero, S.C., Effect of sonde eccentricity on responses of conventional induction-logging tools. *IEEE Transactions on Geoscience Electronics*, GE-16, 4, 332-339, 1978.

Gianzero, S. and Anderson, B., Mathematical theory for the fields due to a finite A.C. coil in an infinitely thick bed with an arbitrary number of co-axial layers. *The Log Analyst*, 25, 2, 25-32, 1984.

Gianzero, S. and Su, S, The response of an induction dipmeter and standard induction tools to dipping beds. *Geophysics*, 55, 9, 1128-1140, 1990.

Hardman, R.H. and Shen, L.C., Theory of induction sonde in dipping beds. *Geophysics*, 51, 3, 800-809, 1986.

Howard jr., A.Q., Induction logging for vertical structures in the presence of a borehole fluid. *Geophysics*, 46, 1, 68-75, 1981.

Kaufman, A.A. and Keller, G.V., *Induction Logging*, Elsevier, New York, 1989.

Keller, G.V. and Frischknecht, F.C., *Electrical Methods in Geophysical Prospecting*, Pergamon Press, New York, 1966.

Moran, J.H. and Kunz, K.S., Basic theory of induction logging and application to study of two-coil sondes. *Geophysics*, 27, 6, 829-858, 1962.

Newman, G. A., and Alumbaugh, D. L., A finite difference solution for 3D induction logging problems: Part II; Accepted for publication in *Geophysics*, 2001.

Newman, G.A. and Alumgaugh, D.L., Frequency-domain modeling of airborne electromagnetic responses using staggered finite differences. *Geophysical Prospecting*, 43, 1021-1042, 1995.

Wait, J.R., General formulation of the induction logging problem for concentric layers about the borehole. *IEEE Transactions on Geoscience and Remote Sensing*, GE-22, 1, 34-42, 1984.

Wang, S.H. and Hohmann, G.W., Electromagnetic theory for geophysical applications. In: *Electromagnetic Methods in Applied Geophysics-Theory*, vol. 1 (ed. M.N. Nabighian), Society for Exploration Geophysics, 130-311, 1993.

Yee, K.S., Numerical solution of initial boundary problems involving Maxwell's equations in isotropic media. *IEEE Transactions on Antennae and Propagation*, AP-14, 302-309, 1987.

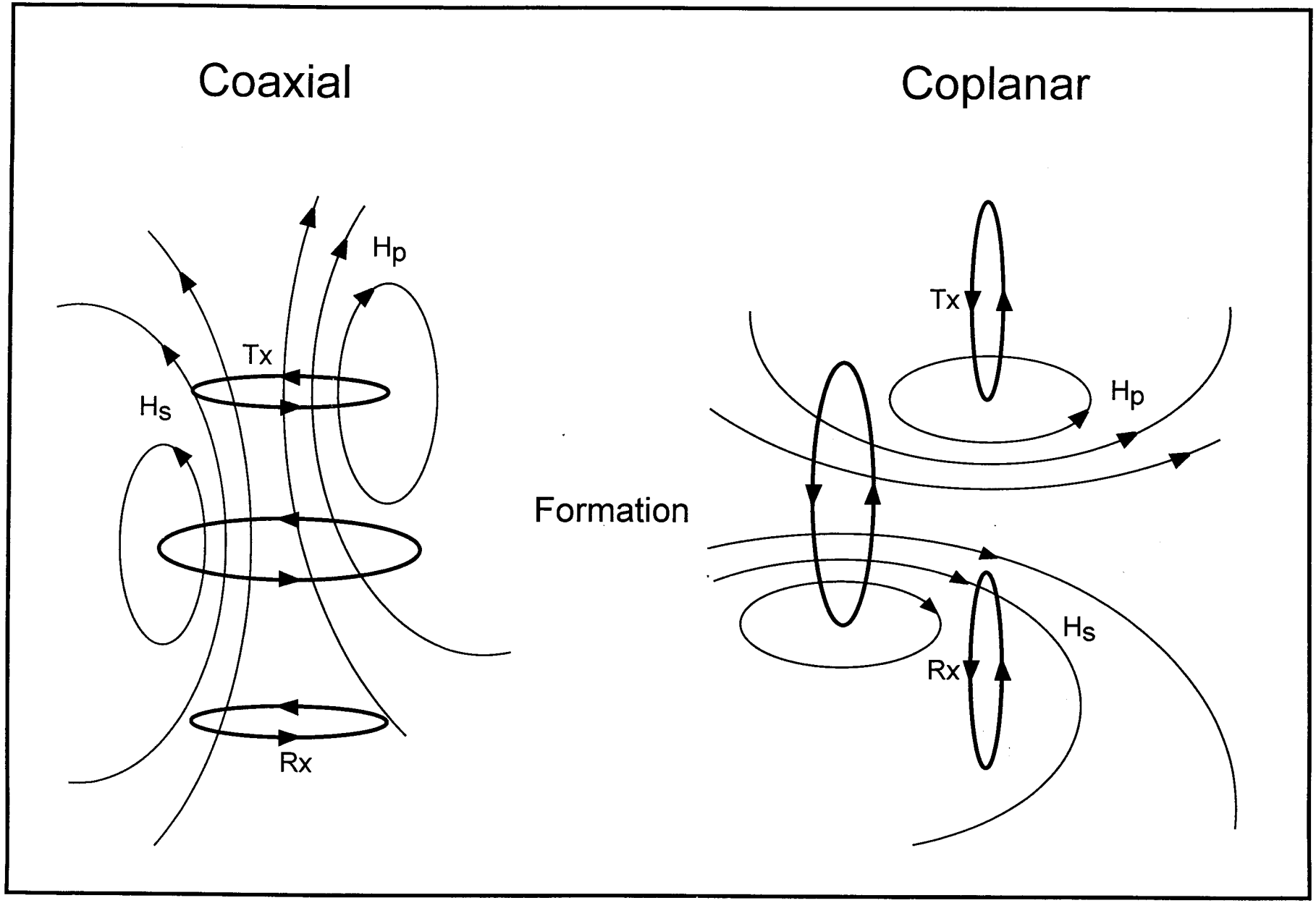


Figure 1. Coaxial and Coplanar configurations. Tx is the transmitter, Rx is the Reciever, Hp is the primary magnetic field, and Hs is the Scattered magnetic field.

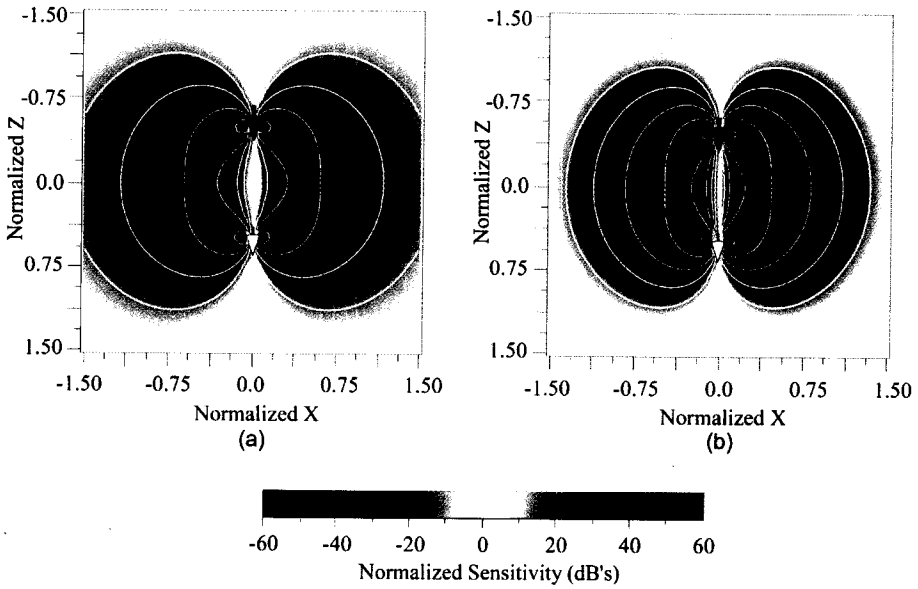


Figure 2. Logarithmically normalized coaxial sensitivity as a function of position in the y=0 plane for an induction number of 1. a) Real component. b) Quadrature component. (From Alumbaugh and Wilt, 2001)

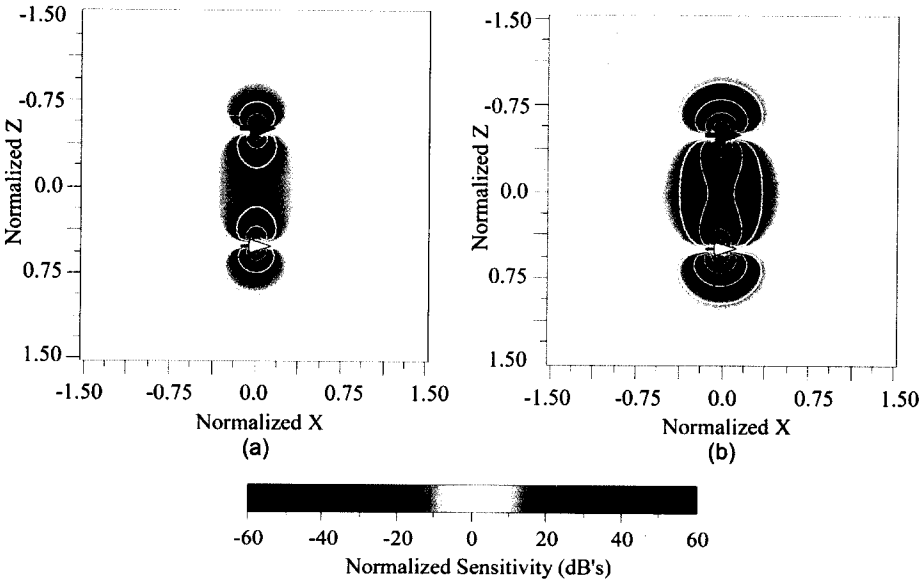


Figure 3. Logarithmically normalized coplanar sensitivity as a function of position in the y=0 plane for an induction number of 1. a) Real component. b) Quadrature component. (From Alumbaugh and Wilt, 2001)

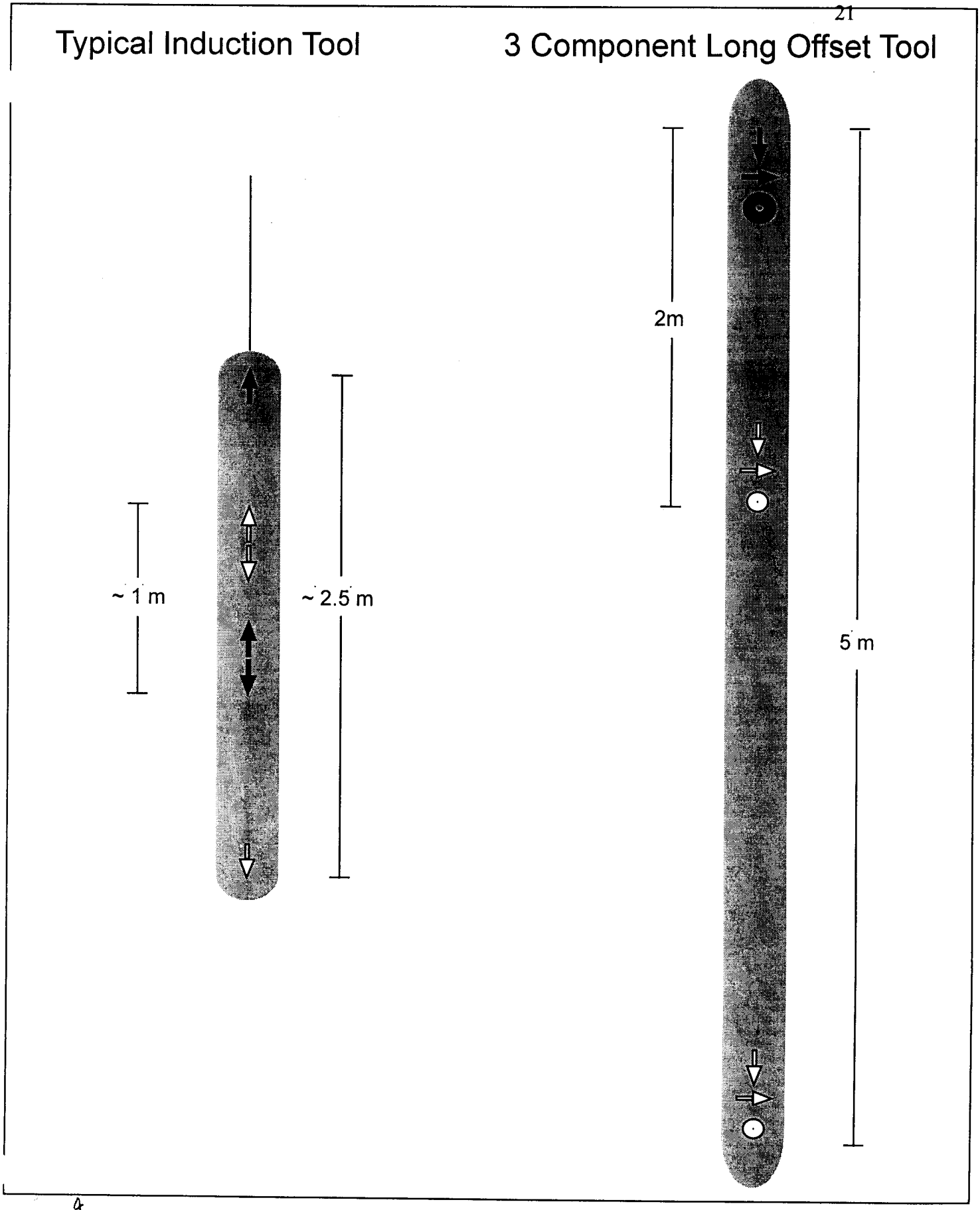


Figure 4. Typical and 3 Component Long Offset tool configurations. Black arrows represent sources and white arrows represent recievers. The direction of the arrow indicates the orientation. Circles represent arrows that point directly out of the page. (After Alumbaugh and Wilt, 2001)

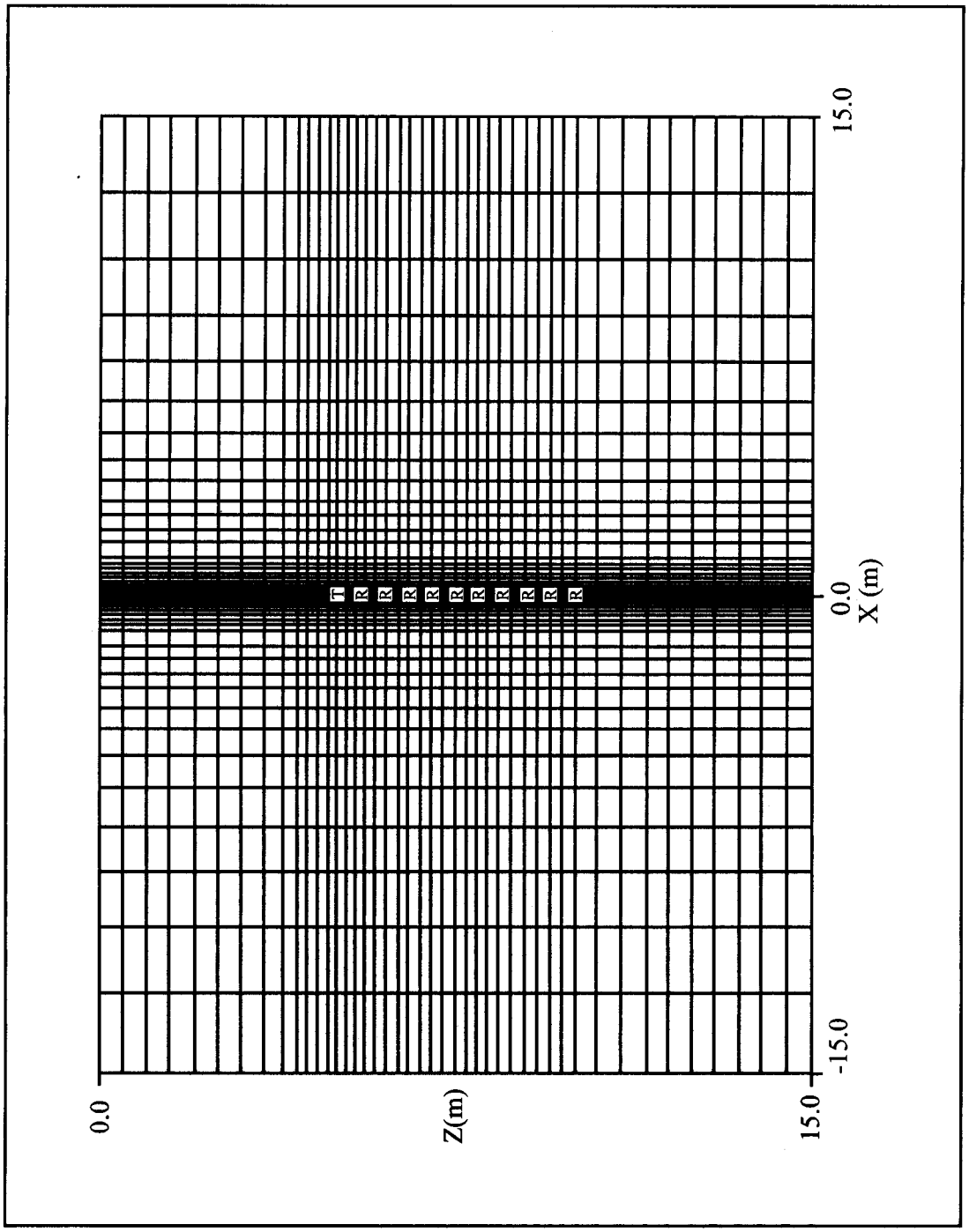


Figure 5a. The X-Z plane of the staggered, grid finite difference model space. T represents the source, and R represents recievers.

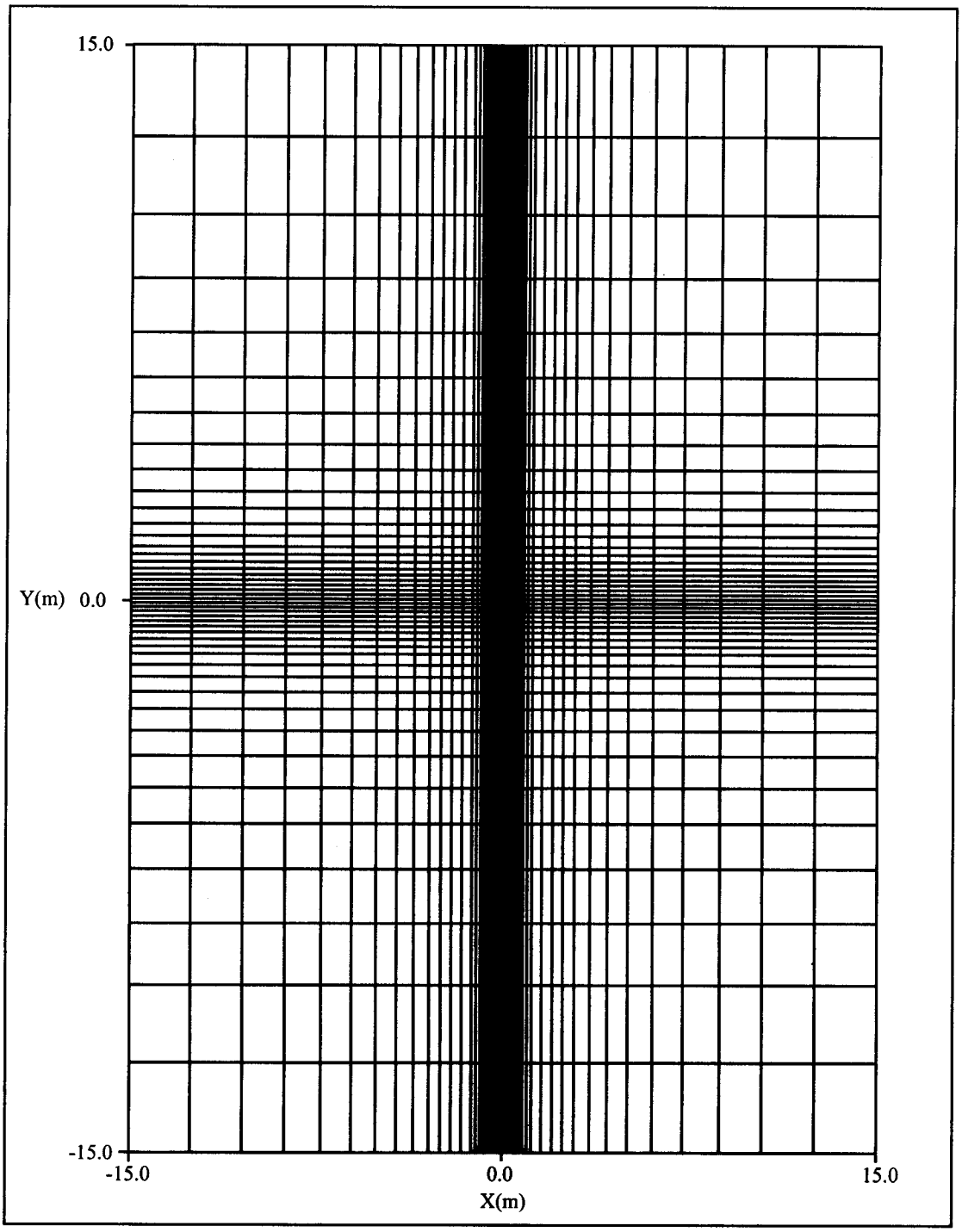


Figure 5b. The X-Y plane of a staggered grid, finite difference model space.

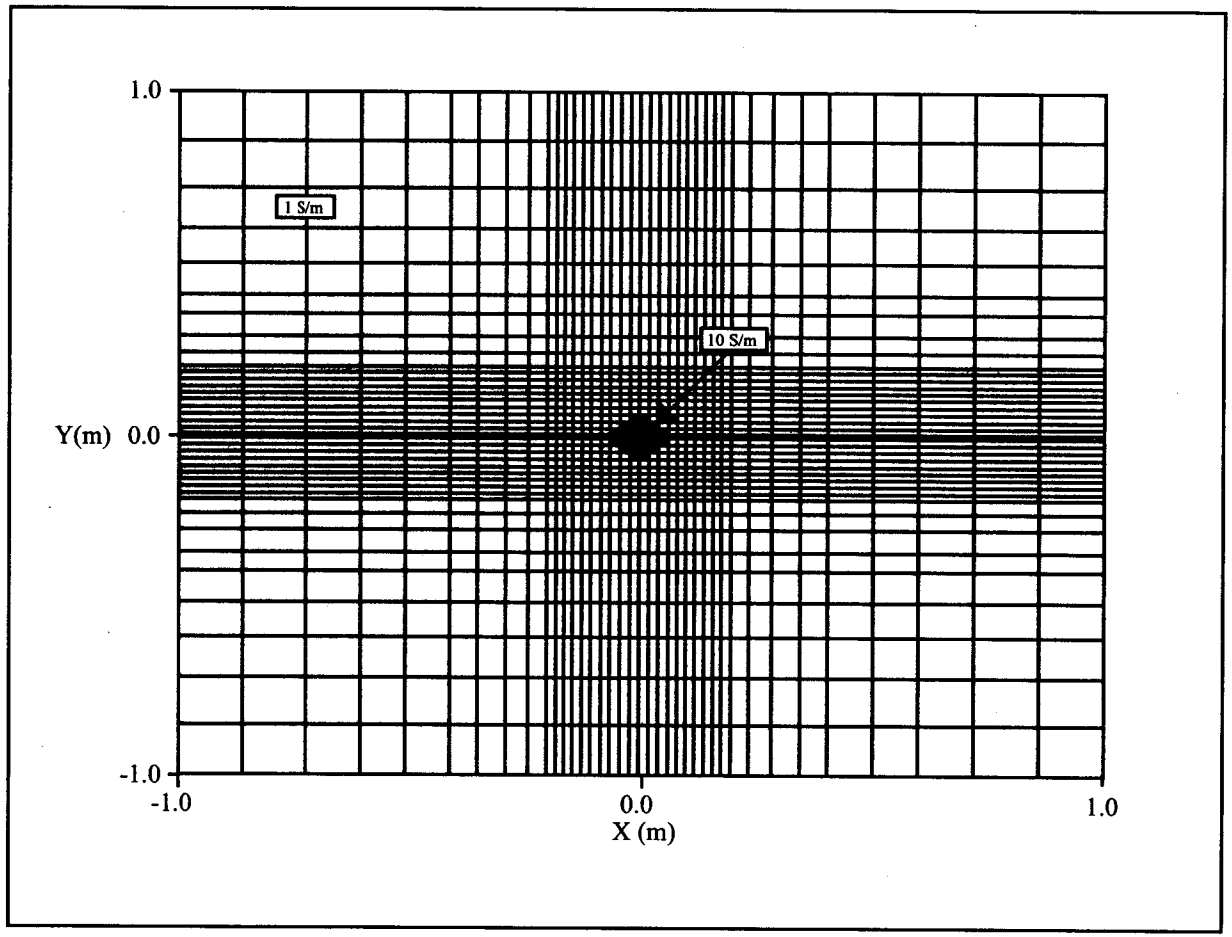


Figure 5c. Expanded view of the X-Y Plane of a staggered grid, finite difference model space. The background conductivity is 1 S/m and the Borehole is 10 S/m

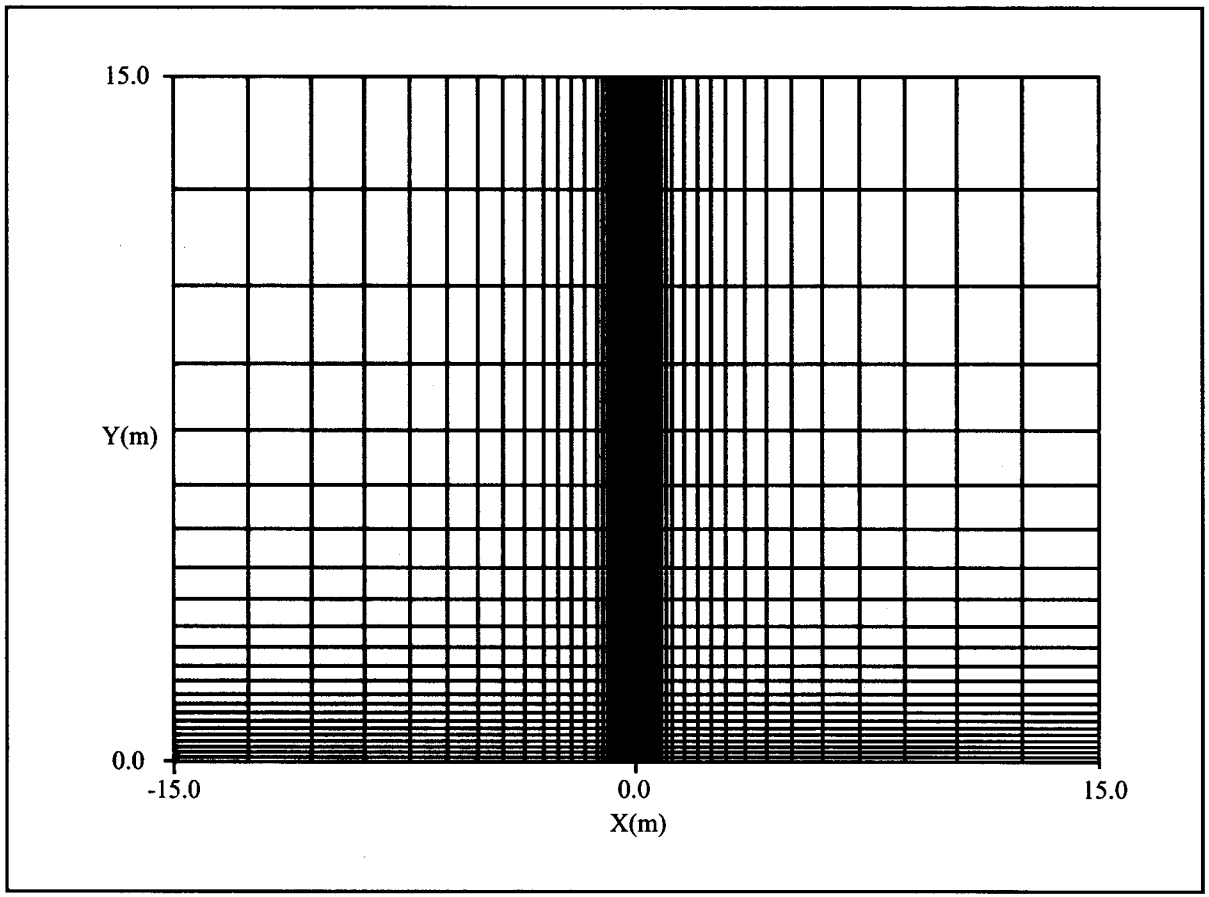


Figure 6a. The X-Y plane of a staggered grid finite difference model space, which is symmetric about the Y axis.

# 0.4 m Borehole

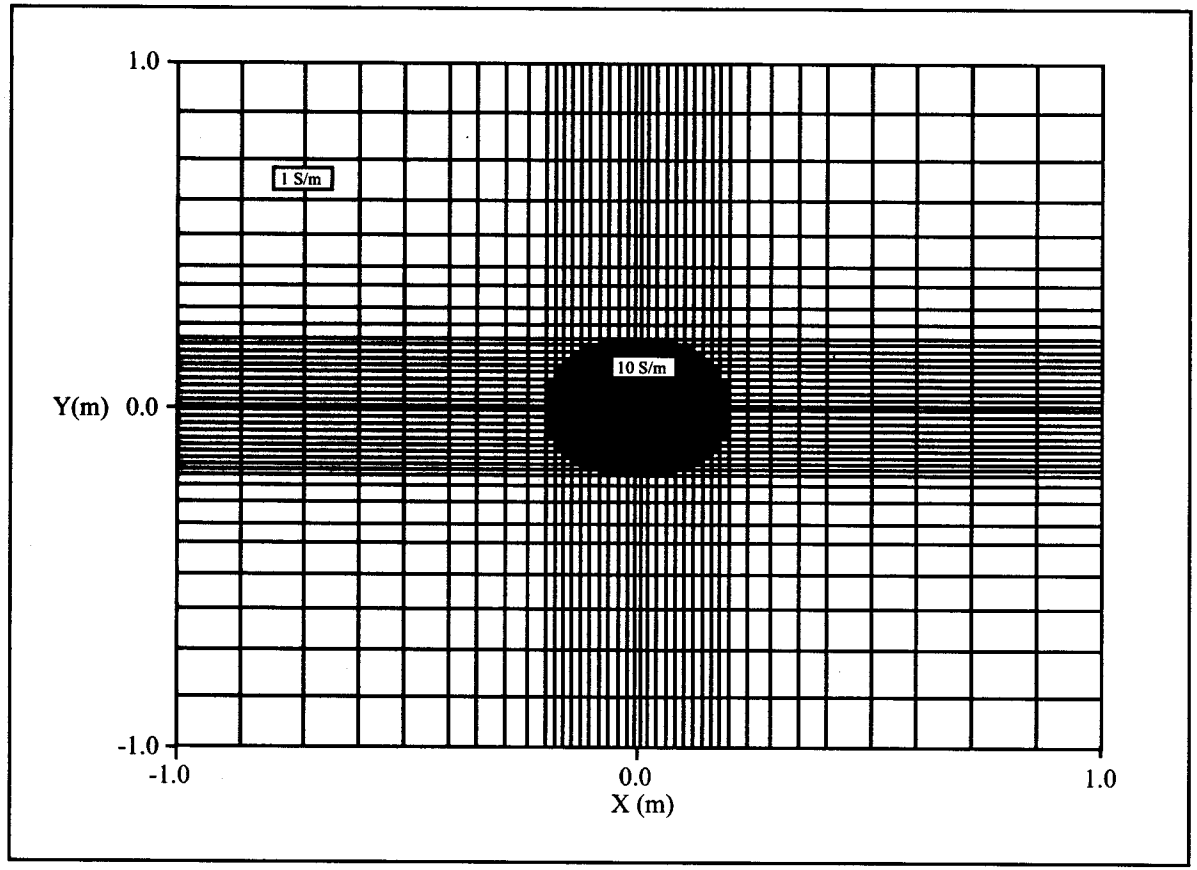


Figure 10b. Expanded view of the X-Y plane of a staggered grid, finite difference model space. Background conductivity is 1 S/m, borehole conductivity is 10 S/m and diamter is 0.4 m.

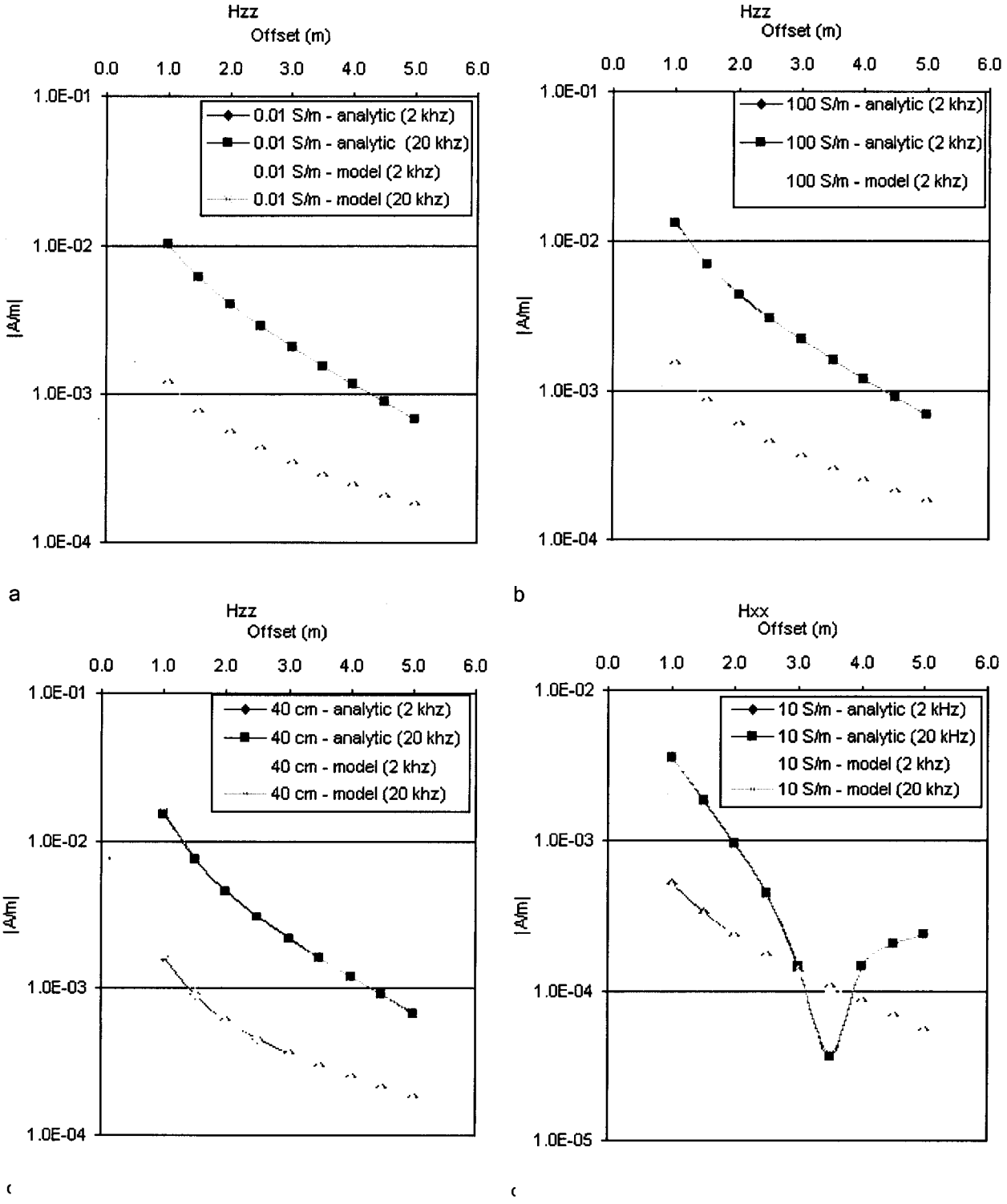


Figure 7. Comparison between analytic and finite difference model solutions. a) Hzz configuration solutions for a 0.01 S/m, 0.1 m diameter borehole. b) Hzz configuration solutions for a 100 S/m, 0.1 m diameter borehole. c) Hzz configuration solutions for a 10 S/m, 0.4 m diameter borehole. d) Hxx configuration solutions for a 10 S/m, 0.1 m diameter borehole.

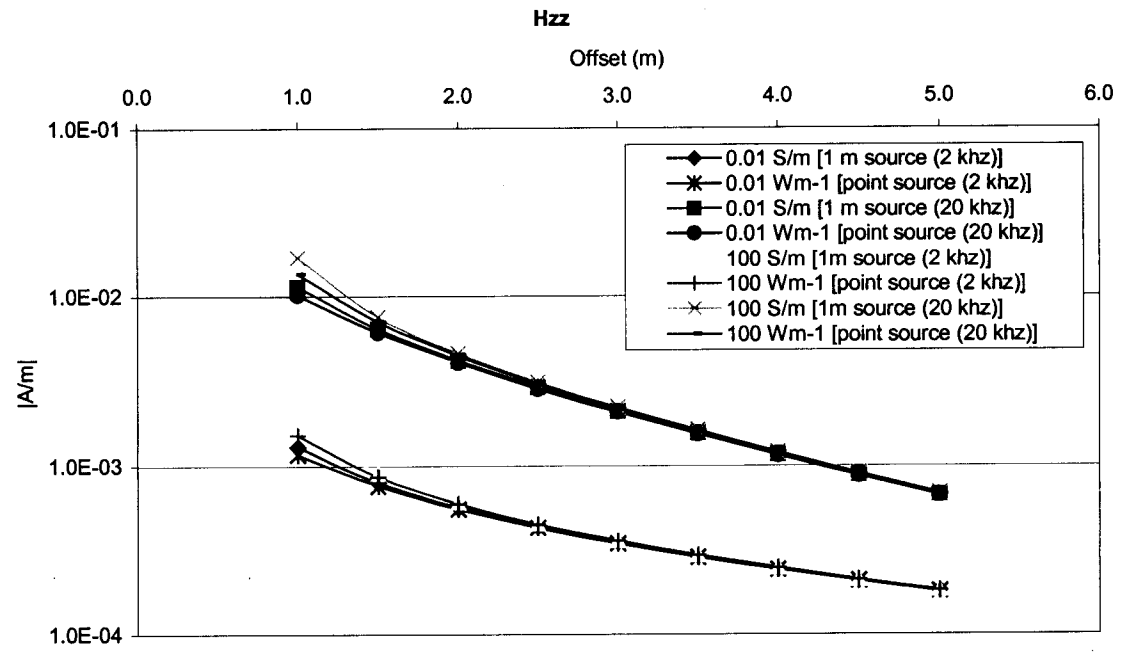


(a)

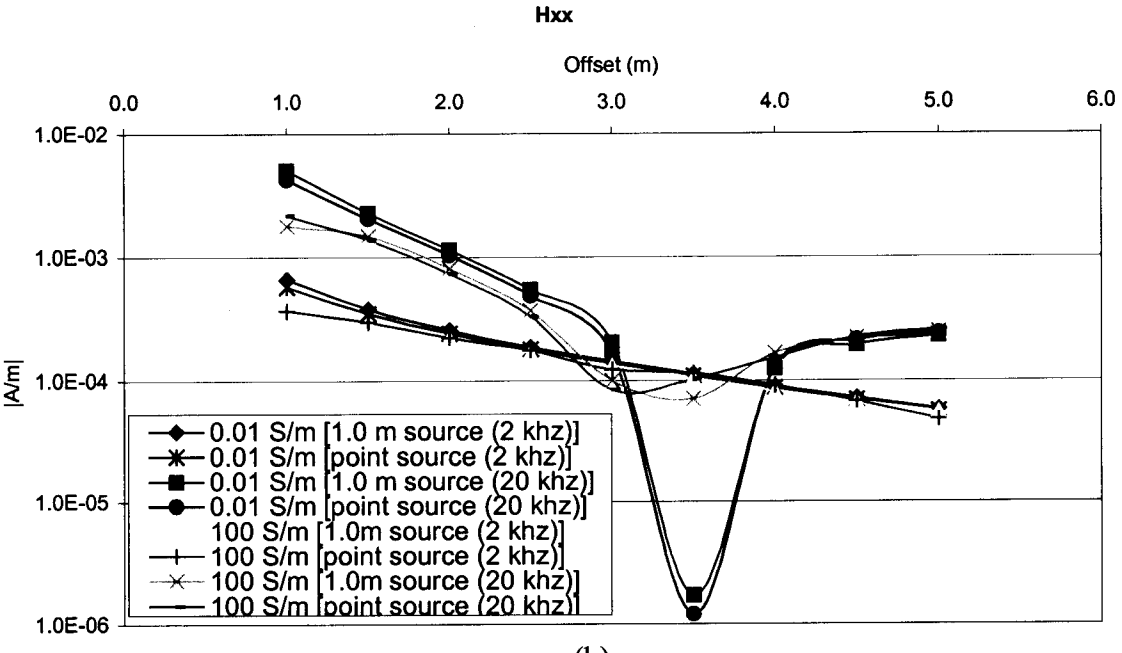


(b)

Figure 8 – Comparison of the total quadrature results between point dipole and finite length sources. (a) Coaxial configuration, with the dipole results compared to that of a solonoid. (b) Coplanar configuration, with the dipole results compared to that of a 1m by 0.08m loop.

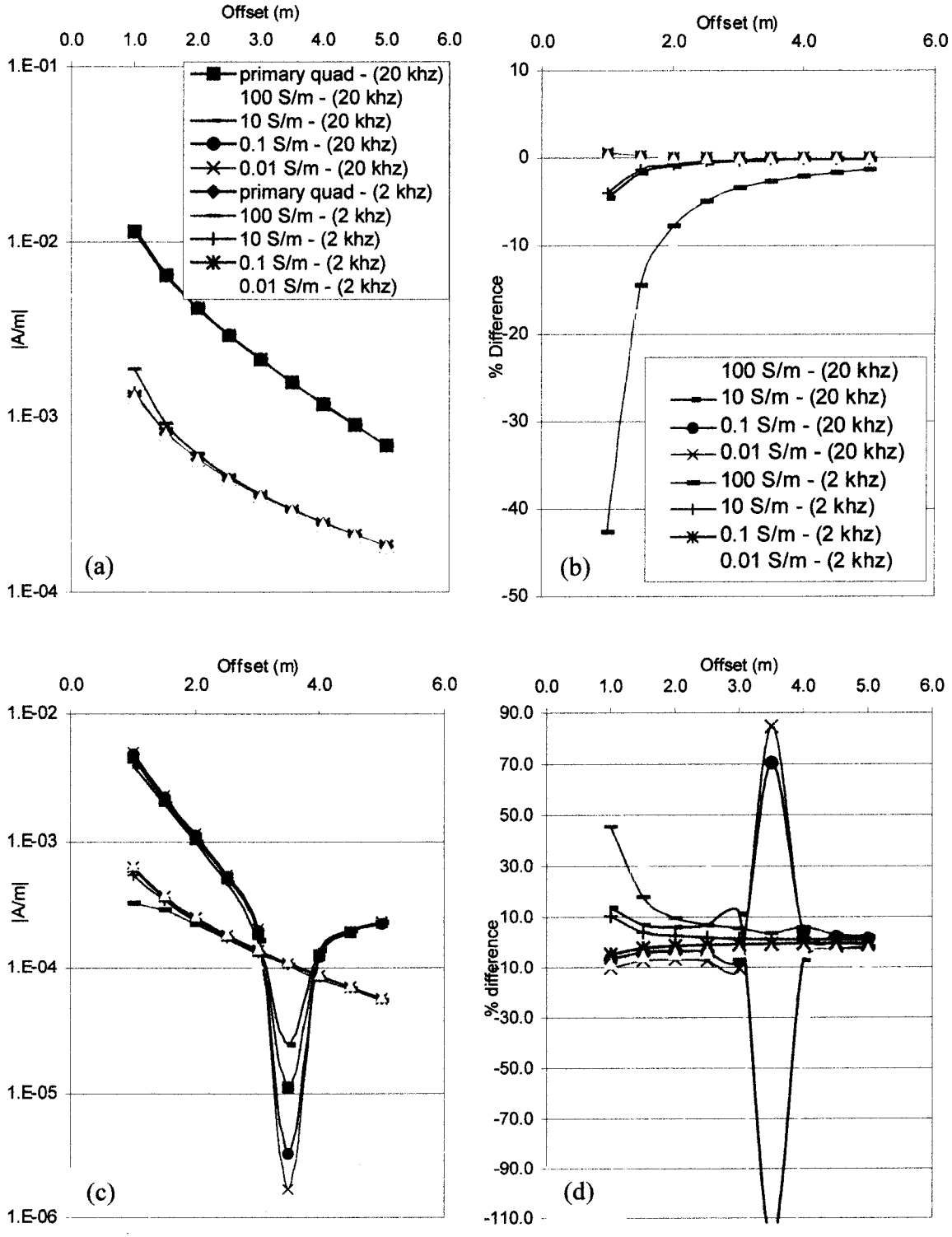


Figure 9 – Variable borehole conductivity results. (a) Magnetic field for coaxial configuration. (b)Percent difference between fields with and without borehole for coaxial configuration. (c) Magnetic field for coplanar configuration. (d) Percent difference between fields with and without borehole for coplanar configuration. The legends for Figures (c) and (d) are identical to those in (a) and (b), respectively.

# 0.2 m Borehole

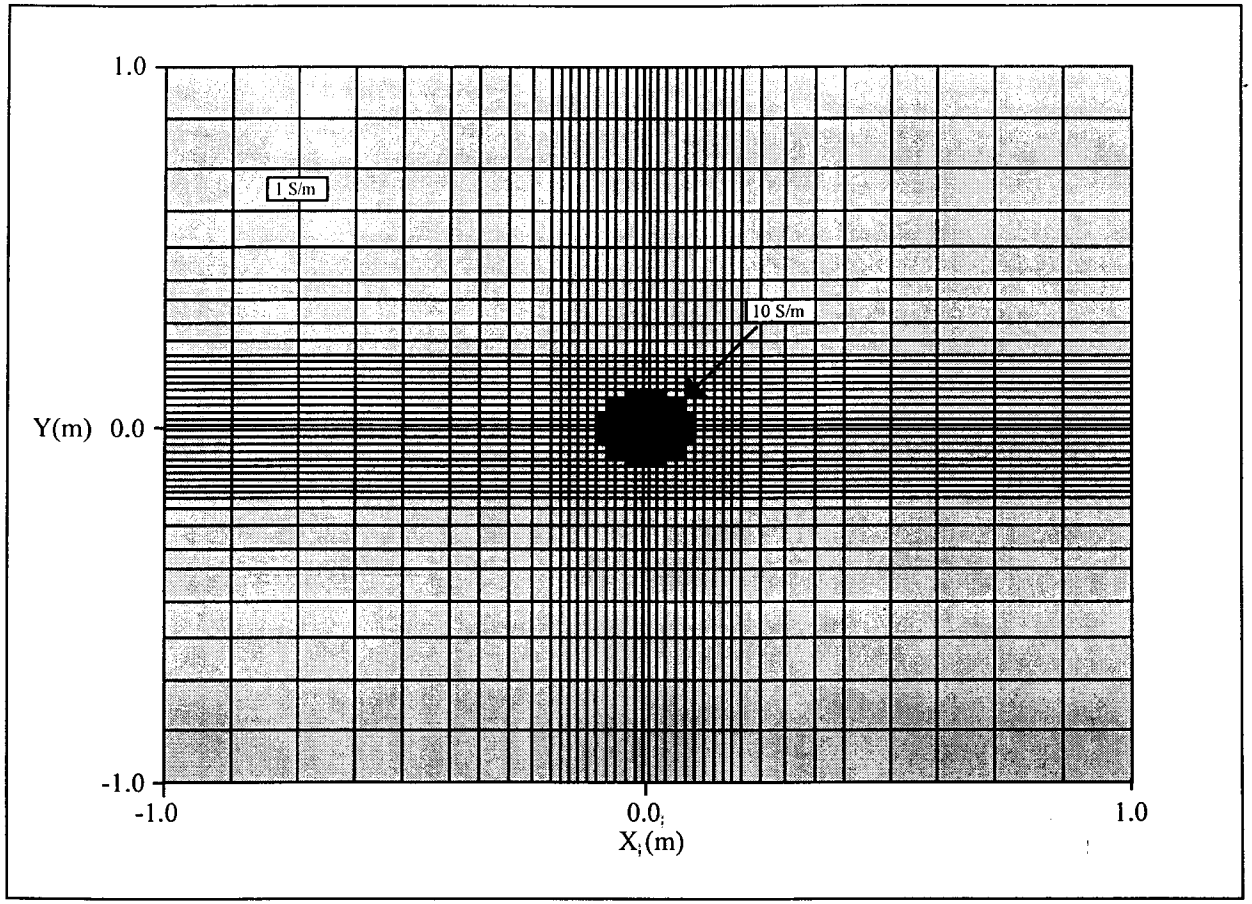


Figure 10a. Expanded view of the X-Y plane of a staggered grid, finite difference model space. Background conductivity is 1 S/m, borehole conductivity is 10 S/m and diamter is 0.2 m.

# X-Y Plane
# 0.2 m Borehole

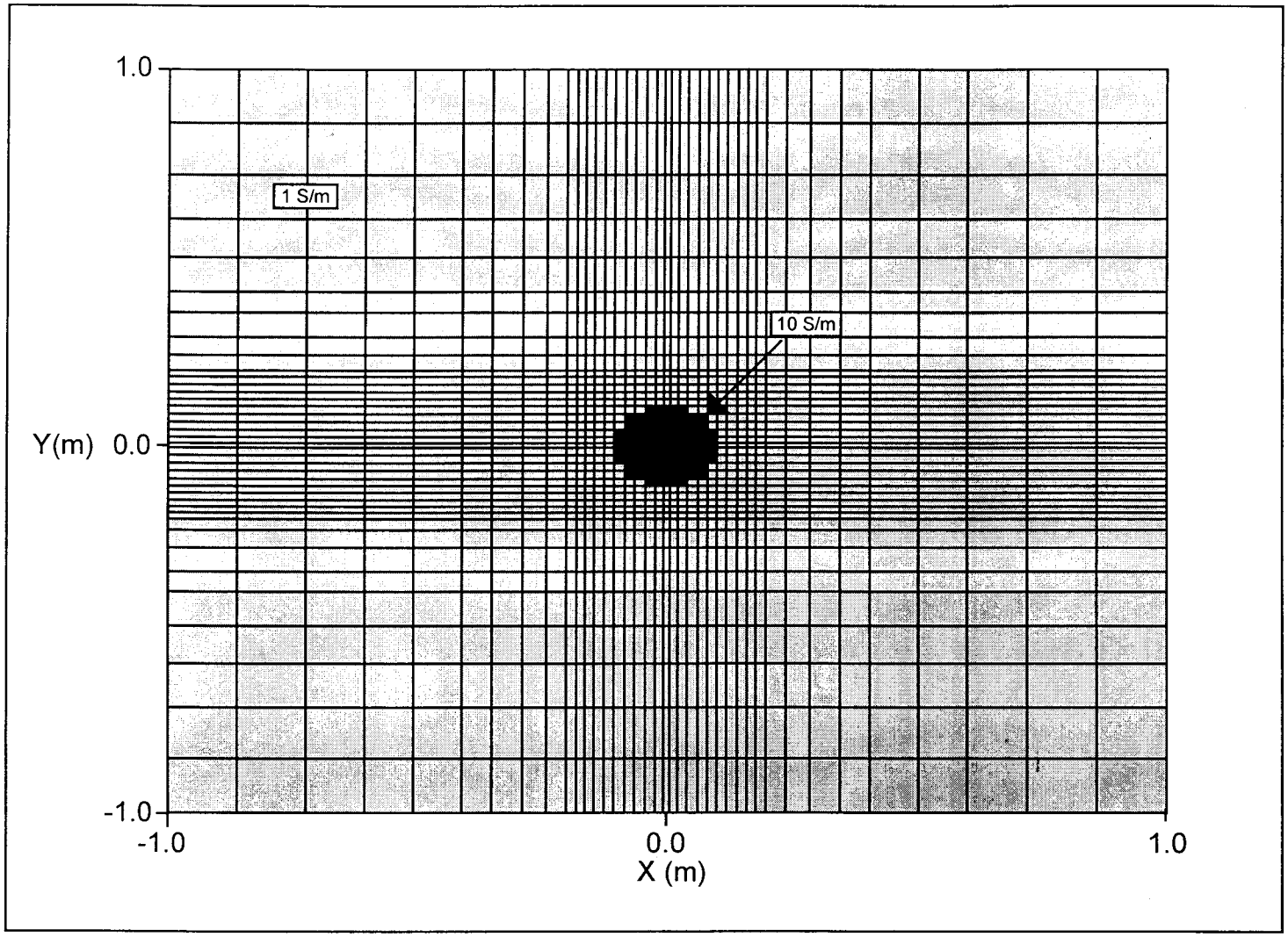


Figure 10a. The X-Y plane of a staggered grid, finite difference model space. Background conductivity is 1 S/m, borehole conductivity is 10 S/m and diamter is 0.2 m.

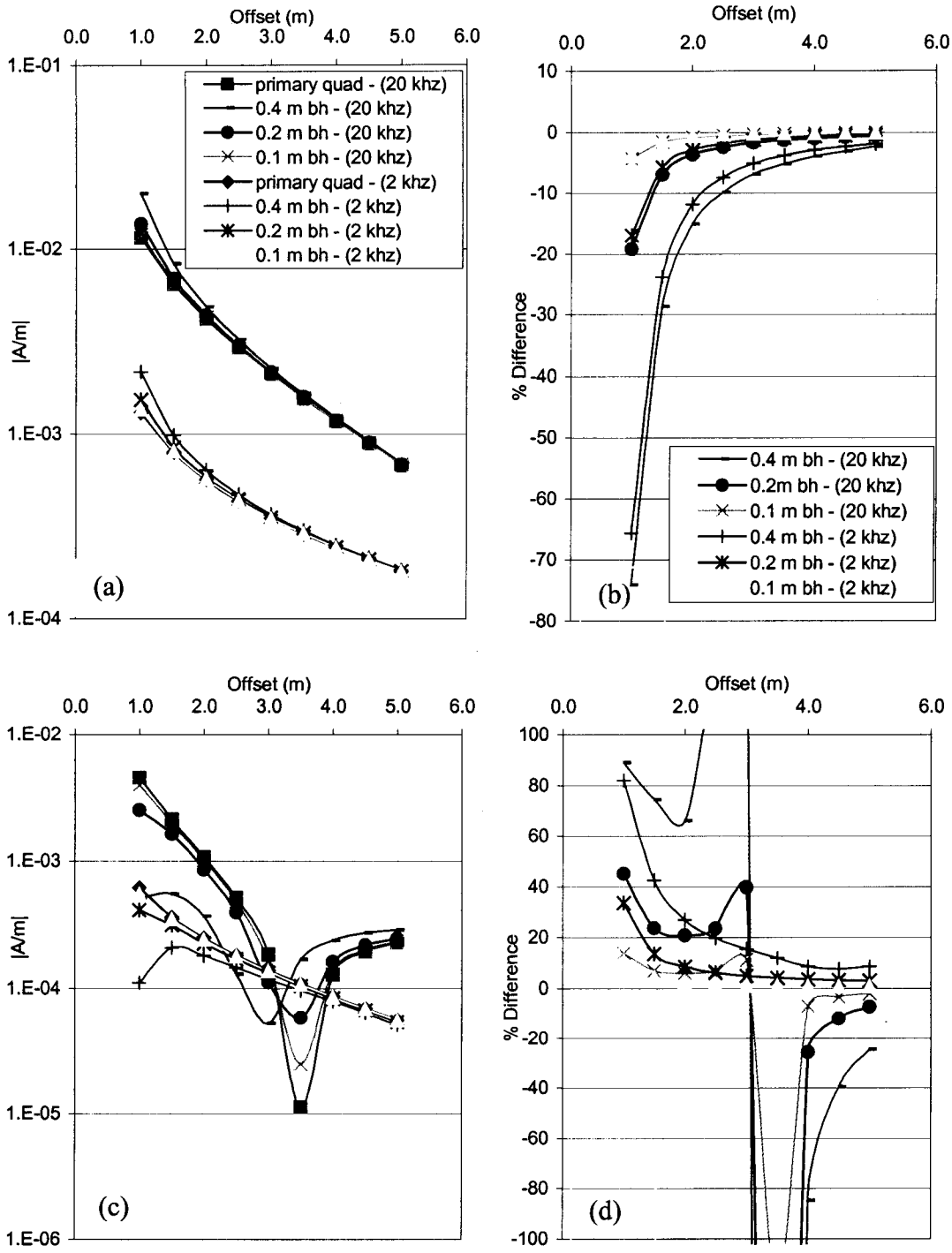


Figure 11 – Results for boreholes of variable diameter. (a) Magnetic field for coaxial configuration. (b)Percent difference between fields with and without borehole for coaxial configuration. (c) Magnetic field for coplanar configuration. (d) Percent difference between fields with and without borehole for coplanar configuration. The legends for Figures (c) and (d) are identical to those in (a) and (b), respectively.

**0.1 m Borehole**
**0.8 m Invasion Zone**

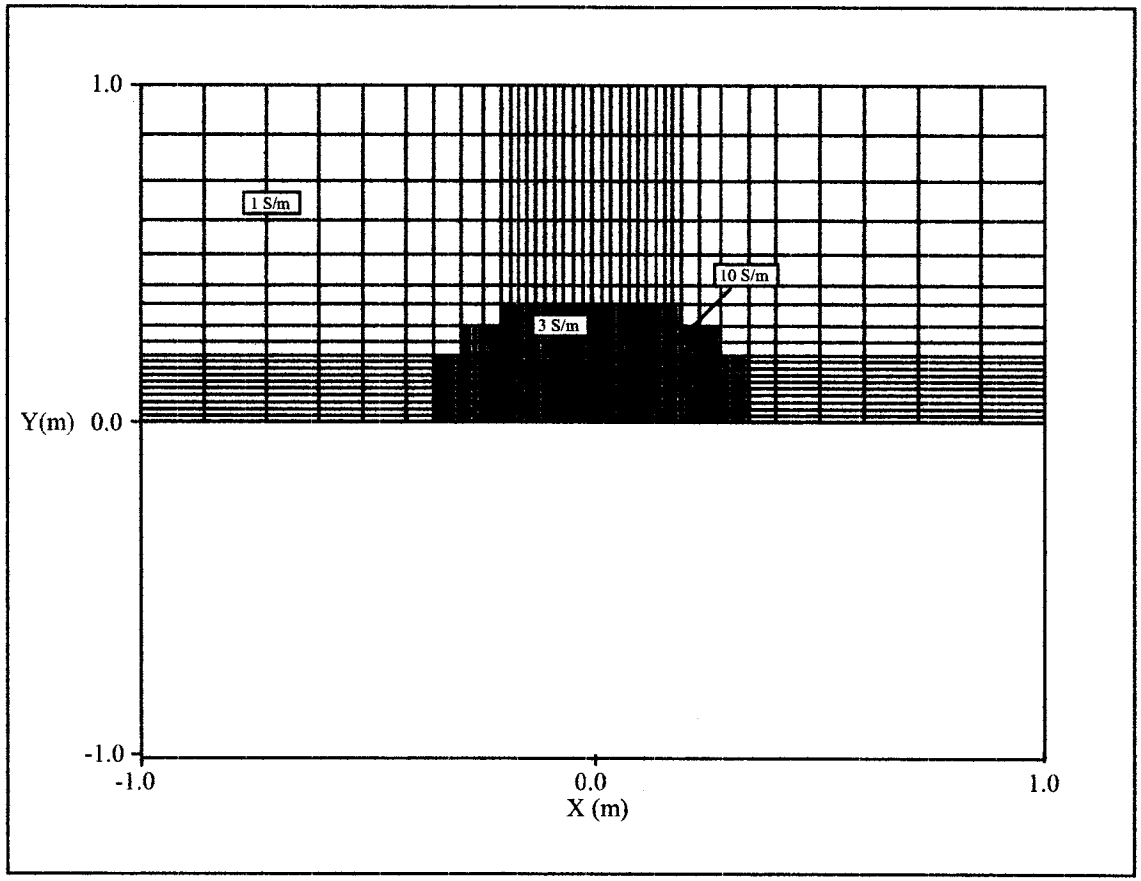


Figure 12a. Expanded view of the X-Y plane of a staggered grid, finite difference model space including a borehole and invasion zone. The background conductivity is 1 S/m, the borehole is 10 S/m and the invasion zone is 3 S/m. The borehole diameter is 0.1 m and the invasion zone diameter is 0.8 m.

**0.1 m Borehole**
**1.2 m Invasion Zone**

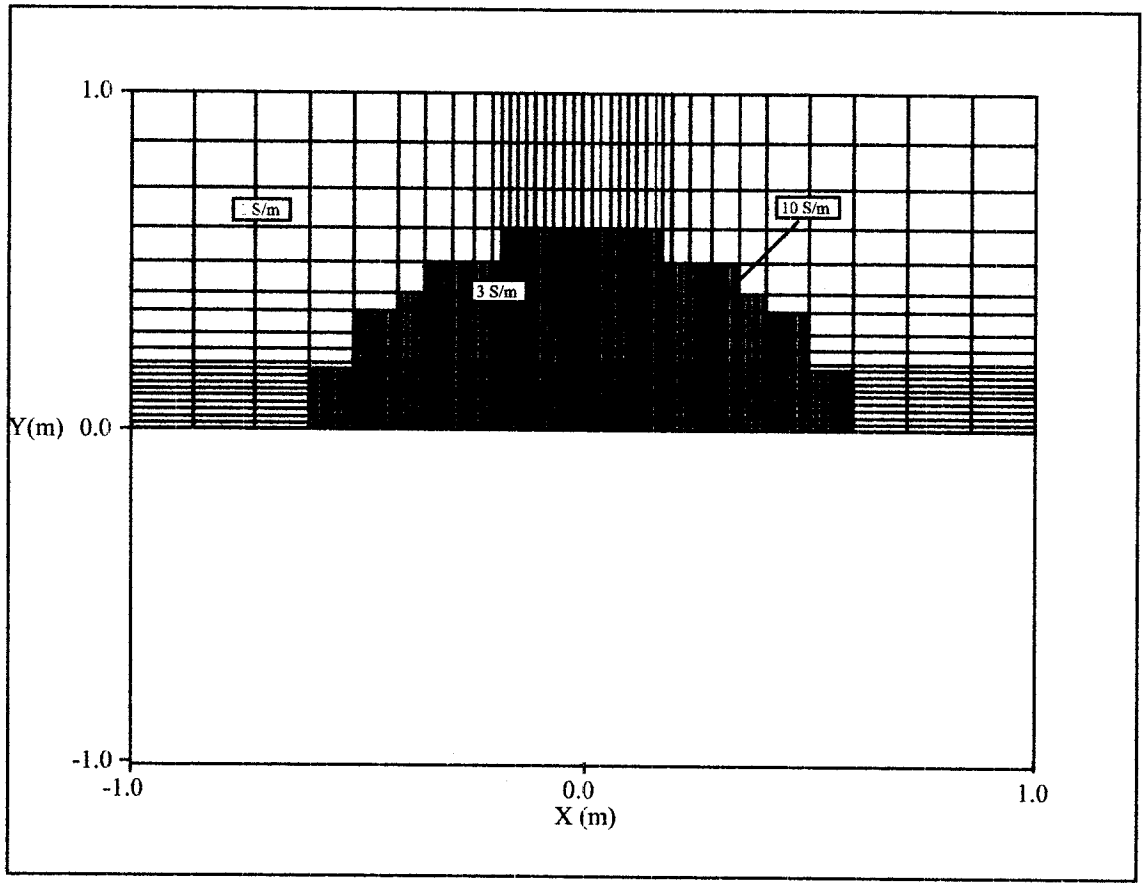


Figure 12b. Expanded view of the X-Y plane of a staggered grid, finite difference model space including a borehole and invasion zone. The background conductivity is 1 S/m, the borehole is 10 S/m and the invasion zone is 3 S/m. The borehole diameter is 0.1 m and the invasion zone diameter is 1.2 m.

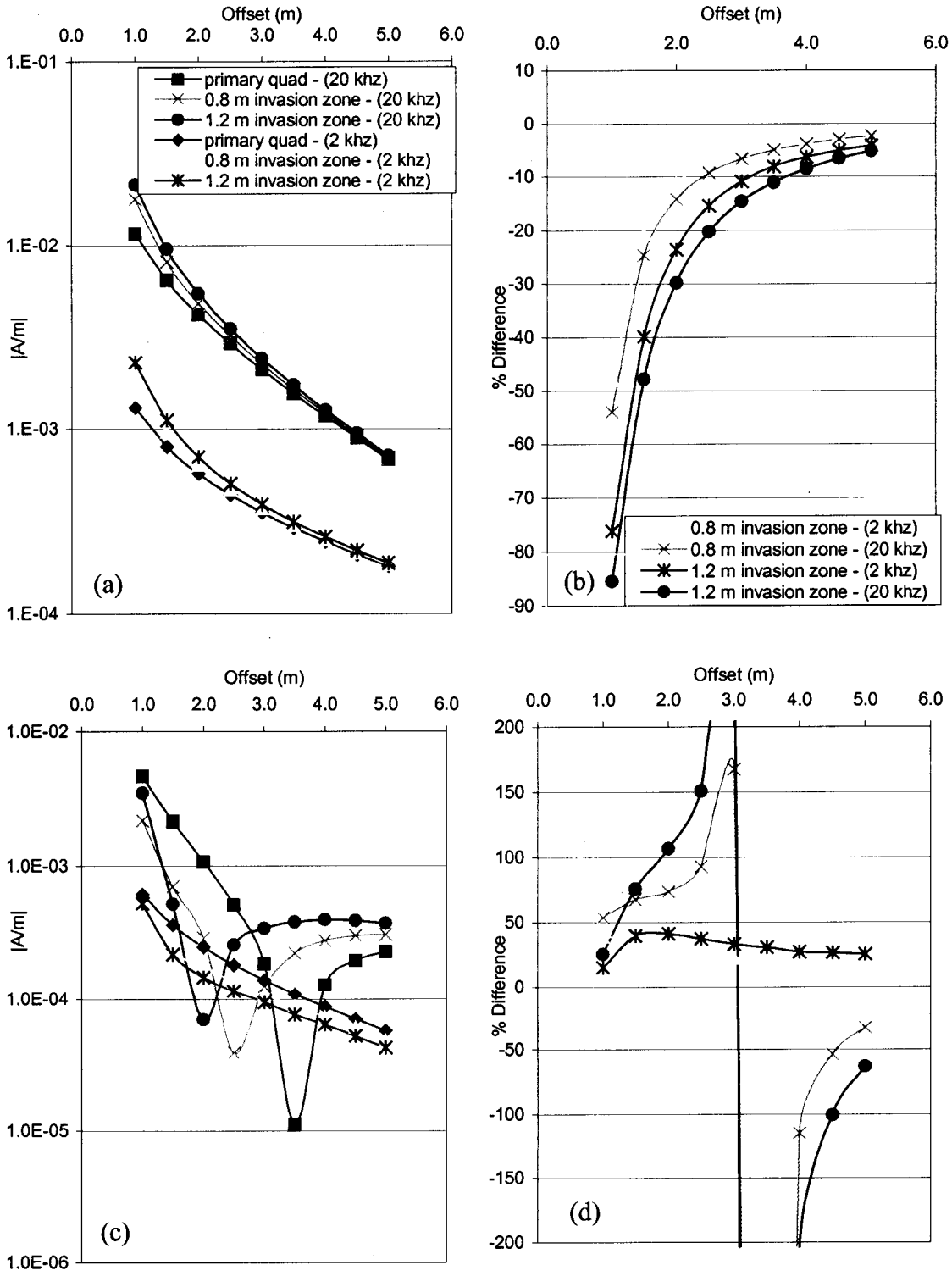


Figure 13 – Results for boreholes plus invasion zone. (a) Magnetic field for coaxial configuration. (b)Percent difference between fields with and without borehole for coaxial configuration. (c) Magnetic field for coplanar configuration. (d) Percent difference between fields with and without borehole for coplanar configuration. The legends for Figures (c) and (d) are identical to those in (a) and (b), respectively.

# 0.4 m borehole
# Off-Center Array

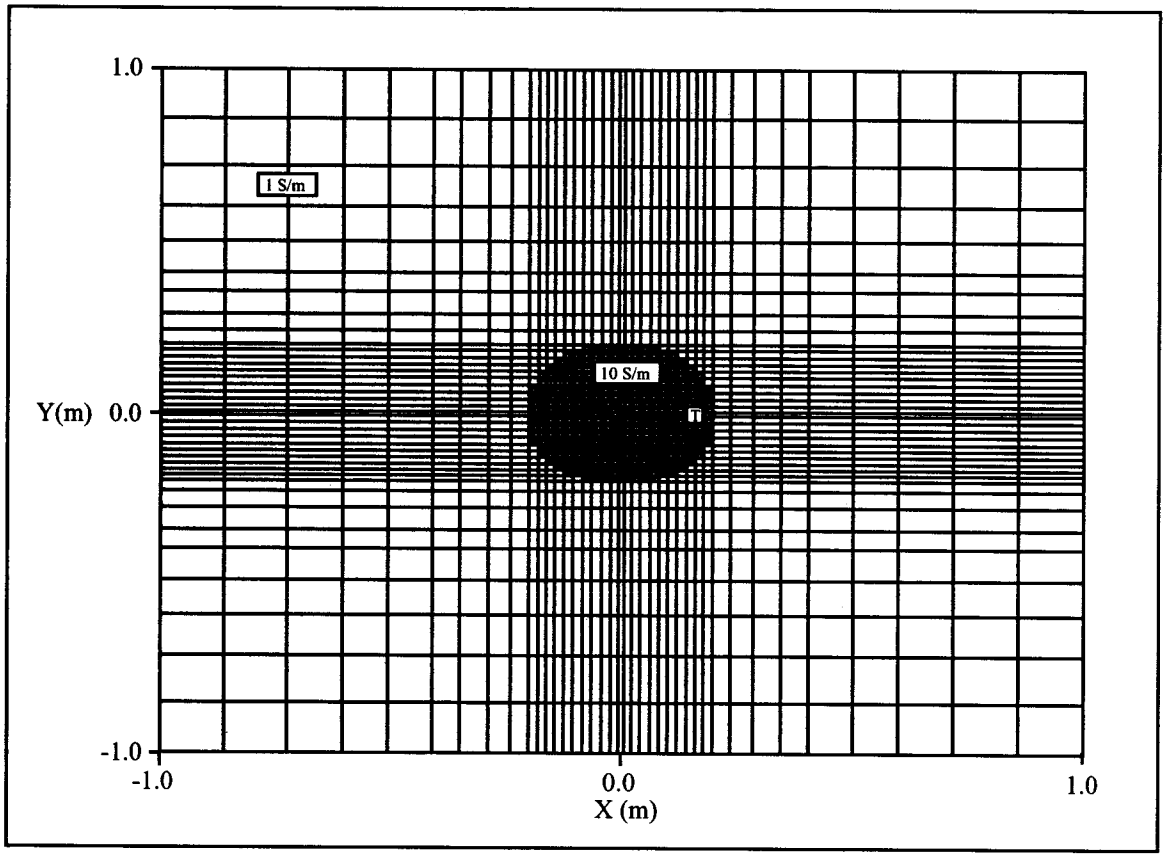


Figure 14. Expanded view of the X-Y plane of a staggered grid, finite difference model space with a source-receiver array that is off-center in the + X direction. The 0.4 m diameter borehole has a conductivity of 10 S/m in a 1 S/m background.

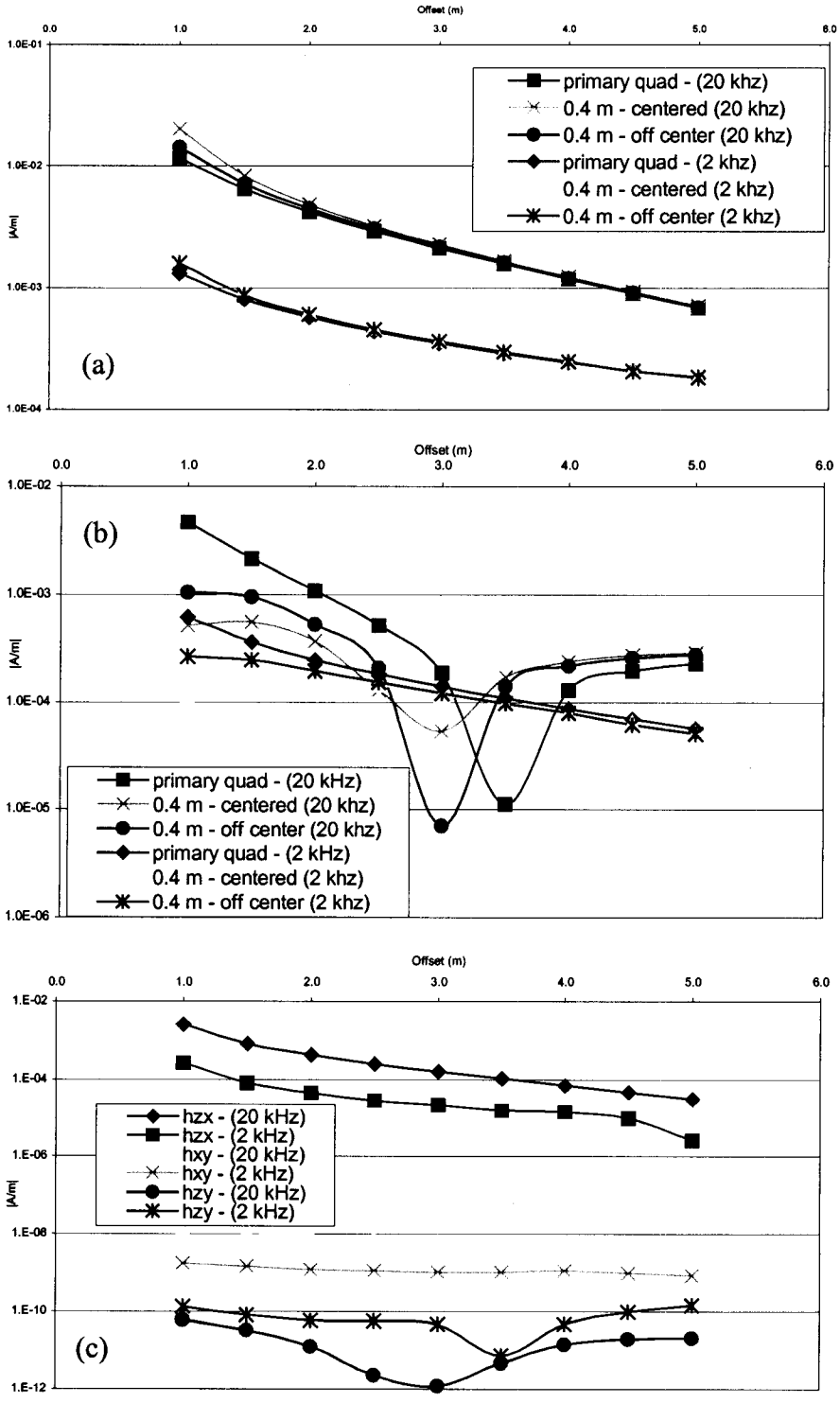


Figure 15 – Results for an array that is located off-center within the borehole. (a) Coaxial results. (b) Coplanar results. (c) Null-coupled results.

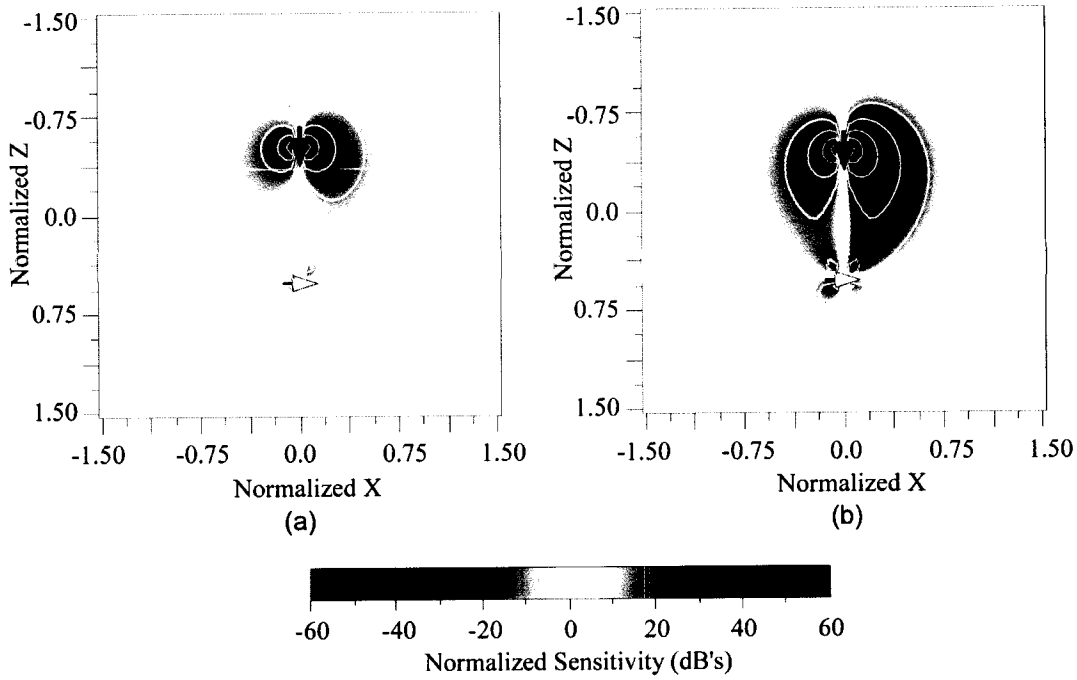


Figure 16 – Logarithmically normalized coaxial null coupled sensitivity as a function of position in the y=0 plane for an induction number of 1. a) Real component. b) Quadrature component. (From Alumbaugh and Wilt, 2001).

# Array Above, Across, and Below Fracture

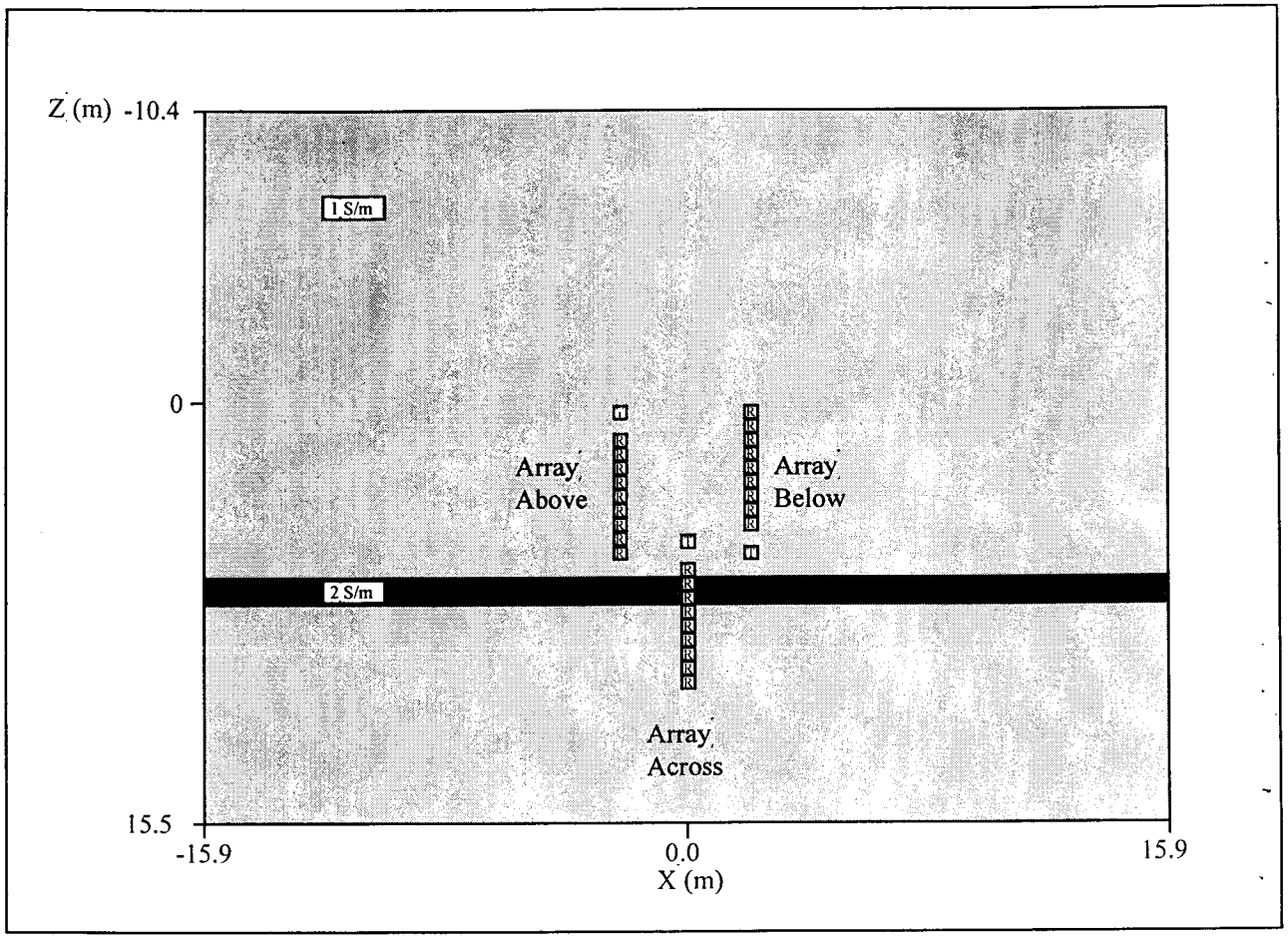


Figure 17. The X-Z plane of a model space that includes a horizontal fracture. Three source-receiver array locations areused: above, across, and below the fracture. All arrays are located at x = y = 0. The array above and below the fracture are in the same location, exept the source and 5 m offset receiver have been switched.

# 2.0 & 4.5 m Array Profiles

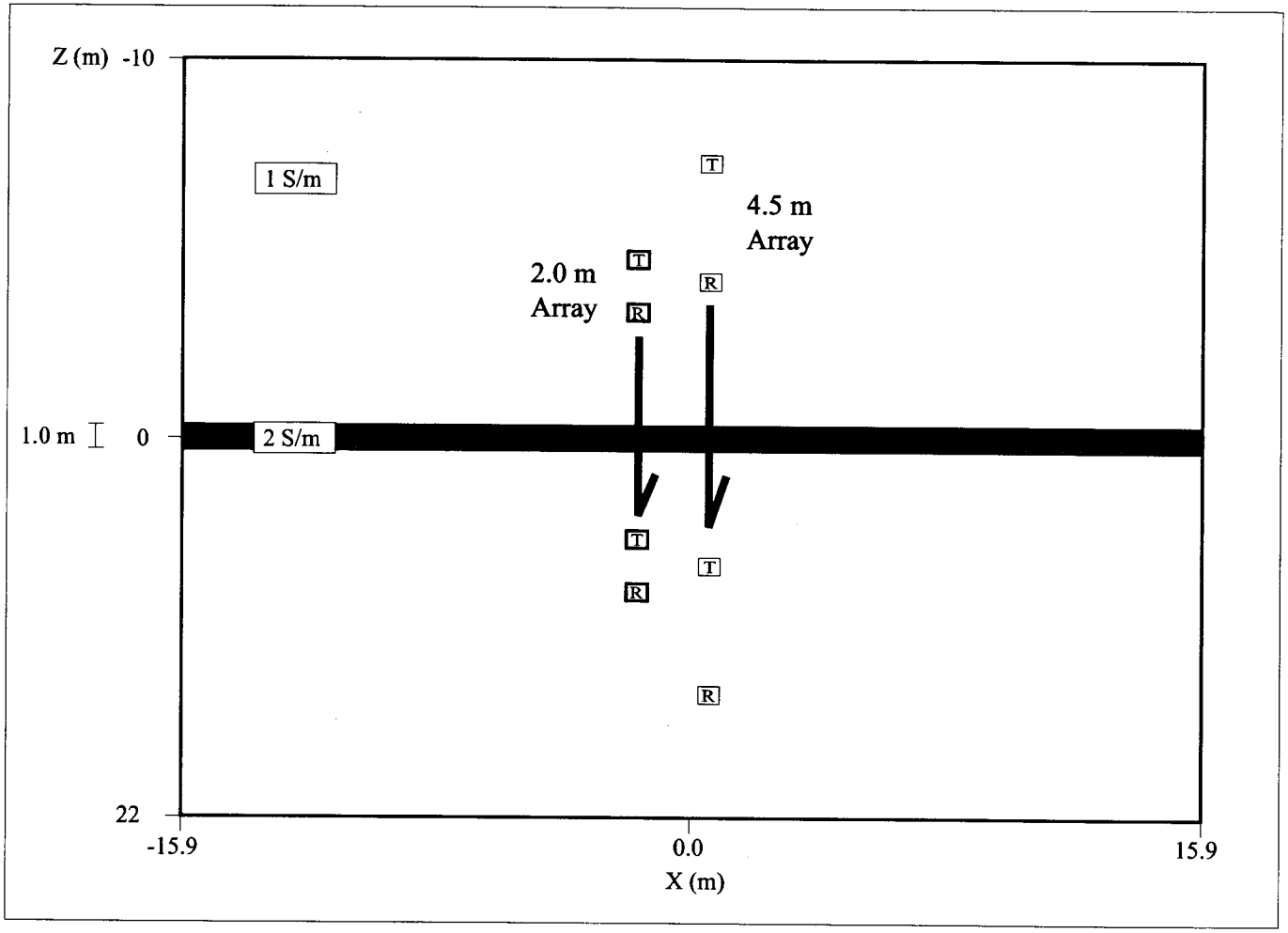


Figure 18. The X-Z plane of a model space that includes a horizontal fracture. The 2 m array crosses the fracture at 0.5 m intervals, and the 4.5 m array crosses the fracture using 1.0 m intervals.

0.1 m Borehole
0.8 m Invasion Zone
1.0 m Fracture

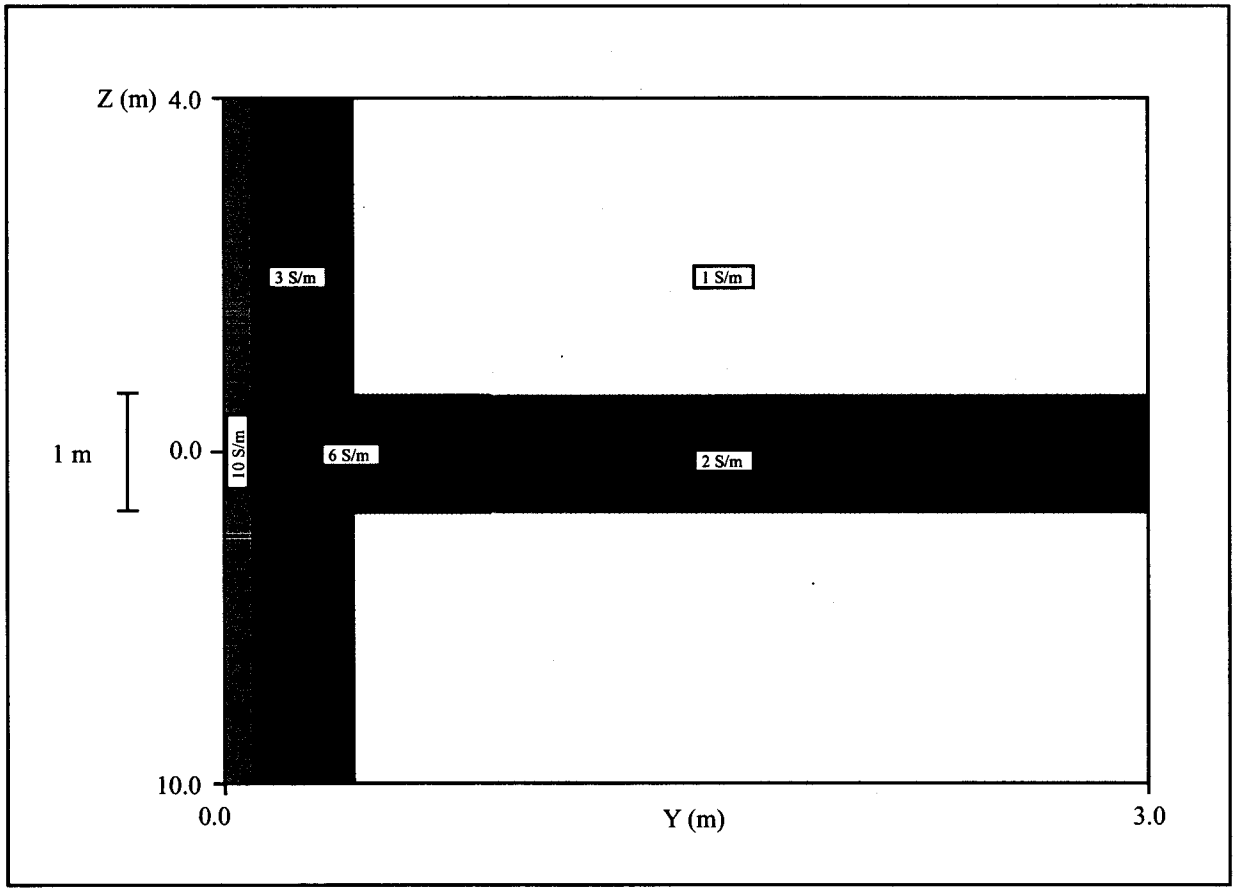


Figure 19. Expanded view of the Y-Z plane of a model space that contains a borehole, invasion zone, and horizontal fracture.

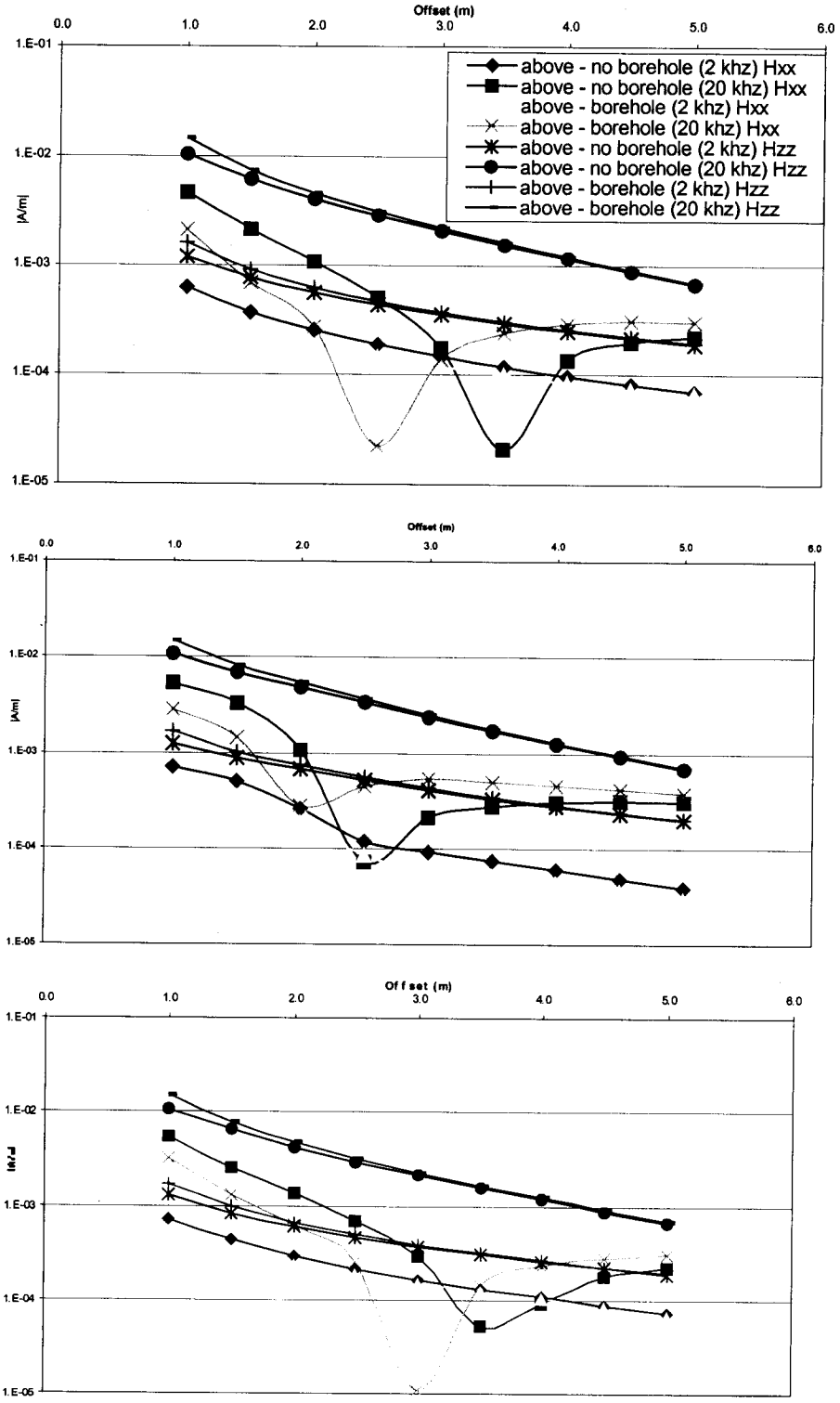


Figure 20 – Modeling results for arrays near a fracture zone. Coaxial and coplanar total quadrature results for a source-receiver array that is located (a) above, (b) below, and (c) below the fracture as shown in Figure 19.

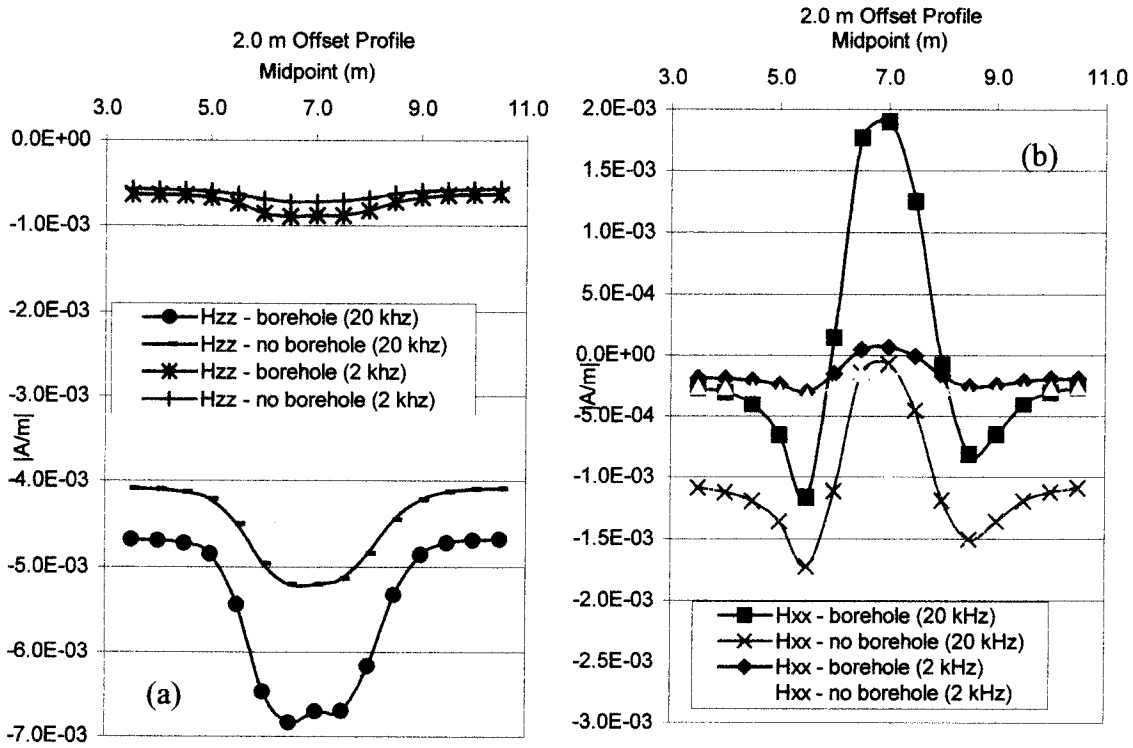


Figure 21. The total quadrature results for a profile across a horizontal fracture using a 2m-offset array. Results are for models with and without the borehole. (a) Coaxial configuration. (b) Coplanar configuration).

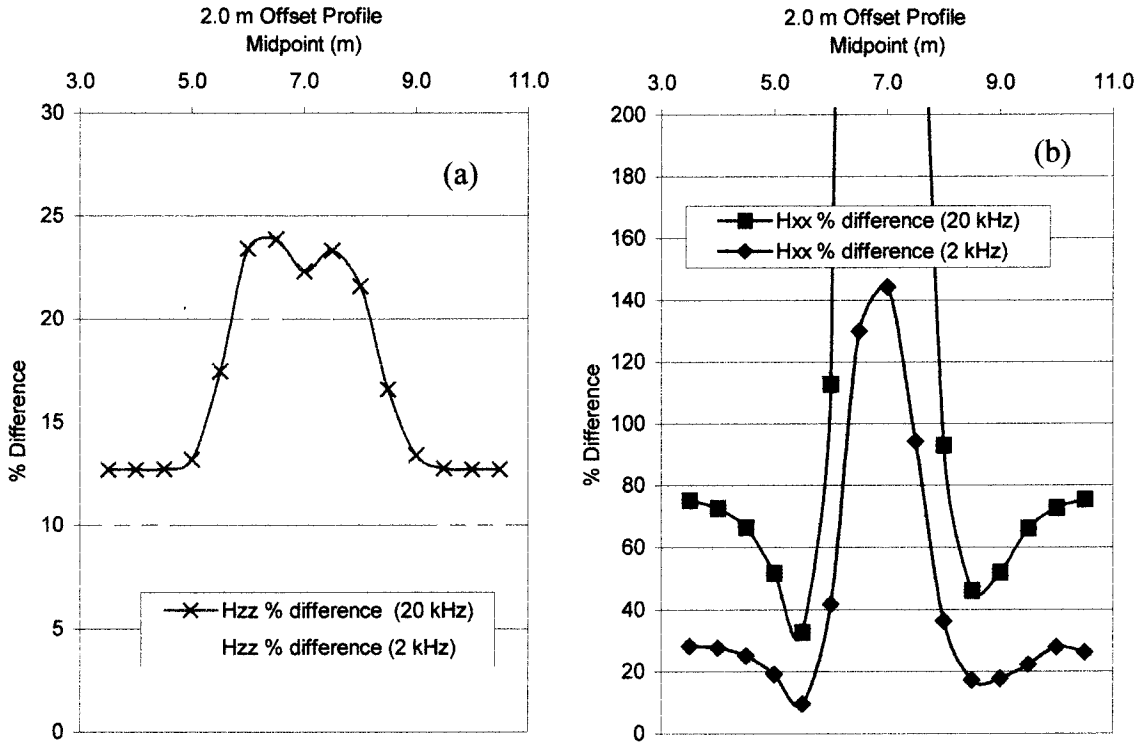


Figure 22. The percentage difference between the total quadrature values from borehole and non-borehole models in Figures 21a and b. a) Coaxial configuration. b) Coplanar configuration.

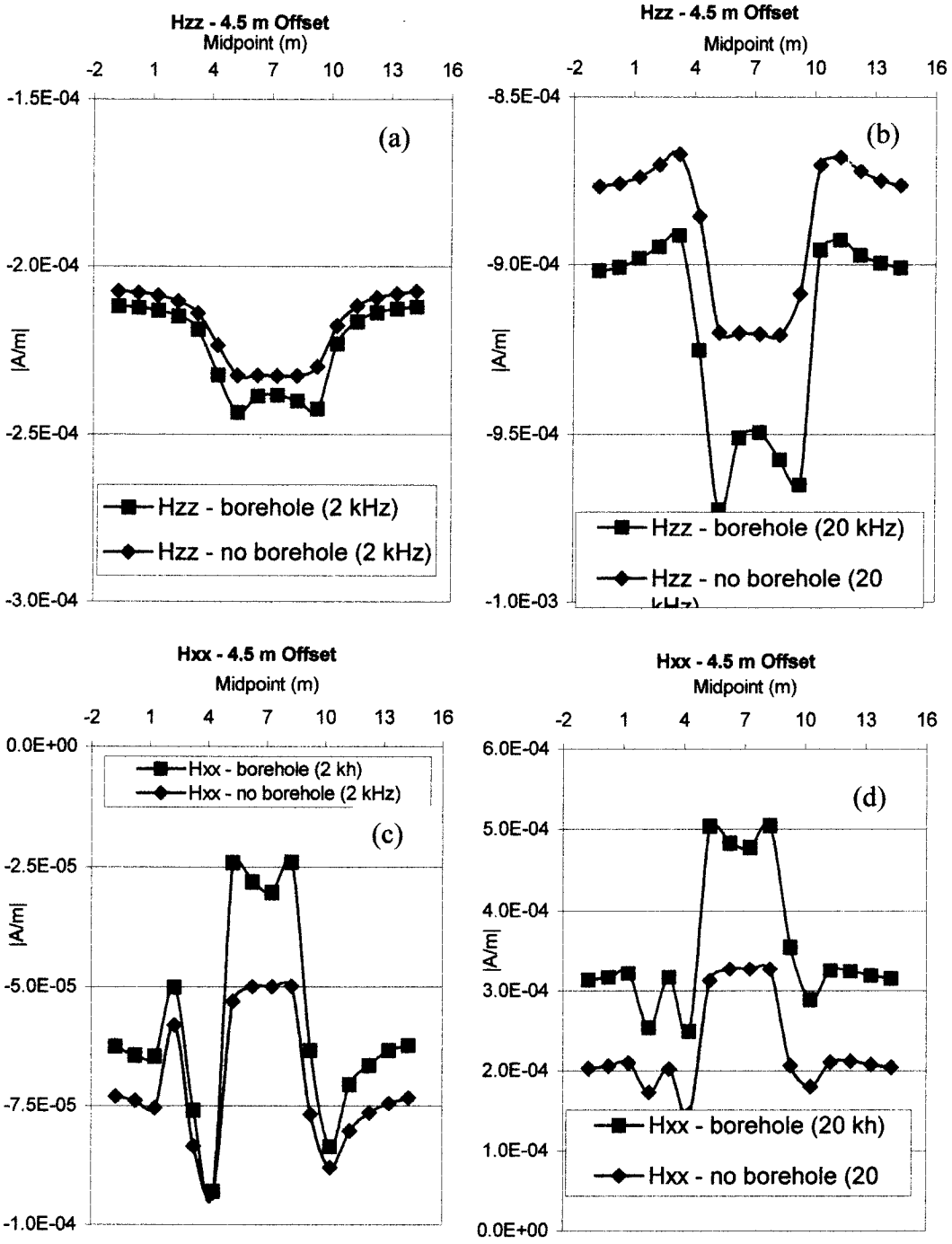


Figure 23. The total quadrature using the coaxial configuration for a profile across a horizontal frature using a 4.5m-offset array. Results are for models with and without a borehole. a) 2 kHz b) 20 kHz. The total quadrature using the coplanar configuration for a profile across a horizontal frature using a4.5m-offset array. Results are for models with and without a borehole. c) 2 kHz d) 20 kHz.

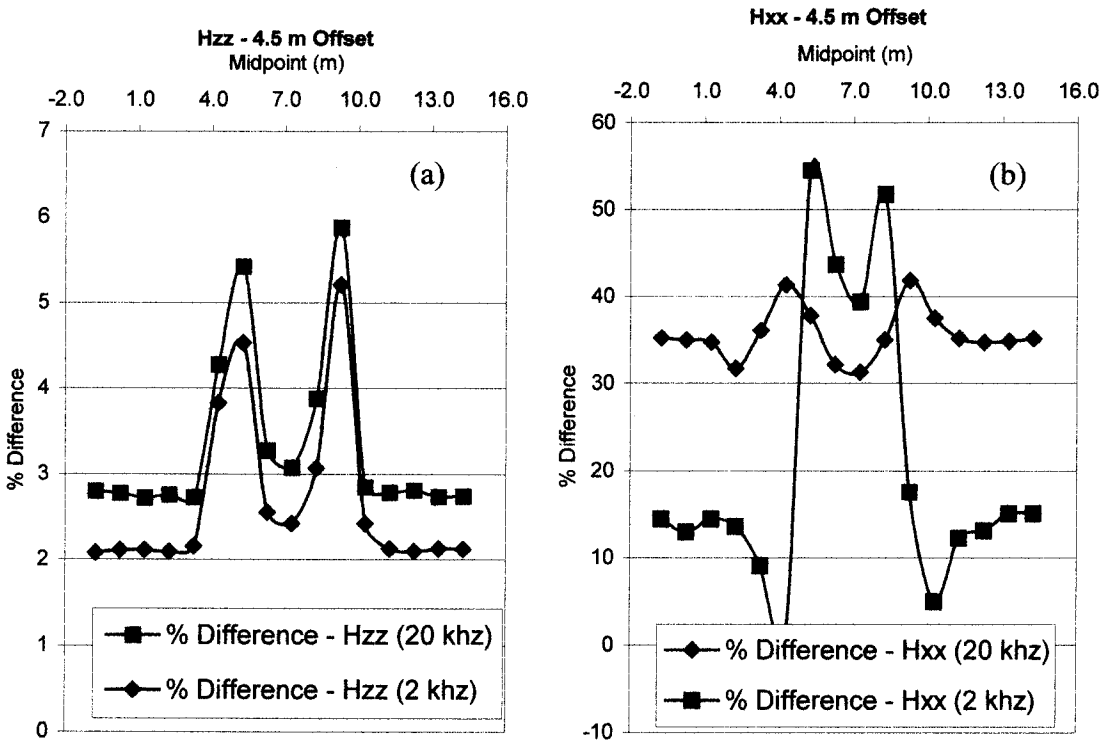


Figure 24. The percentage difference between the total quadrature values from borehole and non-borehole models in Figure 23a-d. a) Coaxial configuration. b) Coplanar configuration.

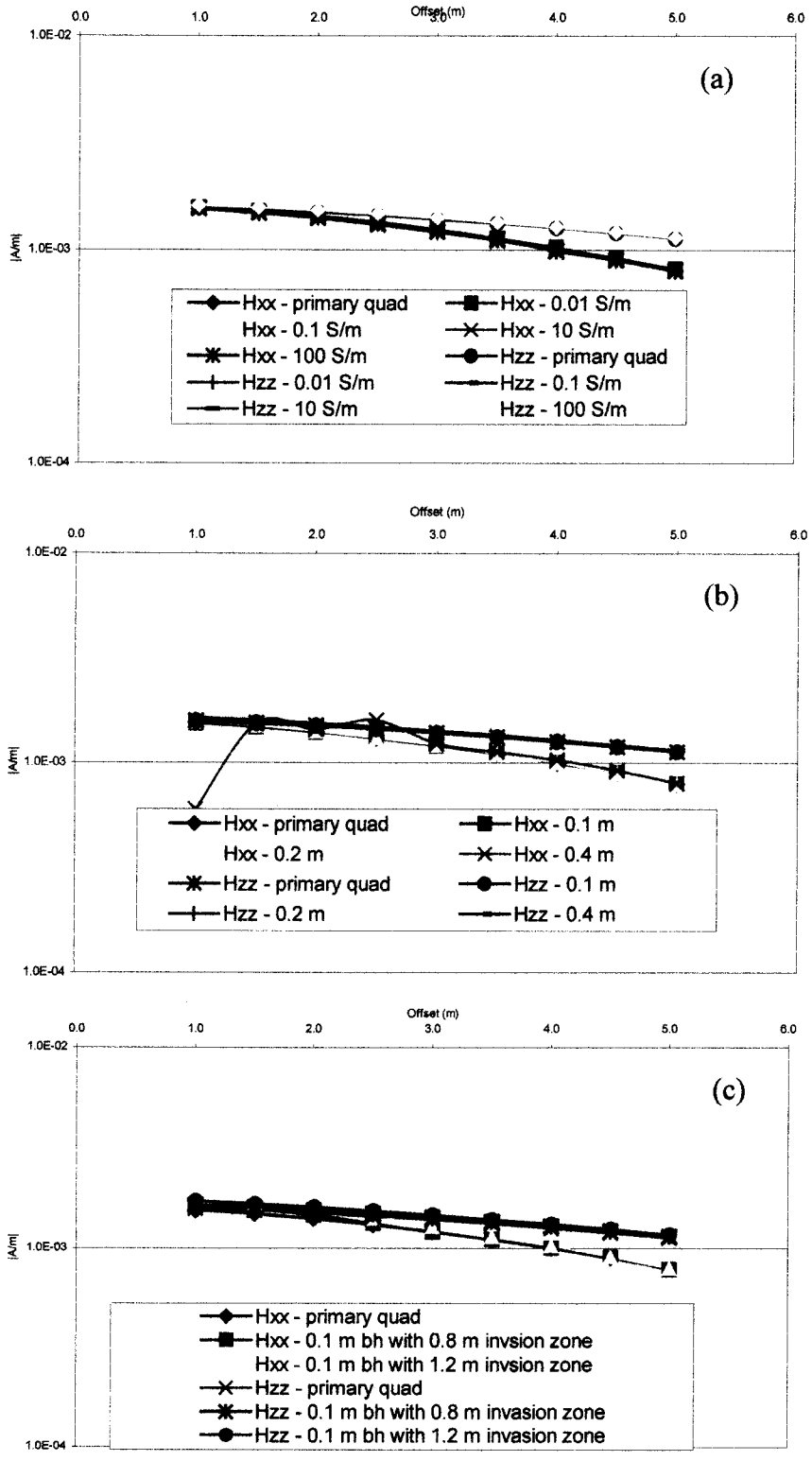


Figure 25. Primary and total quadrature values for the coaxial and coplanar configurations, after frequency differencing, in (a) boreholes of variable conductivity, (b) boreholes of various diameter, and (c) different invasion zone models.

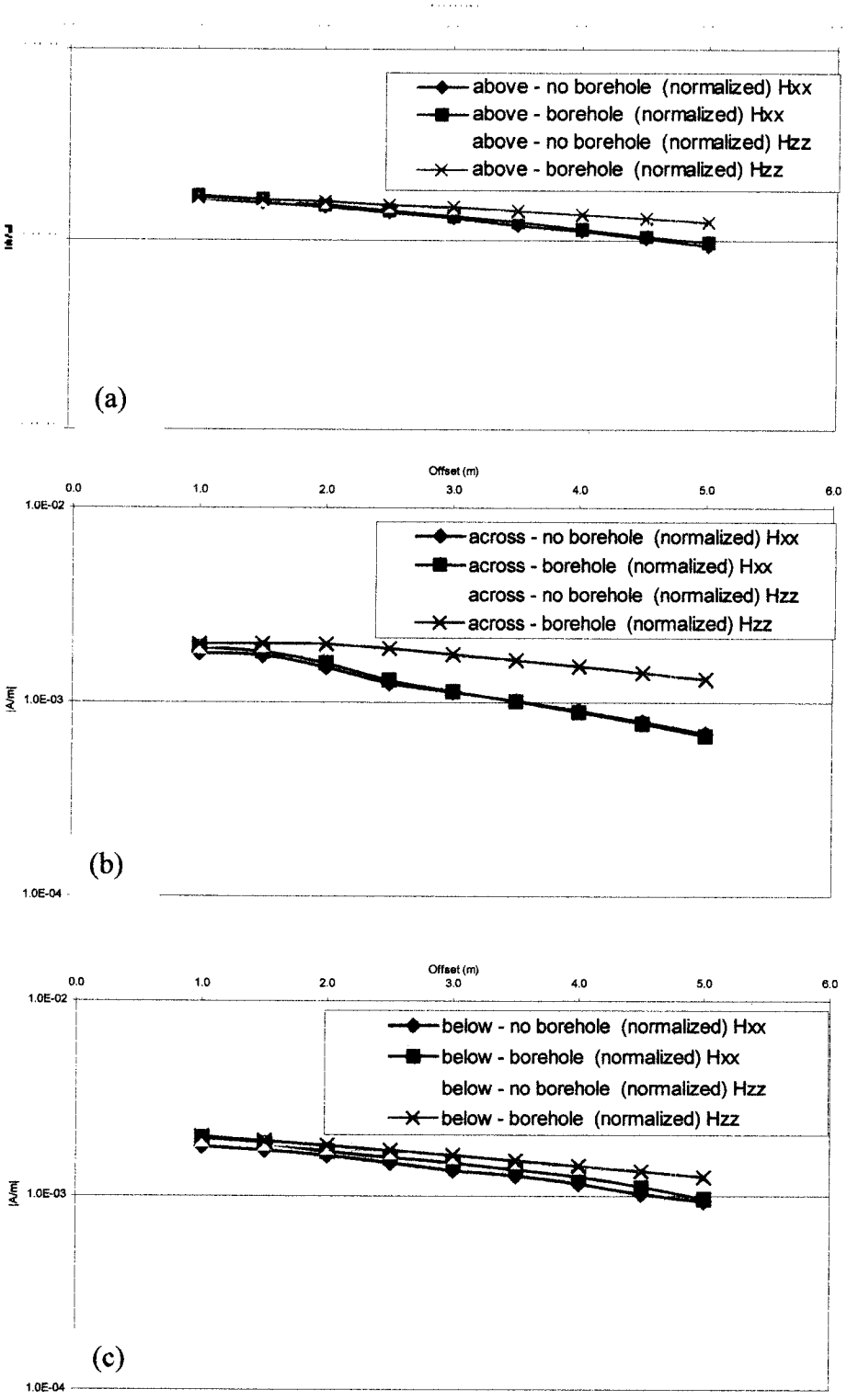


Figure 26- Total quadrature, after frequency differencing, for coaxial and coplanar arrays (a) above, (b) centered on, and (c) below a horizontal fracture. Results are for models with and without boreholes.

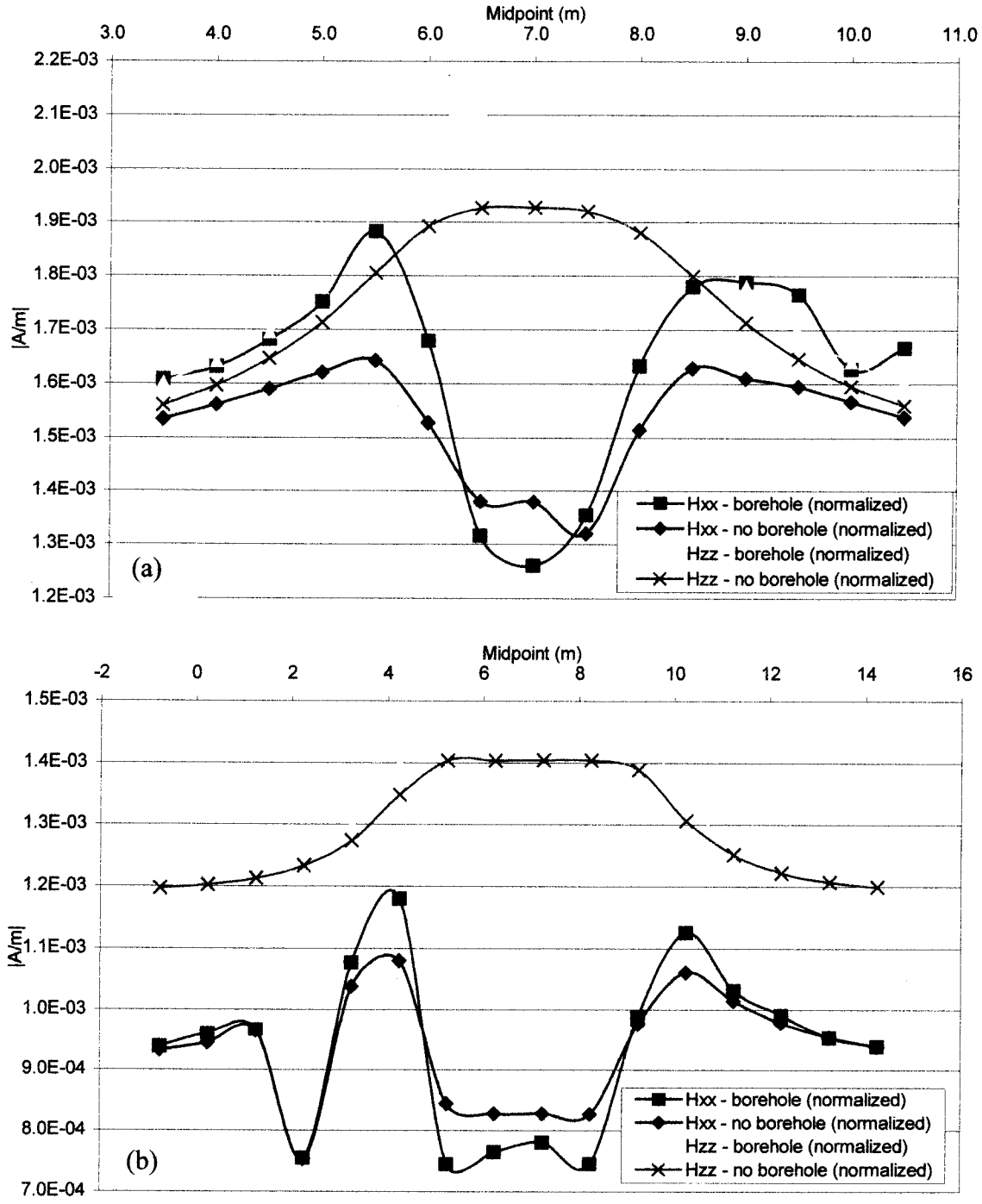


Figure 27- Total quadrature values, after frequency differencing, for a profile across a horizontal fracture using (a) a 2.0 m and (b) 4.5m array in coaxial and coplanar configurations. Results are for models with and without a borehole.

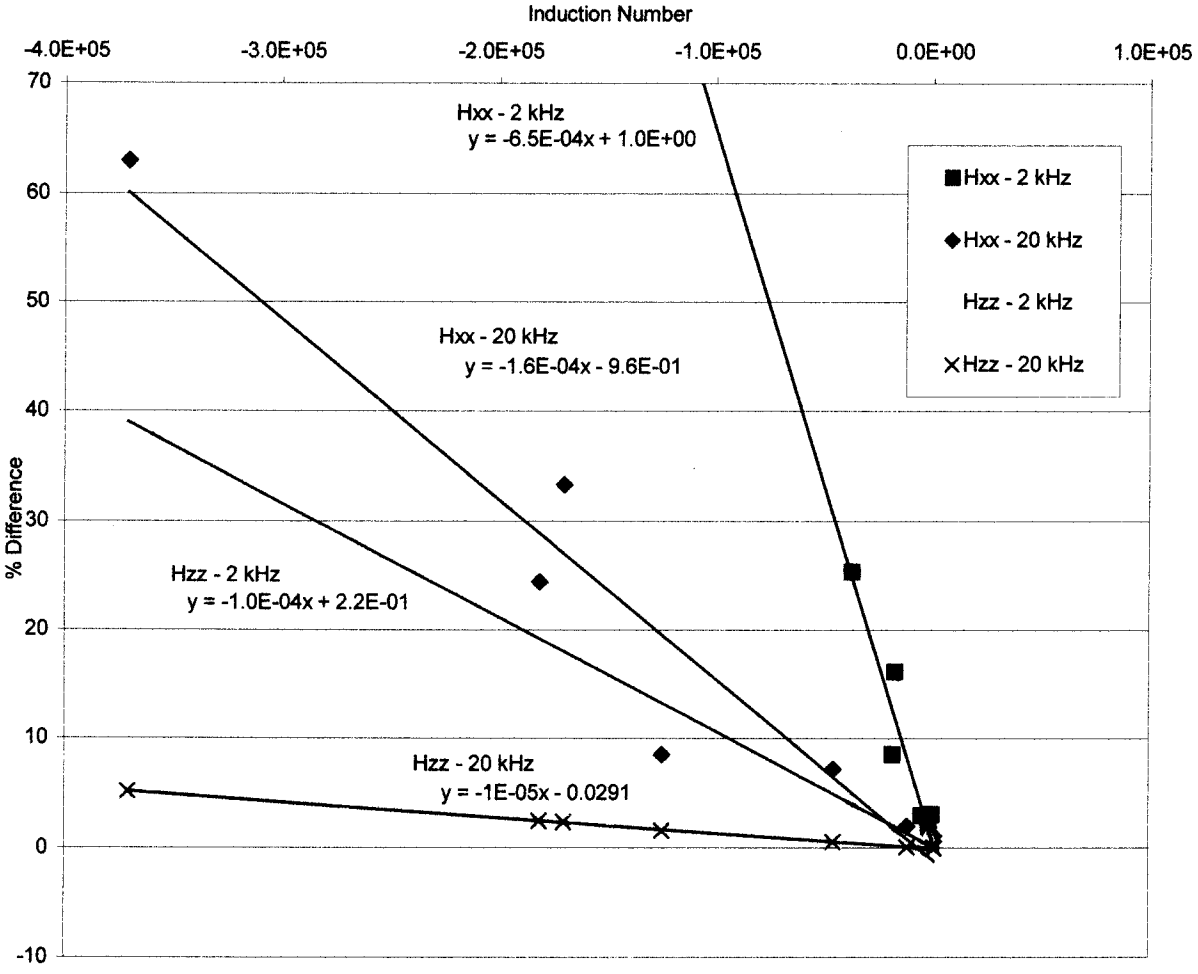


Figure 28. Induction number versus percent difference between the primary and total quadrature values for coaxial and coplanar configurations at 5.0 m offset.

# Chapter 3

# Quantitative analysis of multi-component borehole electromagnetic induction responses using anisotropic forward modeling and inversion

Electromagnetic induction logging procedures are standard accompaniments to well drilling for determining near-borehole rock properties including porosity, oil-versus-water saturation, and fracture location. Typically EM induction measurements are made using a down-hole coaxial magnetic field source and receiver. This configuration allows for at most a 2-D analysis of formation properties when assuming cylindrical symmetry about a vertical axis. With the advent of 3-D induction imaging tools, which utilize multi-component magnetic field receivers and transaxial transmitters, 2-D analysis of EM induction data is insufficient. This is especially true for the analysis of formation electrical properties in deviated well bores (nonvertical) or anisotropic conditions, as the cylindrical geometry often present in vertical wells does not exist.

Electromagnetic Instruments, Inc. is currently developing a 3-D multi-component EM induction tool (GeoBILT$^{TM}$). Because this numerical modeling study is designed to give insight specific to this and like tools, we must consider the GeoBILT$^{TM}$ specifications. The instrument utilizes three-component magnetic field sources and receivers as shown in Figure 1. The tool consists of a sonde which contains two mutually orthogonal, horizontally polarized electric loop sources (dimensions: 0.08m x 1m) and the vertical solenoid source (dimension: 1m). The sonde also contains the receiver array, which consists of receivers with the same three polarizations. Source-receiver offsets include 2m and 5m. Source magnetic fields are generated at five frequencies: between 2 and 40 kHz. At these low frequencies and offsets, the tool is considered to be working in a low-induction number (L) regime:

$$L \leq 1, \text{ where } L=\sigma_b \omega \mu l^2.$$

Here, $\sigma_b$ is electrical conductivity, $\omega$ is angular frequency, $\mu$ is magnetic permeability, and l is the source-receiver separation. Under this condition, the magnetic field response is linearly proportional to frequency and conductivity. Also, at these frequencies $\sigma_b >> \omega\varepsilon$, so propagation is dominantly diffusive and is considered to be dependent only on the conductivity of the medium.

The tool is also able to combine the three component sources and receivers to obtain 9 tool configurations for measurements in 3-D fully anisotropic media (Table 1). Of these 9 components which can be measured, only 4 are needed to uniquely describe a 2-D transversely isotropic structure imbedded in an otherwise homogeneous isotropic whole-space (Figure 2). These components include the coaxial, coplanar X-polarized, coaxial null-coupled, and coplanar Y-polarized configurations. Given that both coplanar configurations produce nearly identical responses when an isotropic conductor is symmetric in both X and Y, I have omitted the coplanar Y-polarized configuration from the simulations. The remaining three configurations constitute those modeled for all simulations.

In the tool design and future data interpretation, source-receiver configurations (e.g., offset and

source size), tool dip angle, and formation anisotropy are important factors controlling the multi-component response. The accuracy of assuming a magnetic dipole source when employing finite-length sources is also a concern in the design of the EMI tool. To this end, much of my work has focused on how the multi-component response deviates when realistic finite-length sources, such as solenoids and rectangular wire loops, are implemented instead of point dipole sources. The effects of anisotropy when coupled with solenoid and loop source configurations are also of interest and are investigated. All of these factors have been studied in relation to several fracture models to investigate the effects on detecting thin conducting bodies. Thin conductors are commonly encountered and represent scenarios of significant interest to the geothermal energy industry.

In order to determine the GeoBILT$^{TM}$ tool response, I am employing the iterative finite difference scheme developed by Newman and Alumbaugh (1995). This isotropic 3-D frequency-domain algorithm solves for the scattered EM fields and gives accurate simulated induction log responses. I will also use the anisotropic finite difference code developed by Newman and Alumbaugh (2001) to simulate the response in anisotropic fractures. Both codes solve the electric field vector Helmholtz equation using an implicit scheme based on a Yee staggered grid solution (Yee, 1966). Approximately 200 simulations have been completed with these techniques including dipping isotropic and anisotropic fracture zone model simulations. Forward models will also serve as input data to test the approximate inversion schemes that I develop.

## MODEL DESCRIPTIONS

In order to test a variety of realistic fracture zone scenarios, we have developed several models. They are based on three different geometries, where a conducting fracture is embedded in a relatively resistive whole-space. The geometries include: a thin infinite layer, a thin half-infinite layer, which is truncated at the borehole, and a finite-width layer, which is centered about the borehole (See Figure 3). All conductors have a thickness of 1 meter, and for simplicity, an infinite extent in the Y direction (Y-plane symmetry). A 1 meter thickness was chosen based on logging data presented by Barton et al. (1998) for the Dixie Valley, Nevada geothermal field. Fracture zone thickness in several wells (e.g., well 37-33) within the producing reservoir ranged from a few centimeters to several meters based on borehole televiewer data. Therefore, 1 meter is a reasonable thickness and is smaller than the shortest source-receiver offset simulated, which is sufficient to consider them thin conductors. In the following discussion, I will consider fracture and conductor synonymous terms, since only conductive fractures are modeled.

We have included several simulations which attempt to characterize the effective depth of

investigation for the coaxial and coplanar tool configurations in the presence of thin conductors. Models which vary the horizontal extent of the centered and half-infinite conductor geometries have been developed, and simulations allow for a semi-quantitative analysis of the effects of conductors on tool depth sensitivity.

Along with geometry, we varied dip angle and fracture-background conductivity contrast to determine the multi-component tool sensitivity to conductive fracture zones of different orientations with respect to the well axis. Each simulation included source frequencies and source-receiver offsets which are representative of the GeoBILT$^{TM}$ tool configurations described before. Solenoid and electric loop sources were simulated for the vertical and horizontal source polarizations, respectively. Coaxial, Coplanar, and Coaxial Null-Coupled tool configurations are included in the modeling results (Figure 2). The Coplanar Null-Coupled configuration is not included, since the response is zero for the conductor geometries considered. In addition to isotropic conducting fracture models, we have included a study of the affect of conductor anisotropy on measured multi-component responses. All plots have vertical depth of source-receiver offset as the abscissa and total quadrature magnetic field amplitude as the Y-axis. The center of the fracture is located at Y=0 on all plots.

## FINITE-DIFFERENCE MESH VERIFICATION

The speed and efficiency for which the finite-difference algorithm can calculate forward solutions is proportional to the total number of unknowns and therefore is sensitive to the total number of cells over which to compute the model parameters (Newman and Alumbaugh, 1995). However, there are a minimum number of mesh cells which are necessary to facilitate accurate results from the numerical scheme. For example, the solution is of 2$^{nd}$ order accuracy. Therefore, at least two cells are necessary across the thin conductors to provide accurate differencing in the conductor. This condition determines the minimum cell size in the mesh, and as demonstrated by Newman and Alumbaugh (1995) there exists a practical limit for the contrast (~10 times) between the largest and smallest cell size dimension in the non-uniform grid. Therefore, non-uniform gridding, which is used to place grid boundries in the far-field without increasing the total number of cells, can be used only to this limit. The 3-D FDFD algorithm forces the tangential electric fields to zero at the grid boundaries, so boundary reflections are present and may cause inaccuracies. Therefore, mesh dimensions must be sufficiently large (>2 skin depths) to avoid solution distortion caused by fields interacting with grid boundaries. In order to optimize the model space for both speed and accuracy, we tested solutions for various model meshes and compared the results to 1-D analytical solutions for agreement. Our tolerance for numerical error was approximately 1% based on the estimated accuracy of the numerical

codes (Newman and Alumbaugh, 1995). That is, the final finite-difference solutions agreed to within 1% of analytical solutions computed with two separate algorithms. An isotropic analytical algorithm was provided by Ki Ha Lee of Lawrence Berkeley Laboratories, and an anisotropic algorithm was provided by Xinyou Lu at the University of Wisconsin-Madison. It should be noted that only the infinite fracture geometries could be compared to the 1-D analytical results, because there exists no closed form solution for the 2-D electromagnetic induction problem that results from the centered and half-infinite geometries.

## TOOL CONFIGURATION EFFECTS

### *Finite length-dipole source agreement*

As mentioned, one of the objectives in this study was to evaluate the validity of assuming point dipoles when using finite-length sources. In order to accomplish this, simulations were first performed using point dipoles then rerun with realistically sized sources. The responses generated by dipole sources perpendicular to the borehole axis yield approximately the same response as the finite-length horizontal loop sources at both the 2 and 5m offsets (note: field amplitudes have been normalized by source moment). The coplanar configuration provides good agreement with point dipole simulations for all conductor geometries and dip angles (Figure 4). This result suggests that modeling of the near-borehole multi-component response assuming horizontally-polarized point dipole sources will suffice for the conductor geometries and offsets modeled here. It should be noted that one finite-length source data point (@ -3.0 meter depth) in Figure 4a shows considerable discrepancy with the dipole data. We are currently investigating the cause of this and believe it may be mesh related.

In contrast to the coplanar simulations, the measured response using a 1m solenoid source deviates significantly from that of a point dipole source at short offsets. For example, the difference between point source and solenoid quadrature magnetic field amplitude reaches a maximum of 4% for the infinite conductor model at an offset of 2m and 0° dip (Figure 5a). Unlike loop sources, the solenoid sources only have a radial field at the ends of the solenoid, which is 1 meter from the simulated dipole point. This difference between point dipole and solenoid source length may explain the observed discrepancies. If this is the case, then we expect the solenoid responses to agree better with simulated point dipole source simulations as offset increases. As shown in Figure 5b, the difference between point dipole and solenoid source amplitude is reduced to less than 1% at 5m offset. This suggests that accurate modeling of solenoid source configurations using point dipoles can be done if the source-receiver offset is sufficiently large. The discrepancy at short offsets appears to be independent of conductor dip.

*Effective investigation depth*

The depth to which typical coaxial induction logging tools are sensitive to near-borehole properties has been determined to be approximately twice the source-receiver separation (e.g., Moran, 1982). Alumbaugh and Wilt (2001) presented effective imaging depth sensitivities for the multi-component induction tool for all four source-receiver configurations used here. We extend the work of Alumbaugh and Wilt here to include simulations which approximate the effective depth of investigation for the GeoBILT™ tool in the presence of a thin conductor. While our results do not include effects due to noise, they may be used to estimate the depth penetration of the tool when thin conductors are present. We simulated the tool's response to the half-infinite and centered half-infinite conductors terminated at varying lateral depths from the borehole axis. We modeled the coaxial, coplanar, and coaxial null-coupled responses for both the 2 and 5m offsets. Since the estimated accuracy of our simulations is 1%, differences less than this are considered numerical noise. The results are plotted in Figures 6 and 7 and demonstrate that effective depth sensitivity is dependent on both source-receiver offset and polarization.

As predicted by Moran (1982) for the coaxial configurations, the investigation depth is approximately twice the source-receiver separation. This is evident in Figure 6a where the difference between the coaxial response at 4m and 6m is less than 1%. A similar result is shown in Figure 6b, where the sensitivity depth is greater than 6m with a 5m source-receiver offset. The coplanar responses are plotted in Figure 7a and 7b and demonstrate a contrasting result. In this case, the coplanar response is sensitive to a depth of approximately 1 source-receiver offset. This effect can be predicted, since the whole-space sensitivities for this configuration are more focused near the borehole than for the coaxial configuration (Figure 8c). Alumbaugh and Wilt (2001) demonstrated that geometric effects in addition to signal to noise considerations limited the effective imaging depth to approximately twice the source-receiver offset for the coaxial configuration and less for the coplanar configuration. Both the 2m and 5m coplanar source-receiver configurations show this diminished depth sensitivity. The coaxial null-coupled response in Figure 6c shows similar depth dependence to the coaxial configuration. Although fewer simulations were completed for the centered half-infinite conductor case, the results agree well with data simulated using the half-infinite geometry.

*Offset-dependent vertical resolution*

As shown in the previous results, the multi-component magnetic field response is dependent on source-receiver configuration. Of particular importance is the distance between the source and receiver coils as this affects both lateral sensitivity and vertical near-borehole resolution. Although

most modern coaxial induction logging tools employ short source-receiver offsets, typically less than 2m, the GeoBILT™ tool implements extended offsets. Increased offsets contribute to greater depth penetration, but decrease the overall vertical resolution of tool. As mentioned, responses have been simulated using a 2m and 5m source-receiver offset to compare and contrast the effects on imaging thin conductors.

Results indicate that at offsets larger than the conductor thickness, the field response is distorted proportional to the offset used. This is shown in Figure 9 where the coaxial responses due to an infinite fracture at $0^{o}$ dip are plotted for both 2 and 5m offsets. It is clear that the 5m data show a magnetic field anomaly that is approximately 2 times the vertical width of the 2m responses. Coplanar results are concurrent with the coaxial results. Simulations indicate that this large offset averaging contributes to smaller measured field values as well. The results shown in Figures 9 suggest that 5m offsets may decrease scattered field amplitudes more than three times that of the 2m configurations. This result is due to the fact that at larger distances from the borehole a larger volume of conductor is needed to produce a similar response at short distances (Alumbaugh and Wilt, 2001). Since our conductor has a static volume, the measured response is smaller at the larger tool offset (i.e., increased lateral depth).

As stated, our simulations were in the low-induction number regime ($L \leq 1$); therefore, varying the source frequency is expected to have a linear effect on the measured field amplitudes; however, since both 4 and 40 kHz are relatively low frequencies, no increase in vertical resolution is apparent for our models of thin conductors (Figure 10). Also apparent, is the inability to recover conductor thickness regardless of frequency or sampling interval (.5m in all simulations). Data simulated at a high dip angle (60 degrees) also shows no increase in vertical resolution with increasing frequency. This result is shown in Figure 10c, where the coplanar field response is plotted for both 4 and 40kHz sources at $60^{o}$ dip. Although the measured responses have slightly different shapes, the inflection points of the curves are superimposed. This substantiates the result that thickness of thin conductors cannot be determined directly from the forward response at typical logging frequencies and that resolution is determined by tool offset not frequency.

We do observe a difference between the responses of the two frequencies in terms of total magnetic field strength. At 4 kHz, the overall amplitude is as much as 1 order of magnitude smaller than that at 40 kHz. At these frequencies, field amplitudes are directly and linearly proportional to induction number for a given source-receiver offset. This suggests that an order of magnitude increase in frequency should yield an order of magnitude increase in amplitude. This is in fact what we see for the coaxial as well as the coplanar configurations.

## GEOLOGICAL EFFECTS

### *Dip angle dependence*

In addition to the previously mentioned tool variations, we simulated the multi-component response to fractures which dip at varying angles from horizontal. These simulations are important, since the measured fields are representative of those recorded in deviated boreholes or dipping formations. We simulated three dip angles: 0°, 30°, and 60°, while the Results are interpreted in terms of the effect of dip on a single component of the total field as well as the variation in the responses between all components. Figure 3 shows two-dimensional slices of the finite difference mesh for the 0° and 60° dip angle models. It should be noted that since the anisotropic finite difference code used in this study could only simulate a horizontal transversely isotropic conductor, the tool, not the fracture, had to be rotated by the appropriate dip angle (see Figure 3b). For example, the 30° dipping conductor model is represented by a horizontal conductor and a 60° dipping tool (i.e., the borehole dip angle is the compliment of the corresponding formation dip angle). Since only the positions of the source and receivers relative to the fracture is important (assuming that the mesh is appropriately designed), this measured response is identical to the dipping fracture case. However for these cases, a post-processing rotation of the field data after the simulations is necessary. This rotation is accomplished by projecting the x and z components of the total field onto the dip angle plane and summing the two components to give the measured total field along the borehole.

Among the results expected is the change in magnitude of the total field response as the conductor dip increases. This is evident if we consider the effective conductor thickness, which the tool will traverse. As we increase the dip of the conductor, the horizontal width of the conductor will decrease as 1/sine of the dip angle. The coaxial configuration is sensitive, or coupled, to the horizontal conductivity of the medium, so we expect the coaxial amplitude to decrease as the horizontal component of the conductor thickness decreases with dip. Additionally, we expect the coplanar configuration, which is affected by both positive and negative sensitivities in the X-Z plane (Figure 8c), to yield a decrease in field amplitude with increasing dip. As dip angle increases from horizontal, progressively more fracture volume intersects the positive lobes of the coplanar sensitivity. The combination of the positive and negative portions of the response result in an amplitude decrease with dip. In contrast, the null-coupled configurations should lead to amplitude increases with dip angle. For the horizontal conductor case, the null-coupled source-receiver configuration records no scattered fields, because all magnetic fields are scattered perpendicular to the receiver polarization. As the dip angle increases, an increasingly large "receiver-parallel" component of the field is scattered and

recorded. Results for the three source-receiver configurations are presented in Figure 11. As predicted, the coaxial and coplanar data show a decrease in the total field response with increasing dip angle (Figure 11a and c). In contrast, the null-coupled response (Figure 11b) shows an increase in the measured field strength with increasing dip angle. The null-coupled fields show less variation with dip angle than does the coplanar response.

Another significant effect of dip is the vertical broadening of the field responses as the tool traverses a steeply dipping fracture. From inspection of Figure 11, it is clear that the measured responses for the 60° dipping fracture are broader in the vertical direction than is the horizontal fracture responses. The source-receiver configurations are sensitive to scatterers away from the borehole axis. As dip angle is increased, progressively more fracture intersects this sensitivity "zone" at depths away from the horizontal fracture depth. The result is a field anomaly which is broad in vertical extent.

*Fracture geometry effects*

Simulations were performed to determine the relationship between tool configuration and varying conductor or fracture geometries. The same three geometries, shown in Figure 3, were modeled at various dip angles. Results are presented for the coaxial and coplanar data in Figure 12. At small dip angles, both configurations give rise to vertically symmetric responses, but as dip angle increases, asymmetry develops for the half-infinite fracture simulations. At shallow dip angles, we expect a vertically symmetric response from the coaxial and coplanar simulations for all geometries, since there is a vertical symmetry of conductor volume near the borehole and both the coaxial and coplanar configurations have symmetric sensitivities in that plane (Figure 8a,c, and d). At large dip angles, we also expect symmetry except for the half-infinite model, since the half-infinite conductor terminates near the borehole. This termination produces a symmetric magnetic field at shallow dip angles, but as the dip angle increases, this truncation produces asymmetry about the vertical borehole and results in an asymmetric field response. In contrast to the coupled configurations, the coaxial null-coupled configuration will give rise to an asymmetric response for all geometries and dip angles (e.g., Figure 11c) due to its asymmetric sensitivity in the X-Z plane (Figure 8b). As dip angle increases, this asymmetry in the magnetic field increases. These observations are significant and suggest that thin fracture geometry cannot be determined from any single source-receiver configuration, because ambiguities exist in the responses due to the similar effect of configuration sensitivity, dip angle, and fracture geometry.

*Anisotropic Models*

Sixteen finite-length source simulations were performed for the infinite and half-infinite

fracture geometries to determine what affect anisotropy has on the multi-component tool response. The dip angle was also varied from 0° to 60°. For all simulations, the fracture-perpendicular conductivity was twice that of the background medium (0.1 S/m), and the fracture-parallel conductivity was chosen to be 10 times the background conductivity (1 S/m).

In general, the anisotropic results agree well with the isotropic simulations for the conductivity contrasts used here. Results are presented in Figures 13 and 14 for all configurations and dip angles and show deviations in amplitude compared to isotropic simulations. At 0°, the computed total magnetic fields are equal or larger for the anisotropic conductor than for the isotropic conductor even though both have the same maximum horizontal conductivity (Figure 13). However at 60° the coaxial configuration yields smaller total field amplitudes than does the isotropic conductor model (Figure 13a). This may be explained by the decrease in effective horizontal conductivity due to the conductor dip. Additionally, this effect may be due to a sensitivity sign change at high dip angles (Figure 15). As shown by Lu et al. (2001), when the angle between the measurement tool and the formation is increased, the effects of anisotropy are increased. For the coaxial configuration, the near-borehole sensitivity changes from strongly negative to positive as dip angle increases (Lu and Alumbaugh, 2001). This change in sensitivity could be responsible for the total field reduction at 60°.

The coaxial response contrasts the coplanar and coaxial null-coupled configurations which always yield higher amplitude values for the anisotropic conductors regardless of dip angle (Figure 13b,c and 14b,c). These results suggest that the scattered currents for the coplanar and null-coupled configurations are focused or channeled in the conductor, which leads to elevated magnetic field amplitudes. This is probable, since anisotropy distorts the coplanar sensitivities (Figure 16) affecting them more in the plane of maximum conductivity (Lu et al., 2001).

Because anisotropy has the effect of altering the total field amplitude over the isotropic case, assumptions used in inverting multi-component data for near-borehole properties can result in error. That is, an isotropic inversion will underestimate (in our coaxial case) the formation conductivity if the formation is anisotropic. The magnitude of this error will depend on the magnitude of the conductivity anisotropy coefficient ( $\lambda = \sqrt{\sigma_h/\sigma_v}$ ) and the dip angle of the formation. In our simulations, the error in measured magnetic field amplitude associated with the coaxial component at 60° dip is approximately 5%. It is less for the coplanar response.

## CONCLUSIONS

We have been able to draw several conclusions about the multi-component response of the GeoBILT™ tool with respect to tool configurations and geological conditions.

1. The magnetic field responses generated by dipole sources perpendicular to the borehole axis yield approximately the same response as the finite-length horizontal loop sources. However, the measured response using a 1m vertical solenoid source deviates significantly from that of a dipole source configuration. The difference between point dipole and solenoid source field positioning may be the source of the observed discrepancies. At longer source-receiver offsets the solenoid responses agree better with simulated point dipole source configurations. This suggests that accurate modeling of solenoid source configurations using point dipoles can be done if the source-receiver offset is sufficiently large.
2. Source-receiver offset has a significant effect on the vertical resolution of the GeoBILT™ tool. As the tool offset increases from 2 to 5m, the resolution decreases by as much as a factor of three. In addition, the measured total field amplitude decreases as offset is increased. This is a direct result of an increase in depth sensitivity at larger offsets, and implies that both long and short offsets should be employed to properly sample the near-borehole environment both vertically and horizontally.
3. The effective depth sensitivity of the tool is controlled by source-receiver offset as well as configuration. Results provide evidence that fields recorded for coaxial and null-coupled sources and receivers sample a lateral depth of twice the tool offset. This distance is significantly reduced when coplanar source and receiver polarizations are used. Coplanar configurations are sensitive to the very near-borehole and may be significantly effected by unwanted EM scattering from the borehole itself.
4. Dip angle has significant effects on the measured magnetic field intensity for all source-receiver offsets. The coaxial and coplanar data show a decrease in the total field response as we increase the dip angle. In contrast, the null-coupled responses show an increase in the measured field strength with increasing dip angle. Additionally, the degree to which the measured fields are affected by dip angle depends on the depth sensitivity of each source-receiver configuration.
5. Fracture geometry affects measured field amplitudes by creating symmetric or asymmetric responses based on the near-borehole conductivity contrasts of the fracture. For infinite fractures, the coaxial and coplanar configurations give rise to symmetric field anomalies, while the null-coupled responses are asymmetric. All responses are asymmetric when a steeply dipping fracture is truncated at the borehole. Therefore, all configurations must be considered if symmetry is used to determine fracture depth or dip.
6. Finite-length source simulations containing transversely isotropic conductors show small but

measurable differences from isotropic results. Coaxial configurations record identical total field responses for the isotropic and anisotropic horizontal conductors. However, these configurations record smaller total field amplitudes for anisotropic conductor when conductor dip angles are large. The coplanar and null-coupled configurations record larger total field amplitudes for the anisotropic conductors at all dip angles. Distortions of the multi-component sensitivities in anisotropic conductors are responsible for these observed total field variations with anisotropy. Modeling and inversion which assumes isotropy in the presence of anisotropy will result in error.

## REFERENCES

D.L. Alumbaugh, and M.J. Wilt, 2001, A numerical sensitivity study of three-dimensional imaging from a single borehole, *Petrophysics*, v. 42, 19-31.

X. Lu and D.L. Alumbaugh, 2001, Three-dimensional sensitivity analysis of induction logging in anisotropic media, *Petrophysics,* in press.

X. Lu, D.L. Alumbaugh, and C.Weiss, 2001, Three-dimensional sensitivity analysis for multi-component induction logging in anisotropic media, Sandia National Laboratories Technical Report, in preparation.

J.H. Moran, 1982, Induction logging-geometrical factors with skin effect, *The Log Analyst*, v. 32, 4-10.

G.A. Newman and D.L. Alumbaugh, 1995, Frequency-domain modeling of airborne electromagnetic responses using staggered finite differences, *Geophysical Prospecting*, v. 43, 1021-1042.

G.A. Newman and D.L. Alumbaugh, 2001, A finite-difference solution for 3-D induction logging problems: Part II, *Geophysics*, in press.

K.S. Yee, 1966, Numerical solution of initial boundary problems involving Maxwell's equations in isotropic media, *IEEE Transactions on Antennas and Propagation*, AP-14, 302-309.

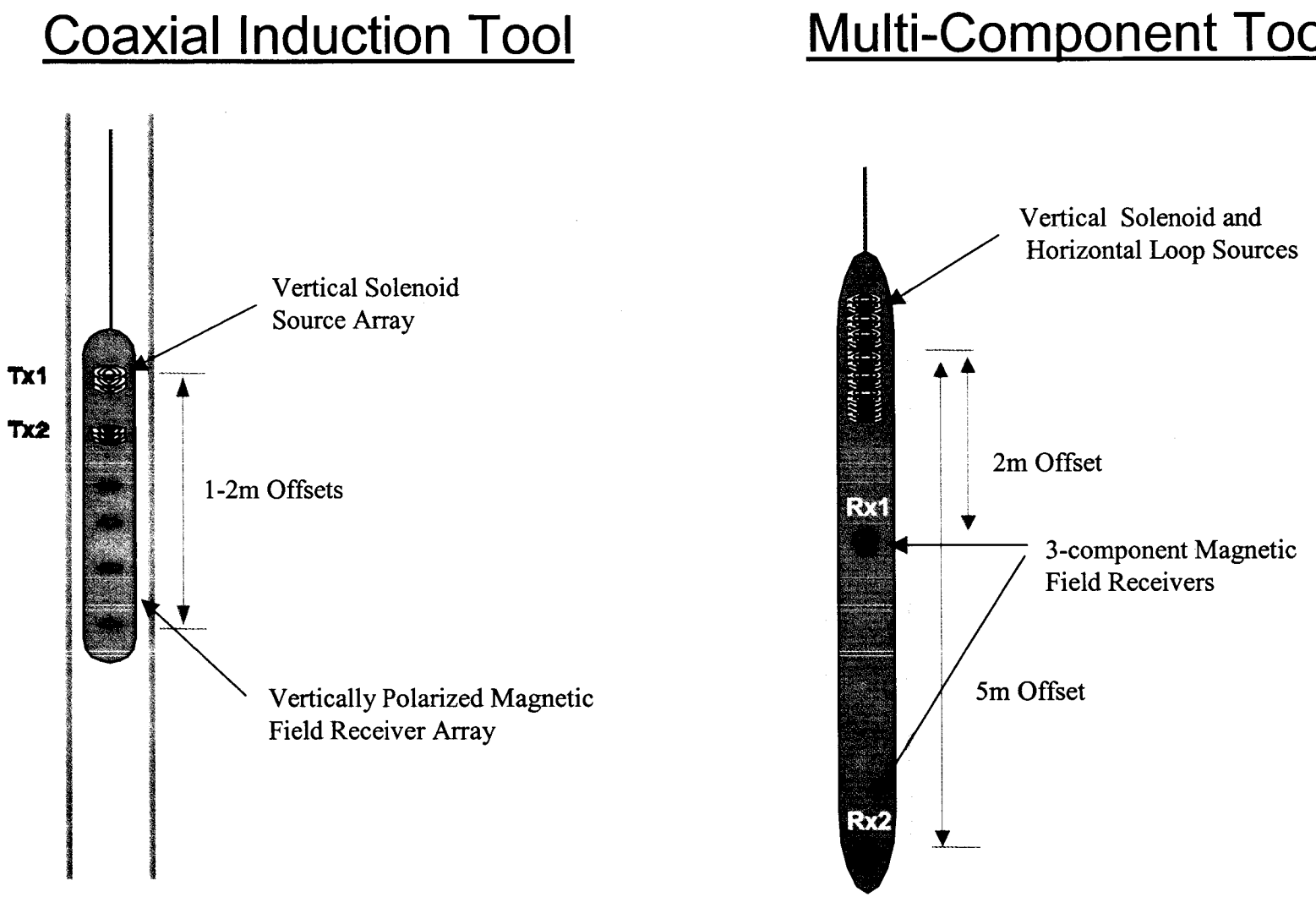


Figure 1. Schematic diagram of a typical coaxial induction logging tool and a prototype multi-component induction tool (GeoBILT).

3(a)

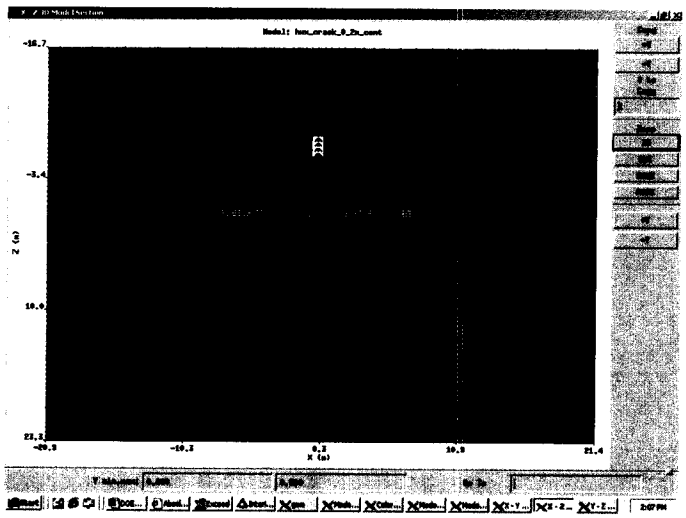

3(b)

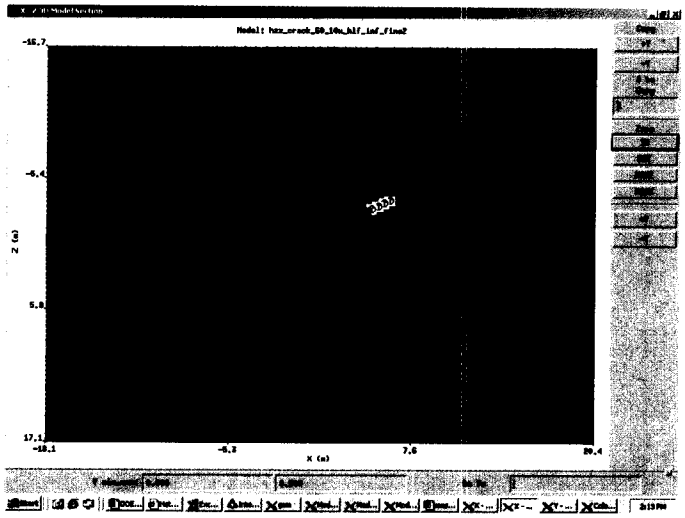

3(c)

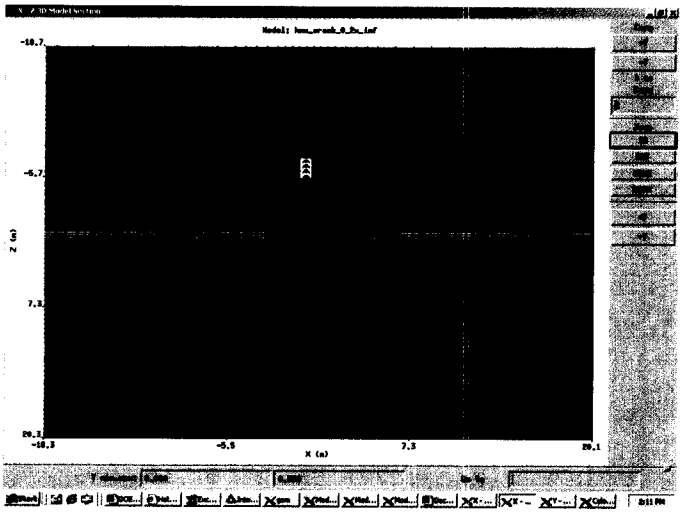

Figure 3. 2-D slices of 3-D Finite-difference meshes showing non-uniform gridding. a) X-Z plane slice of 3-D mesh showing the "centered" fracture model. b) X-Z plane of 3-D mesh showing the "half-Infinite" fracture model. Also shown is a conductor model at 60° dip with respect to the tool axis. c) X-Z plane slice of 3-D finite-difference mesh showing the "Infinite" fracture geometry model.

a.

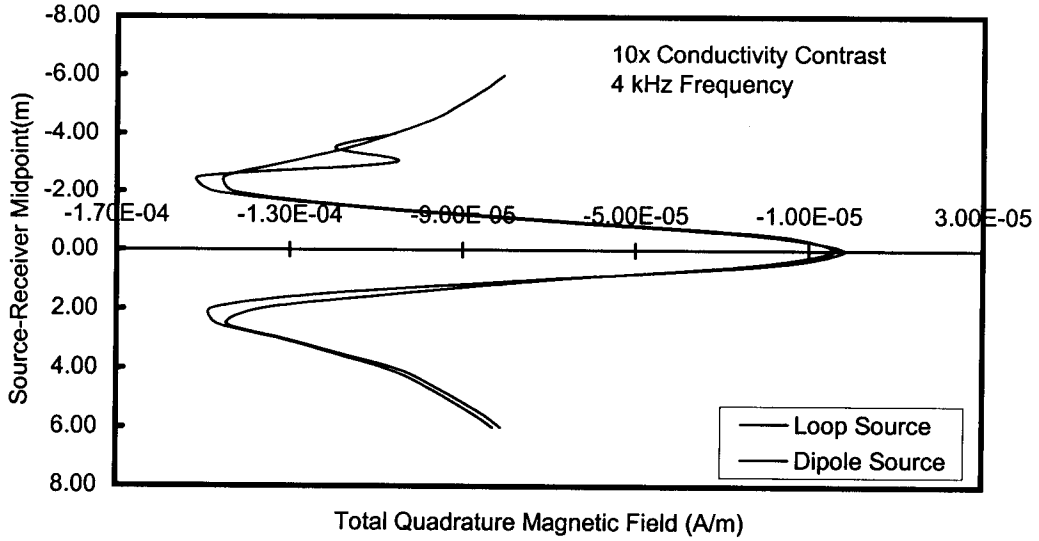


b.

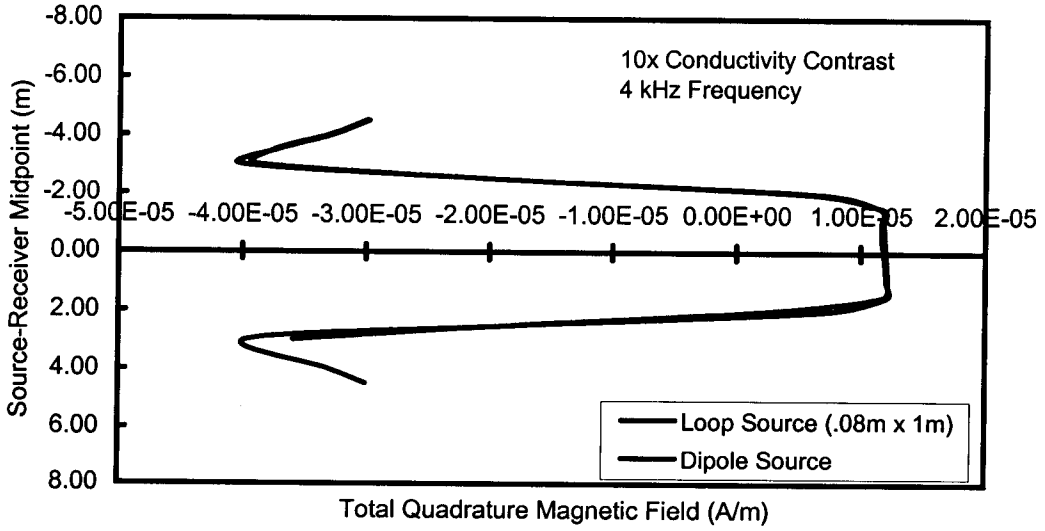


Figure 4. Point dipole and electric loop source comparisons for ther coplanar configuration at 2m (a) and 5m (b) offsets. Simulations are for an infinite conductor model at 0° dip and 4kHz source frequency. The fracture is centered at source-receiver midpoint =0.0.

**a.**

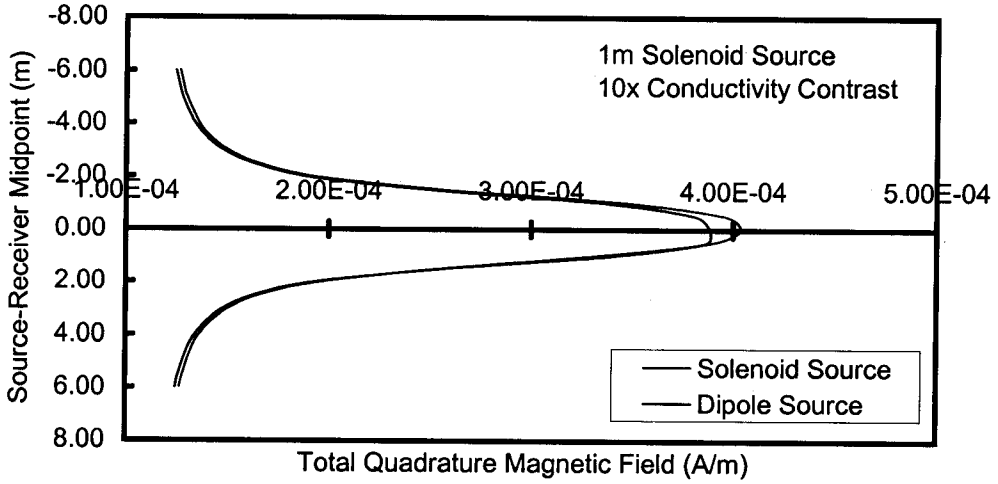


**b.**

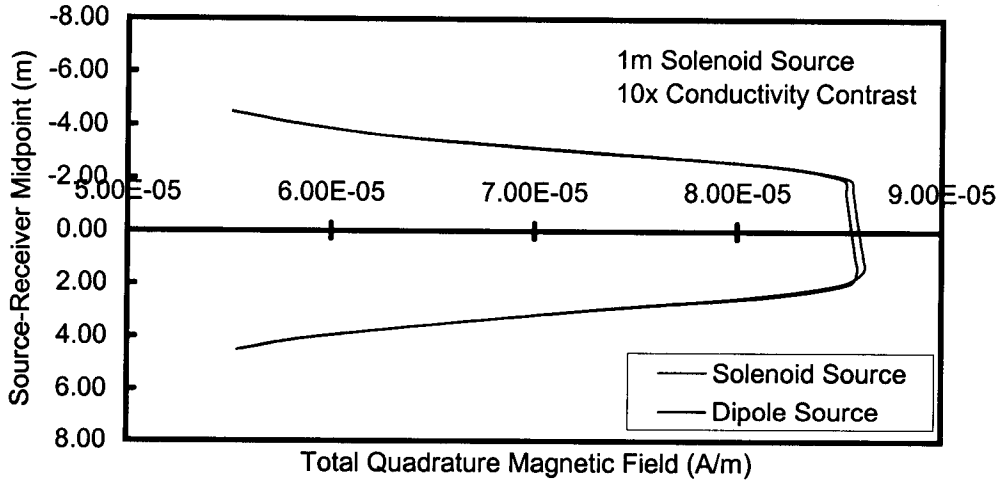


Figure 5. Point dipole and solenoid data comparisons at 2 and 5m offsets and 4kHz. a) Coaxial configuration response at 2m and 0° for an infinite conductor. b) Coaxial response at 5m and 0° for an infinite conductor. Note that the Y-axes for the two plots are scaled differently.

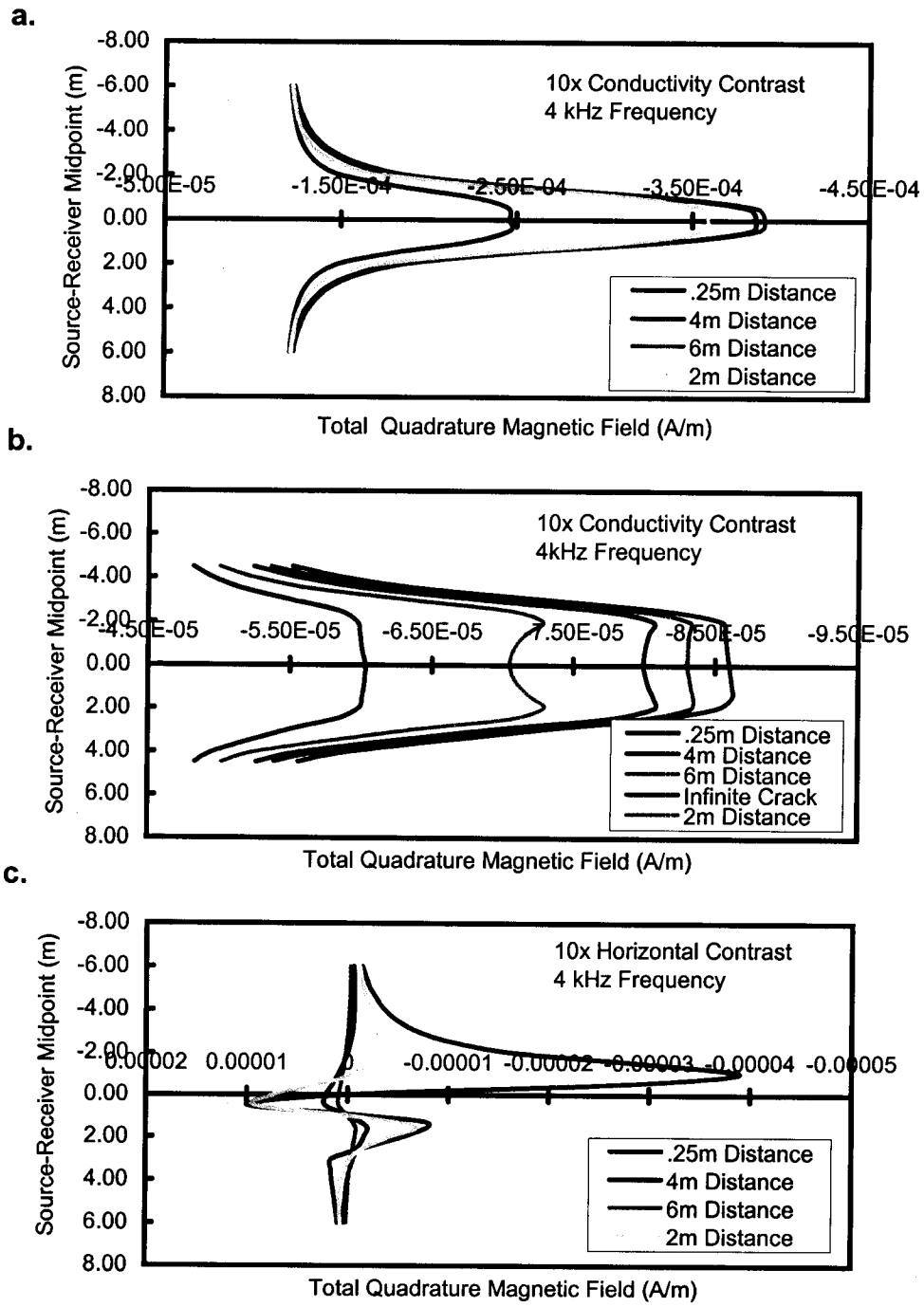


Figure 6. Simulated data showing the effective depth sensitivity for two tool configurations. Data represent the half-infinite conductor model, which has varying lateral extent away from the borehole axis. a) Coaxial data at 2m source-recevier offset. b) Coaxial data at 5m offset. c) Coaxial null-coupled data at 2m offset.

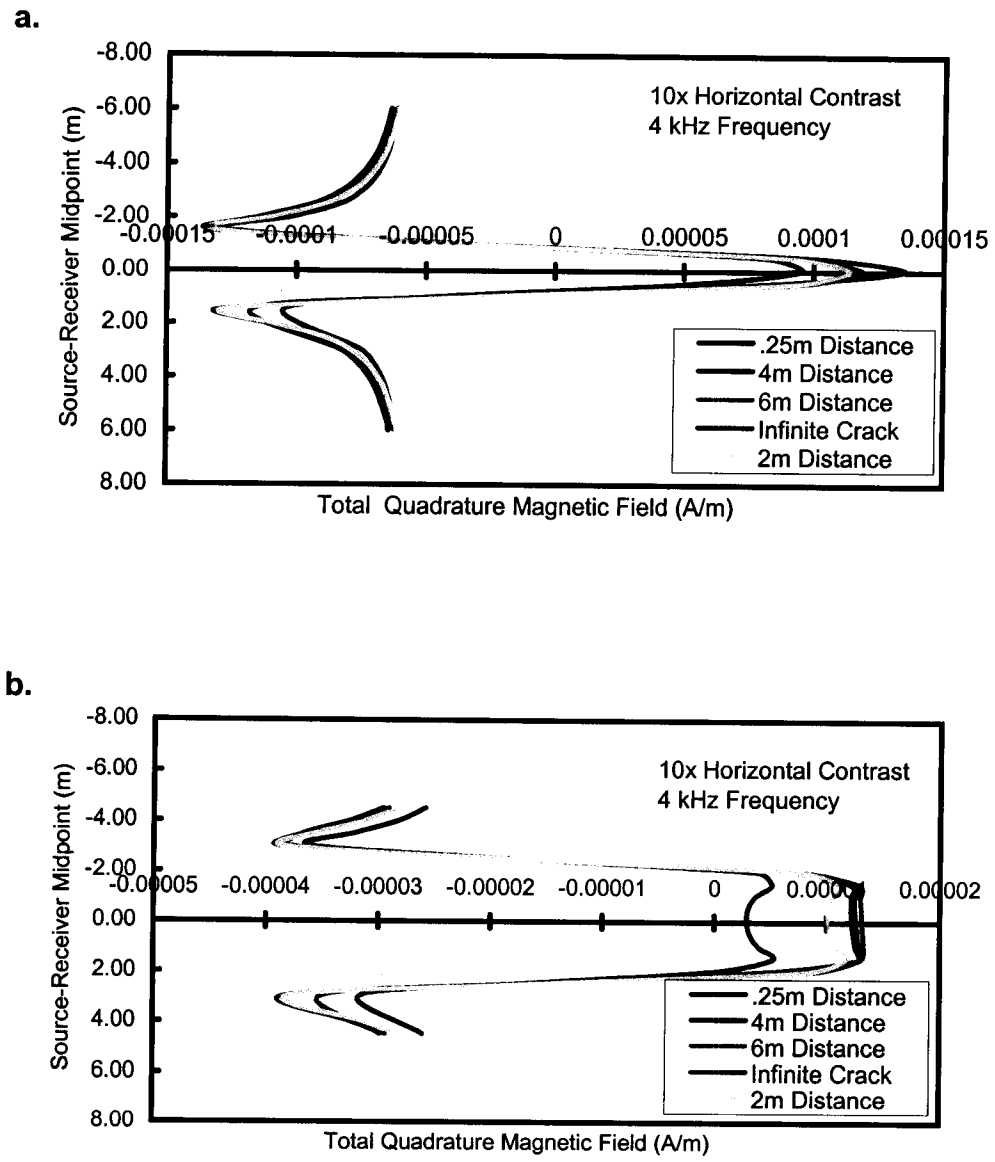


Figure 7. Simulated data showing the effective depth sensitivity for the coplanar tool configuration. Data represent the half-infinite conductor model, which has varying lateral extent away from the borehole axis. a) Coplanar data at 2m offset. b) Coplanar data at 5m offset.

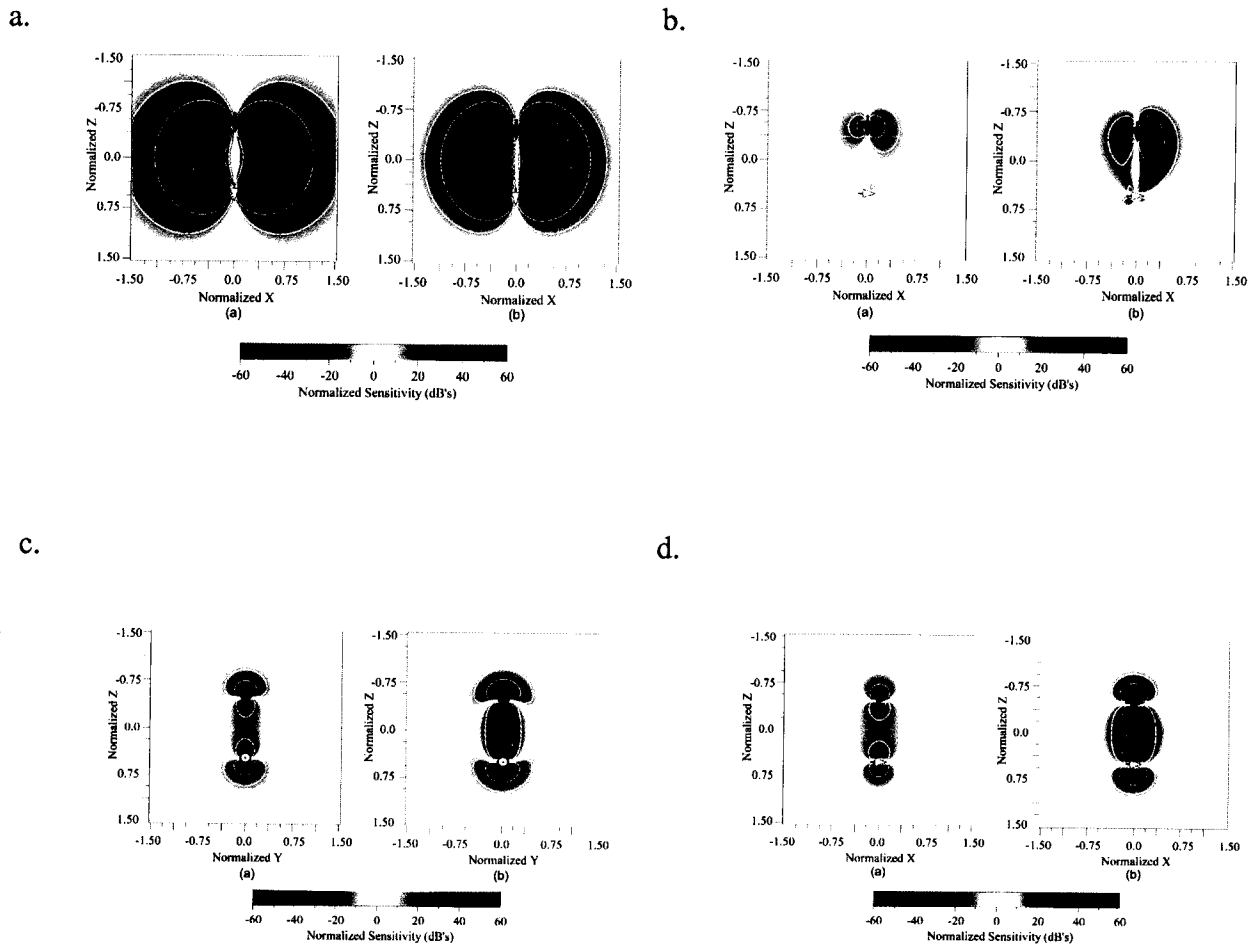


Figure 8. Logarithmically normalized multi-component sensitivities as a function of position in a homogeneous isotropic whole-space. Left panes are real components, and right panes are quadrature components. All data are presented at an induction number of 1. a) coaxial sensitivity in the y=0 plane. b) coaxial null-coupled sensitivity in the y=0 plane. c) Coplanar X-polarized sensitivity in the X=0 plane. d) Coplanar Y-polarized sensitivity in the Y=0 plane. (After Alumbaugh and Wilt, 2001).

a.

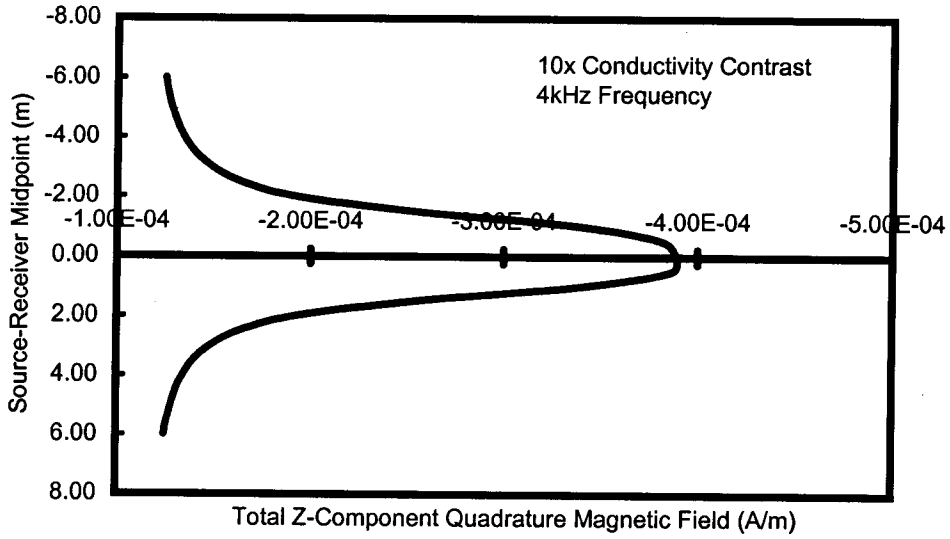


b.

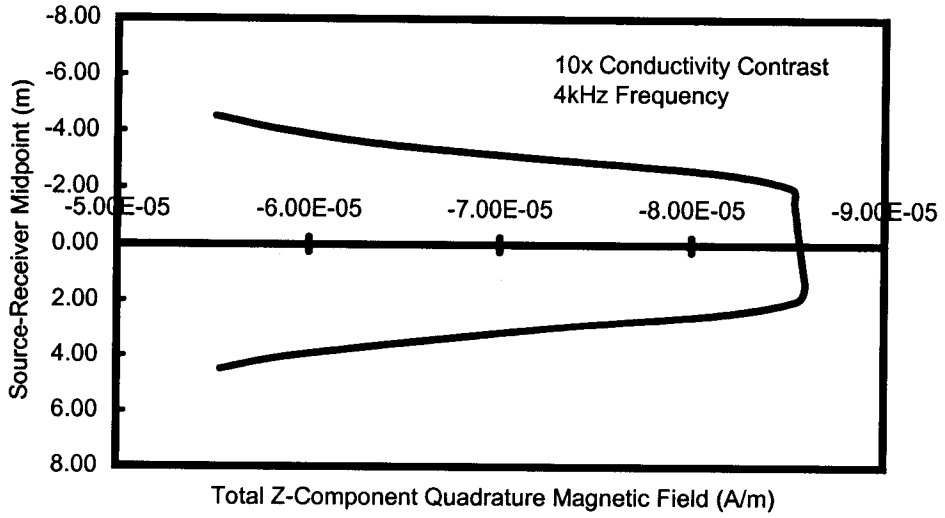


Figure 9. Coaxial configuration simulations showing the effect of source-receiver offset on measured magnetic field amplitudes. a) Coaxial data at a source-receiver offset of 2m for the "infinite" conductor model. b) The same "infinite" conductor model at 5m offset and 0 degree dip.

a.

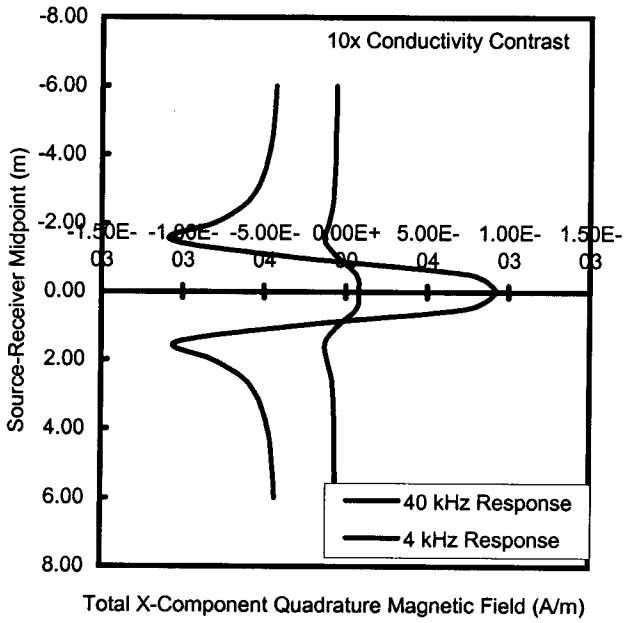


b.

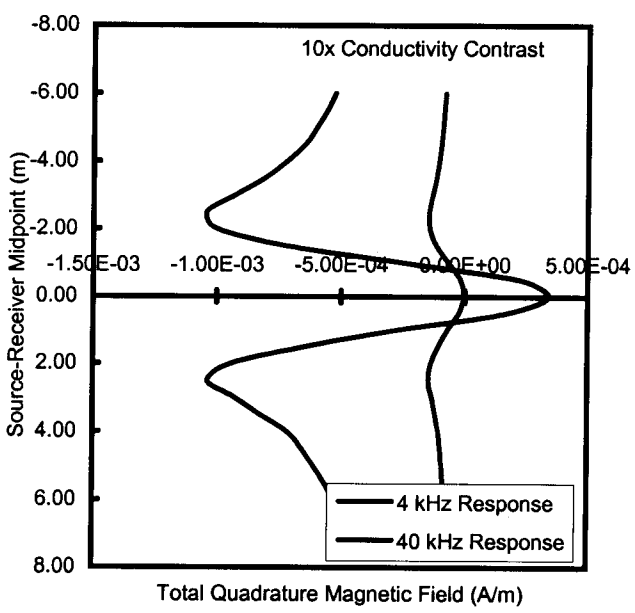


c.

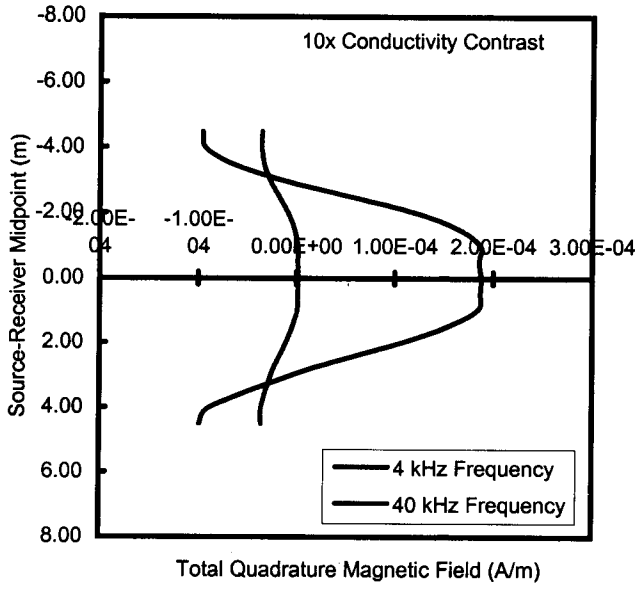


Figure 10. Plots of coplanar configuration responses showing variation at low (4kHz) and high (40 kHz) frequency. a) Half-infinite model simulation at 0 deg dip and 2m offset. b) Infinite model simulation at 60 deg dip and 2m source-receiver offset. c) Infinite model simulation at 60 deg dip and 5m source-receiver offset.

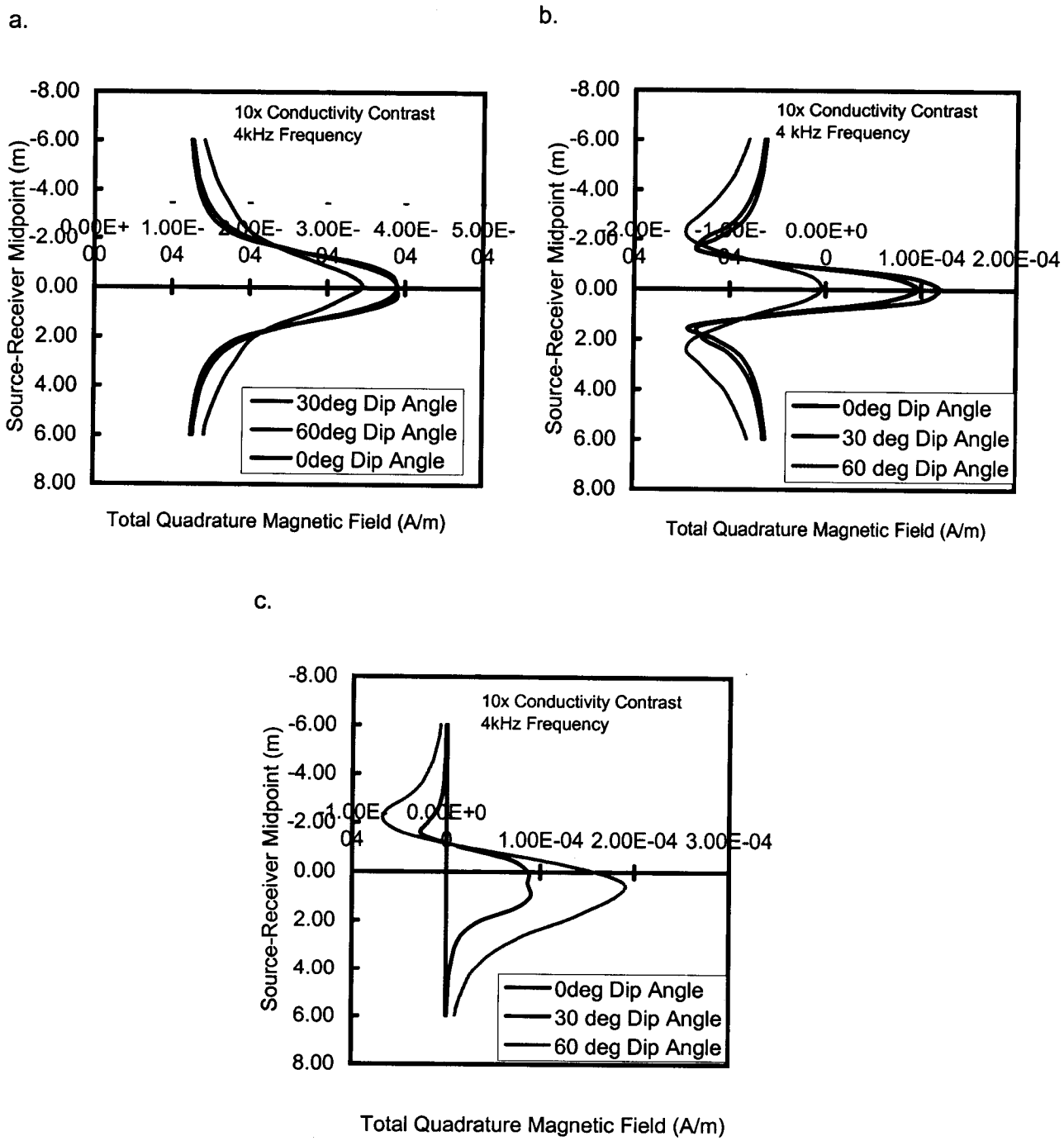


Figure 11. Plots showing the variation in magnetic field ampliude with fracture dip angle and source-receiver configuration. a) Coaxial response from the infinite fracture model at an offset of 2m. b) The coplanar response to an infinite fracture model at an offset of 2m. c) The coaxial null-coupled response for an infinite fracture model at 2m offset.

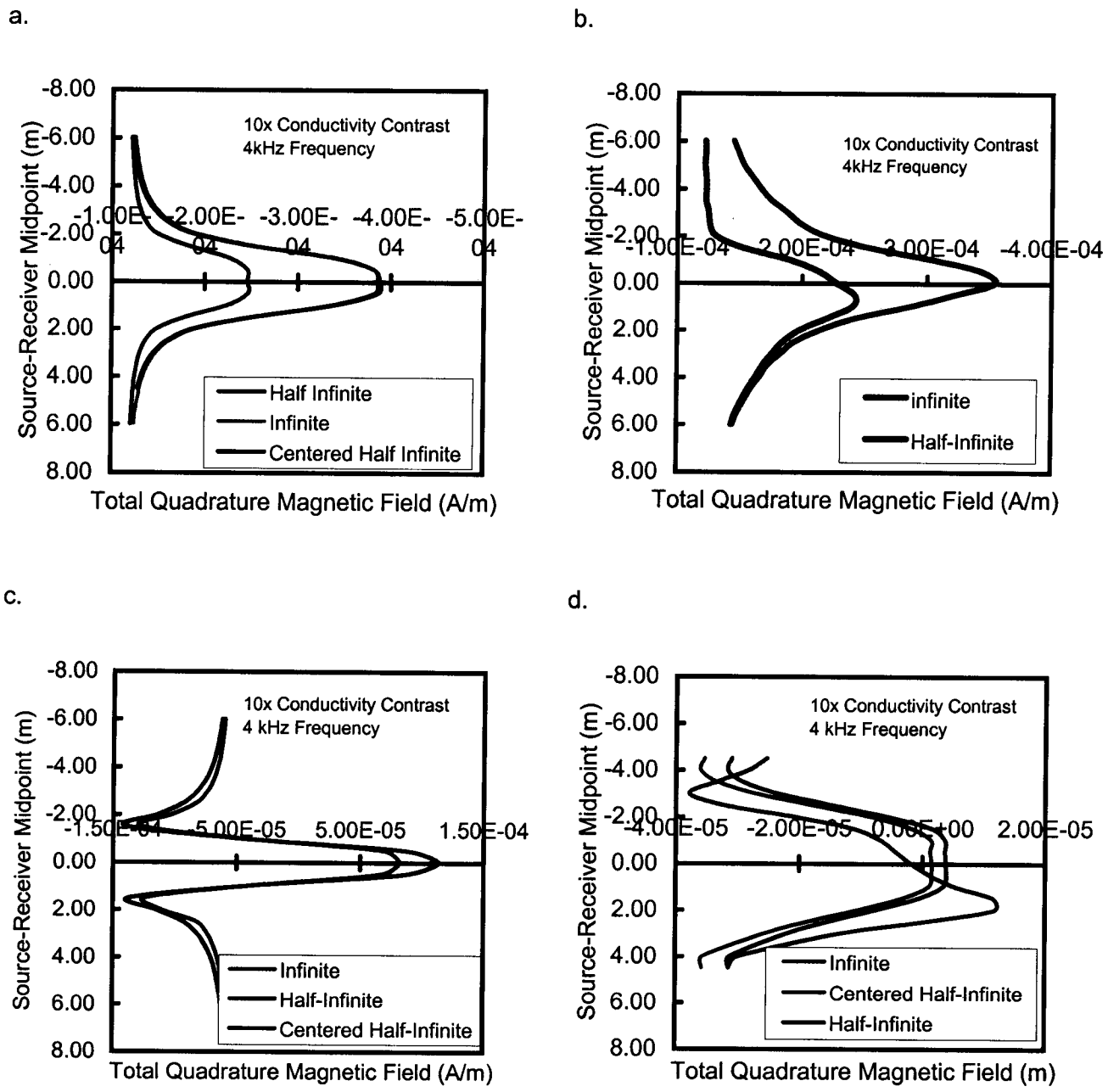


Figure 12. Plots showing the effect of fracture geometry on measured magnetic field strength for two dip angles. a) 2m coaxial data for threehorizontal fracture geometries. b) 2m coaxial null-coupled data for two fracture geometries dipping at 60 degrees from the horizontal. c) 2m coplanar data for three horizontal fracture geometries. d) 5m coplanar data for three fracture geometries dipping at 60 degrees from the horizontal.

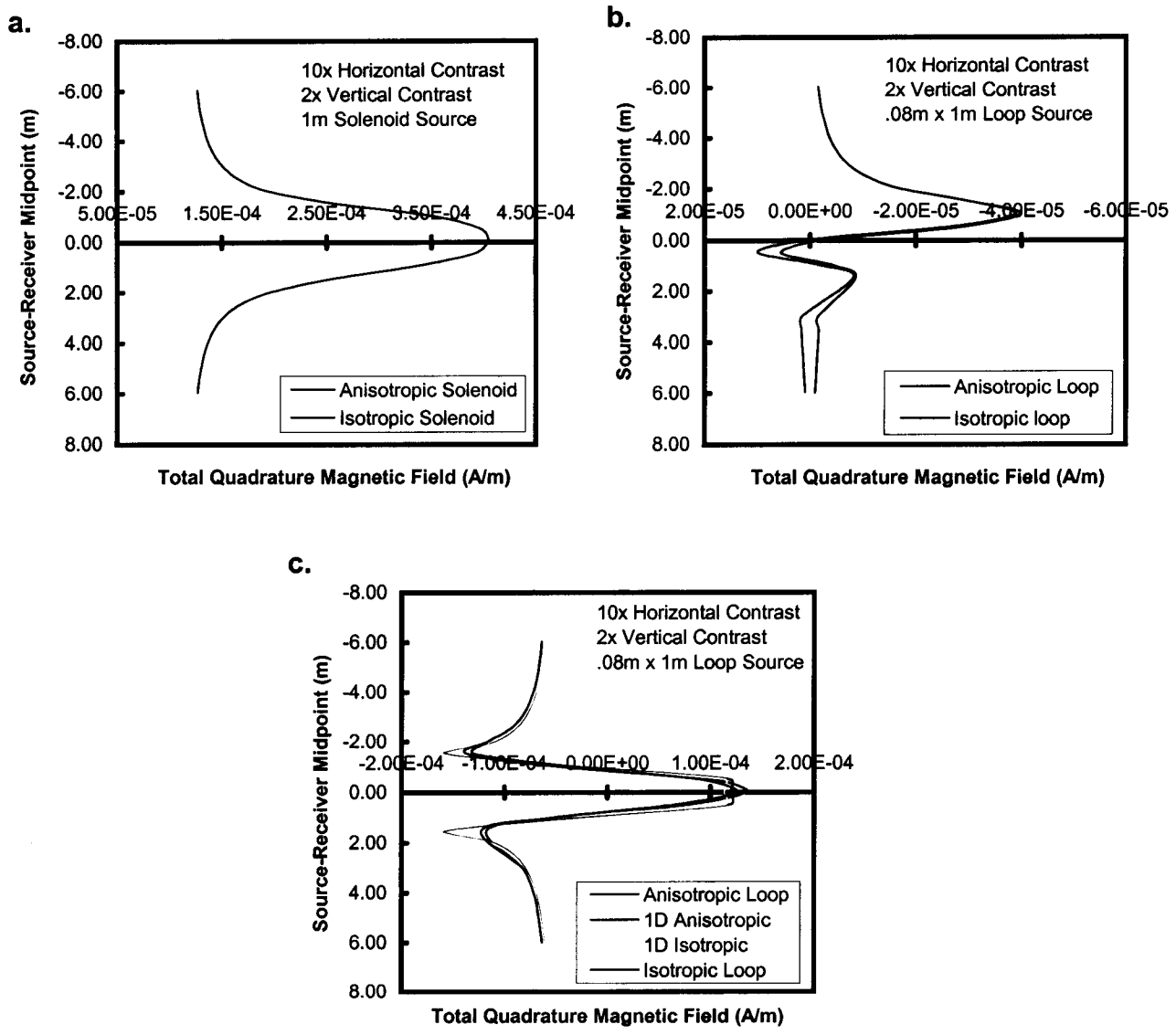


Figure 13. Isotropic and anisotropic comparisons for various configurations at 2m offset and $0^{o}$ dip. a) Coaxial response for an infinite conductor at 4 kHz. Note that the isotropic response lies on top the anisotropic response. b) Coaxial null-coupled response for the half-infinite conductor geometry at 4kHz. c) Coplanar configuration response for an infinite conductor at 4kHz. Also included is the 1-D analytical solutions for the isotropic and anisotropic case.

a.

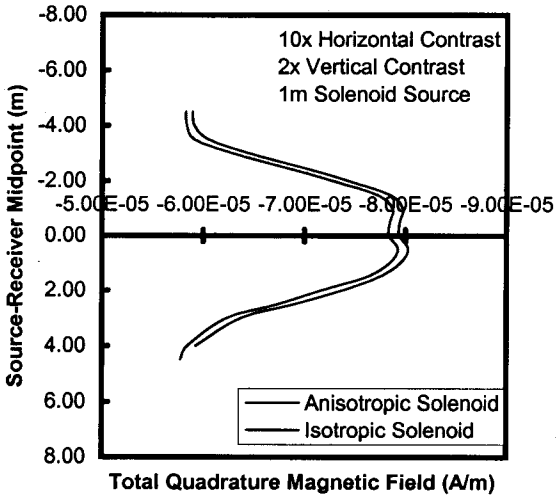


b.

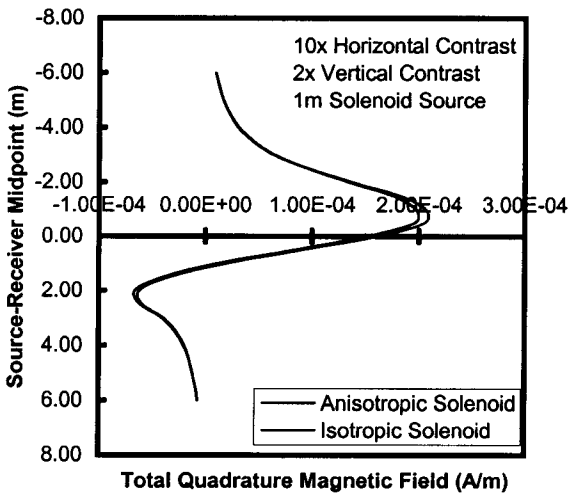


c.

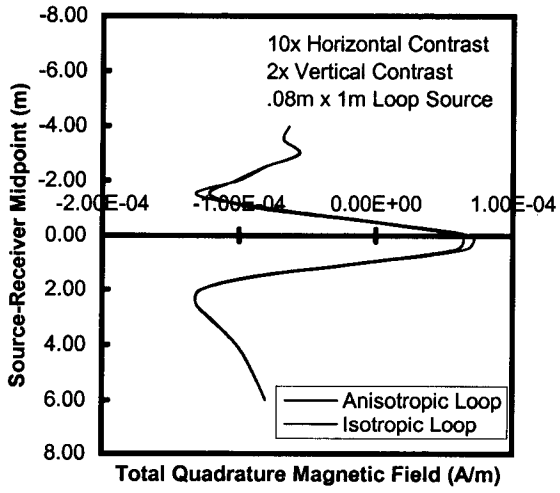


Figure 14. Isotropic and anisotropic comparisons for various configurations at 2m offset and 60° fracture dip. a) Coaxial response for an infinite conductor at 5m offset and 4 kHz. b) Coaxial null-coupled response for an infinite conductor at 2m offset and 4kHz. c) Coplanar configuration response for a half-infinite conductor at 2m offset and 4kHz.

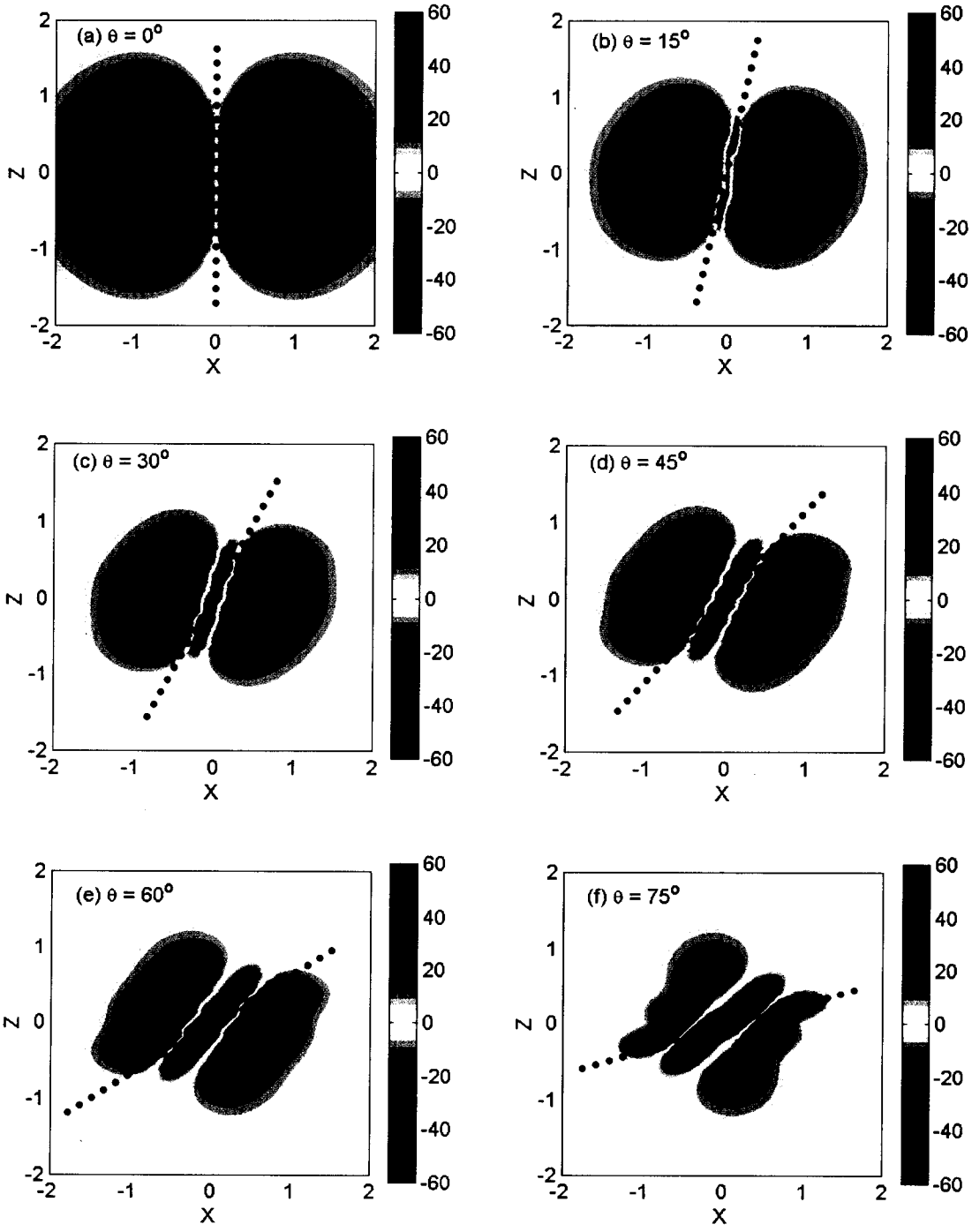


Figure 15. Coaxial sensitivities as a function of increasing tool or formation dip (θ) in the presence of transverse isotropy. Plots represent projections of 3-D sensitivities of +-20 dB. As dip angle increases, the positive sensitivity region near the tool axis becomes negative. The tool axis is indicated by the dotted line. (After Lu and Alumbaugh, 2001c)

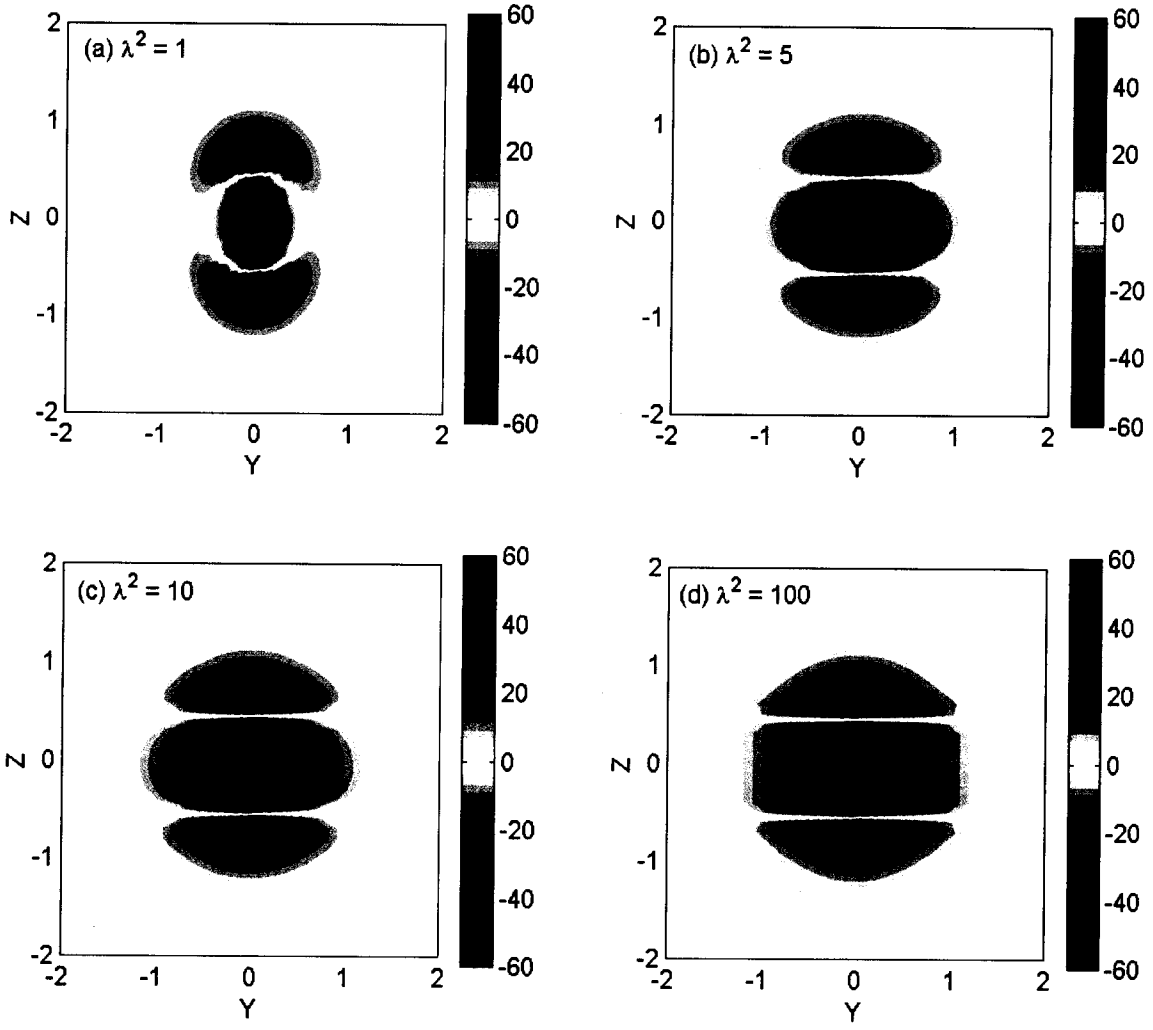


Figure 16. Sensitivities for the coplanar configuration as a function of increasing anisotropy ($\lambda$). 2-D projections represent isosurfaces of sensitivity of ±20 dB. Surfaces are distorted in the direction of maximum anisotropy. (a) $\lambda^2 = 1$. (b) $\lambda^2 = 5$. (c) $\lambda^2 = 10$. (d) $\lambda^2 = 100$. (After Lu and et al., 2001)

## Chapter 4 – Conclusions and Recommendations

This forward modeling study has determined important aspects regarding the effects of the borehole and invasion zone on three-component induction measurements made with the new EMI GeoBILT tool. It has been determined that the effects can be significant, and that they increase with $f\Delta\sigma r^2$, where f is the frequency, $\Delta\sigma$ is the difference in conductivity between the formation and the borehole/invasion zone, and r is the radius of the borehole/invasions zone. A normalizing procedure involving differencing the measurements made at two different frequencies reduces the borehole effect, but will not totally eliminate them. This is especially true for larger values of $f\Delta\sigma r^2$, and when the formation and borehole/invasion radius varies along the length of the borehole.

Fracture-zone simulations have yielded important information on the tool resolution and depth of investigation. The coaxial configuration has greater depth sensitivity than the coplanar, and the resolution is dominated by the source-receiver separation rather than frequency. Anisotropy has significant effects on the results; the magnitude of the coaxial response is decreased by transverse anisotropy, while the coplanar response increases slightly. Three-dimensional structures can produce complicated signatures, especially in the null-coupled components when the fracture terminates near the borehole.

The results to this point have been generated via forward modeling experiments. Future work should focus on 3D inversion, including developing faster schemes that may be run on a single workstation, and that will work for the lower induction numbers that the tool operates at. In addition, the schemes should be designed to invert on the frequency-differenced results rather than the raw data itself.